Chem Soc Rev

REVIEW ARTICLE

View Article Online
View Journal

Cite this: DOI: 10.1039/c5cs00739a

Silicon based radicals, radical ions, diradicals and diradicaloids

Kartik Chandra Mondal, Sudipta Roy and Herbert W. Roesky*

Received 27th September 2015

DOI: 10.1039/c5cs00739a

www.rsc.org/chemsocrev

Radicals are an important class of species which act as intermediates in numerous chemical and biological processes. Most of the radicals have short lifetimes. However, radicals with longer lifetimes can be isolated and stored in a pure form. They are called stable radicals. Over the last five decades, the syntheses of several stable radicals have been reported. Recently, highly unstable radicals have been successfully stabilized *via* strong σ-donation of singlet carbenes. Cyclic aklyl(amino) carbene (cAAC) is regarded as a stronger σ-donor and a better π-acceptor when compared with that of an N-heterocyclic carbene (NHC). In this article we review preferentially the results of our group to generate stable radical centers on the carbene carbon atoms by employing the so far hidden and unique ability of the cAACs. We focus on the development of new synthetic routes to stable and isolable radicals containing silicon atoms. All the compounds have been well characterized by single crystal X-ray analysis; the mono-radicals have been distinguished by EPR spectroscpy and the ground state of the diradicals has been studied by magnetic susceptibility measurements and theoretical calculations. Many of these compounds are studied by cyclic voltammetry and are often converted to their corresponding radical cations or radical anions *via* electron abstraction or addition processes. Some of them are stable, having long lifetimes and hence are isolated and characterized thoroughly. Not much information has been obtained on the short lived persistent radical species. Herein, we discuss some of the examples of such a type of species and focus on what kind of chemical reactions are initiated by these short-lived radical species in solution. We also briefly mention the syntheses and charaterization of the so far reported stable silicon centered radicals.

Institut für Anorganische Chemie, Georg-August-Universität, 37077 Göttingen, Germany. E-mail: hroesky@gwdg.de; Fax: +49 551 39 33373; Tel: +49 551 39 33001

Introduction

Radicals are captivating chemical species which have attracted the interest of experimental as well as theoretical chemists and

Kartik Chandra Mondal

Kartik Chandra Mondal received his PhD in 2011 from Karlsruhe Institute of Technology (KIT) under the supervision of Professor Annie K. Powell. He worked on mixed 3d–4f ion based single molecule magnets. After a short stay as a postdoctoral researcher in the same group he moved to University of Göttingen in October, 2011. Since then he has been working with Professor Herbert W. Roesky as a postdoctoral fellow. His research interest mainly focuses on the stabilization of low valent low coordinate group 14 elements and transition metal complexes. Dr Mondal has coauthored more than 45 peer-reviewed publications in leading scientific journals.

Sudipta Roy

Sudipta Roy received her PhD in 2012 from the University of Regensburg under the supervision of Professor Oliver Reiser. Afterwards she worked as a postdoctoral fellow at the Institute of Organic and Biomolecular Chemistry, University of Göttingen on transition metal catalyzed C–H bond activation. Since 2014 she has been working as a postdoctoral fellow with Professor Herbert W. Roesky. Her research interests include the synthesis of cyclic alkyl(amino) carbene stabilized highly sensitive Si–P compounds, and transition metal complexes with their application in catalysis.

physicists for over a century.[1] The first organic radical (trityl radical; $Ph_3C^{\bullet}$) was synthesized in 1897 by the Russian scientist Moses Gomberg and was reported in 1900.[1a] Trityl radical is the first organic radical which was produced within a glass container in a laboratory. It was accidentally obtained in an attempt to synthesize sterically crowded $Ph_3C–CPh_3$ by reduction of $Ph_3C–Cl$ with Zn or Ag metal. A trityl radical ($Ph_3C^{\bullet}$) mostly exists in the dimeric form and a small percentage of the monomeric radical form is in equilibrium with its dimer. Seven decades later the molecular structure of $Ph_3C^{\bullet}$ analogues were studied and confirmed by X-ray single crystal diffraction. The chemists then tried to understand and unlock the hidden mystery behind the unusual stability of such open shell species. Finally, it has been concluded that substitution with six chlorine atoms (at the 2,6-position of each phenyl ring) is enough to make this class of radicals to be stable in air. Radicals are mostly stabilized by the steric effect preventing them from taking part in further chemical processes such as dimerization and proton abstraction. A large number of chemical[2,3] and biological[4] procedures are functioning *via* radical pathways.[2–4] Radicals play crucial roles in our daily biological systems to laboratory chemical processes. A large number of radical species have been even found in the interstellar atmosphere such as methylidyne ($^{\bullet}CH$), ethynyl radical ($^{\bullet}C_2H$), methylene diradical ($^{\bullet\bullet}CH_2$), amino radical ($^{\bullet}NH_2$), formyl radical ($HCO^{\bullet}$), hydroxyl radical ($^{\bullet}OH$), and cyanogen radical ($^{\bullet}CN$). They could not combine with each other due to the very low density of the interstellar medium.

In general most of the radicals are short-lived species.[1h,5] The lifetimes of some radicals are extremely short and thus they cannot be even characterized by electron paramagnetic resonance (EPR) measurements. Radicals having relatively longer lifetimes can be studied by EPR spectroscopy at low temperatures. The instability of the unstable radicals arises mainly from their high reactivity due to thermodynamic and kinetic reasons. Highly reactive radicals are prone to undergo dimerization, polymerization, bond activation, fragmentation or atom abstraction from solvents, *etc.* The radicals are mainly divided into two categories, *viz.* persistent radicals[5] and stable radicals. The former have sufficiently long lifetimes and can be characterized in solution by EPR. The persistent radicals cannot be isolated in a pure form, while the stable radicals are isolable and storable even at room temperature (rt).[1h,5] Stable radicals can be structurally characterized by X-ray single crystal diffraction.[6] They are utilized in many areas of chemistry for different means. They can catalyse polymerization reactions and hence are of huge interest in polymer chemistry.[7] They have been combined with metal salts for oxidation of alcohols to the corresponding aldehydes.[8] Stable radicals have often been used for trapping unstable radical intermediates in organic and inorganic chemical transformations.[9] When radicals are combined with anisotropic metal ions at the molecular level, the composite can act as single molecule magnets (SMMs)[10] or single chain magnets (SCMs),[11] which are promising candidates for the construction of molecule based electronics.[12] Moreover, radicals have the ability to act as antioxidants.[13]

Herbert W. Roesky

Herbert W. Roesky obtained his doctorate from University of Göttingen. After working at Du Pont in the United States, he returned to Göttingen and finished his habilitation. Then he became a professor at the Johann-Wolfgang-Goethe-Universität, Frankfurt am Main in 1971. He moved to the University of Göttingen in 1980 and was the director of the Institute for Inorganic Chemistry until 2004. He is primarily known for his pioneering work on fluorides of both transition and main group elements. His current research interest is focused on the synthesis and reactivity of compounds with heavier group 13 and 14 elements in low oxidation states. More than 1250 peer-reviewed papers, articles, patents, and books record his research activities in the areas of Inorganic Chemistry and Material sciences.

Monoradical, biradical, diradical and diradicaloid

Monoradical

An atom or a functional group or a molecule containing an unpaired electron is called a monoradical. A free electron has a spin quantum number $S = 1/2$ and further possesses an electric charge. An electron has a magnetic momentum with magnetic components $m_s = +1/2$ and $m_s = -1/2$ which are energetically degenerate in the absence of a magnetic field. However, the degeneracy is lifted when an external magnetic field (H) is applied in a certain direction. The magnetic moment of an electron can align itself either parallel ($m_s = -1/2$, β spin) or antiparallel ($m_s = +1/2$, α spin) to the direction of the applied magnetic field (Fig. 1a).

The spin multiplicity ($2S + 1$) of monoradicals is two and hence they are also called doublet species. Two fine energy states (β and α) of a monoradical are split into well resolved energy states (by the Zeeman effect) and their separation is proportional to the strength of the applied magnetic field (H). These energies (E_α and E_β) are calculated by the equation of $E = m_s g_e \mu_e H$, where g_e is the so-called g factor ($g_e = 2.0023$ for a free electron), and μ_e is the Bohr magnetron (9.274078×10^{-24} J T^{-1}). The only possible electronic transition is from β → α or β ← α ($\Delta m_s = \pm 1$) for a monoradical. The separation ($\Delta E = E_\alpha - E_\beta$) between two Zeeman energy states (β and α) is given by $\Delta E = g_e \mu_e H$. Electron paramagnetic resonance (EPR) occurs when the frequency (ν) matches the energy $\Delta E = E_\alpha - E_\beta = g_e \mu_e H = h\nu$. In principle a free electron will produce one EPR signal due to $\Delta m_s = \pm 1$ transition. An unpaired electron of an atom or a functional group or a molecule further interacts with the magnetic moment of the spin-active nucleus (if any) to produce

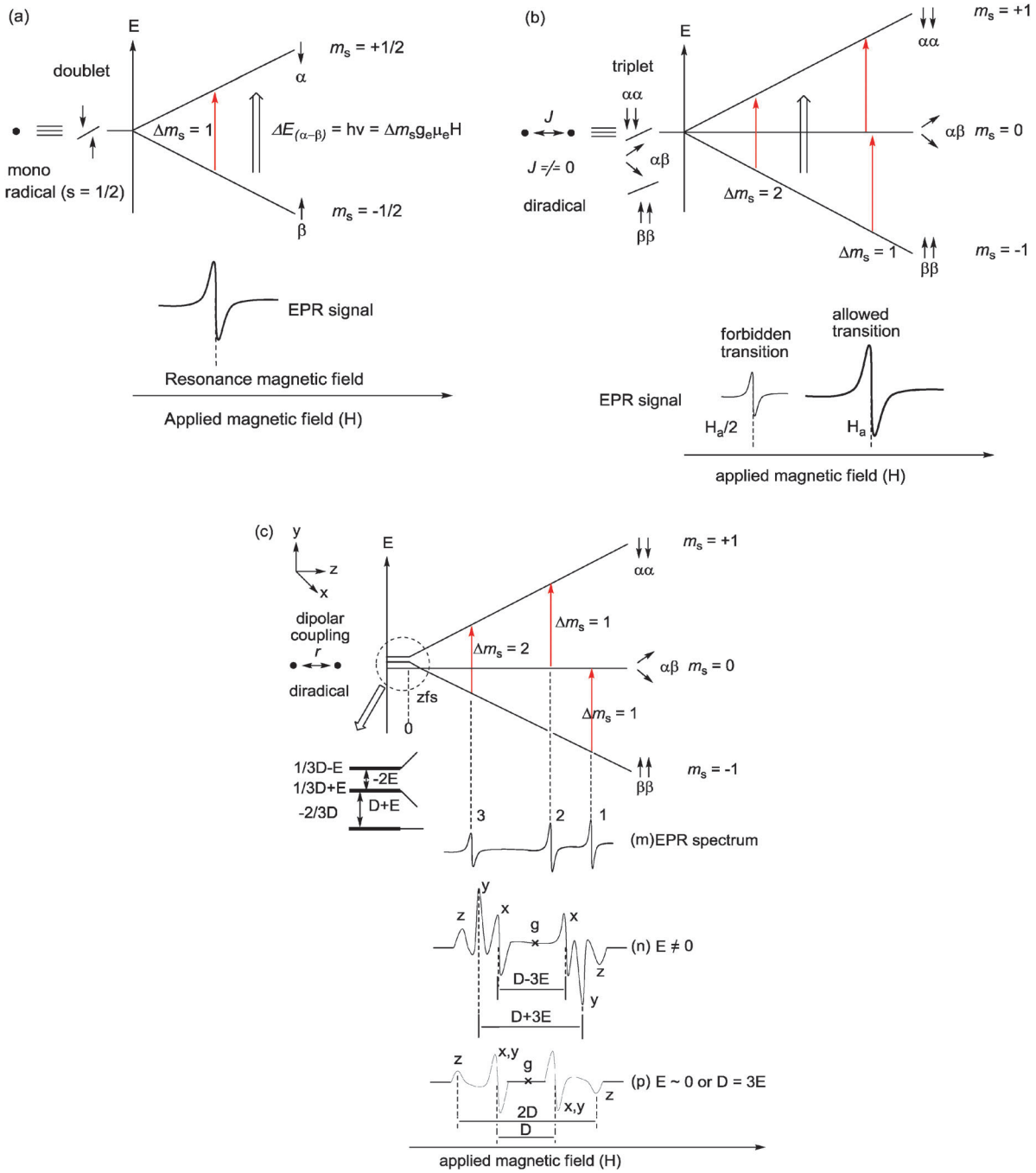

Fig. 1 (a) Zeeman effect on unpaired electrons and the EPR spectrum ($\Delta m_s = \pm 1$ transition) of a free electron, (b) electron-electron interaction in a diradical and EPR resonances ($\Delta m_s = \pm 1$ and ± 2 transitions) and (c) effect of zfs in $S = 1$ ground state.

additional hyperfine line energy states. The satellites will be observed due to the interaction of the nuclear spin with the electron spin. When a radical electron resides on an atom having spin-active nucleus then a number of hyperfine lines can be given by $(2nI + 1)$ [n = number of nucleus and I = spin of that nucleus]. The radical electron can further interact with neighboring nuclei *via* bond or space. In that case, the number of hyperfine lines can be calculated by $(2n_1I_1 + 1)(2n_2I_2 + 1)\ldots$ and so on. A radical electron in general couples with its own nucleus (on which it is localized) more strongly than to its neighboring nuclei and thus might have a higher hyperfine coupling constant for its own nucleus than those of neighboring nuclei. It might not be always the case. However, the magnitude of the hyperfine coupling constants is expected to decrease with decreasing spin density due to radical electrons (if all these nuclei are identical). It also depends upon the spin density of that atom as well as the particular element (isotope). EPR coupling constants of some nuclei are frequently large due to the high nuclear magnetic moment, not necessarily reflecting very large spin densities. Often it occurs that the magnitudes of

hyperfine coupling constants of different atomic nuclei are close to each other and the hyperfine lines appear in similar regions leading to less number of hyperfine lines than one can expect from the above mentioned formula.

Biradical and diradical

When two unpaired electrons (radicals) of a molecule interact with each other, the molecule is termed a biradical[14a] or diradical (open-shell molecule).[1d,h,14b] In general the shorter the distance between two radical centers, the stronger is the interaction. For biradicals the electron exchange interaction (J) between the two unpaired electrons is negligible or nearly negligible ($J \approx 0$) due to the long distance (r) between them.[1a] Biradicals are like two doublets within the same molecule. The stronger electron dipole–dipole interactions lead to two classical situations; (1) both spins align in the same direction ($\uparrow\uparrow$; $S = 1$, $2S + 1 = 3$; triplet) in a triplet diradical or (2) two spins are directed opposite to each other ($\uparrow\downarrow$; $S = 0$, $2S + 1 = 1$; singlet) in a singlet diradical (Fig. 1b). Two electrons occupy two separate orbitals in both the ground state triplet diradical and singlet diradical. For example, molecular oxygen (O_2) has a triplet ground state since two electrons occupy a double degenerated π*-orbital ($\uparrow\uparrow$). The strength of the exchange interaction is evaluated in terms of J which is positive for a triplet diradical and negative for a single diradical. The exchange interaction between two electrons in a (non radical) closed-shell singlet molecule is negative and extremely high in magnitude. Both the electrons occupy the same orbital with opposite spin in a closed-shell singlet molecule. For example, the exchange interactions between two π-electrons of an ethylene ($H_2C{=}CH_2$) molecule are extremely negative and hence they eventually form a π-bond between two p_z-orbitals of each CH_2 group. Both the CH_2 groups of ethylene are in the same plane and thus it does not have radical character. Ethylene has a singlet ground state (with $S = 0$). The radical character can be induced in an ethylene molecule if the CH_2 groups are twisted around each other making the overlap between two p_z orbitals weaker. When the twisting angle reaches 90°, the orbital overlaping between two p_z-orbitals becomes negligible and the molecule attains a diradical ground state. Such an electronic state is not the ground state of an ethylene molecule rather an excited state.

The through-space exchange interaction (J) between the two radical spins can be experimentally studied by the electron paramagnetic resonance (EPR) spectroscopic analysis using stable radicals (Fig. 1b). For example, when the two carbon centered radicals [R_2N–$C^{\bullet}(R_2)$] in a molecule are isolated or separated from each other at a large distance, three hyperfine line signals ($2nI + 1 = 2 \times 1 \times 1 + 1 = 3$) will be typically observed from the coupling of the electron with a nitrogen nucleus (^{14}N; $I = 1$), appearing in the EPR spectrum (for biradical). Additionally, satellites with low intensity are observed due to coupling of the radical electron with the ^{13}C nucleus ($I = 1/2$). Thus, interaction between the two spins is negligible. When the J value is large enough ($J \gg \alpha(^{14}N)$) due to the short distance (r), five hyperfine line signals ($2 \times 2I + 1 = 5$) will be observed with additional satellites in the EPR spectrum (for a diradical).

Diradicals can be divided into two categories; localized and delocalized diradicals. Delocalized diradicals have been even divided into Kekulé and non-Kekulé molecules. Antiaromatic molecules can be regarded as delocalized diradicals.

The singlet diradicals ($\uparrow\downarrow$; $S = 0$, $2S + 1 = 1$; singlet) do not have a net magnetic moment and hence they are diamagnetic and are EPR silent. If a molecule with a singlet diradical character has a low lying triplet (excited state) state which can be fractionally populated, then such a molecule can show EPR signals. The temperature dependent intensity of the EPR signal can be used to predict the nature of the ground state. The intensity of the signal will decrease with decreasing temperature due to depopulation of the low lying excited state (magnetic) and population of the diamagnetic ground state. This is typically the case when J is negative (antiferromagnetic exchange interaction or dipole–dipole interaction) for a diradical. When J is positive, the triplet ($S = 1$) is the ground state and hence the intensity of the EPR signal will increase with decreasing temperature due to the population of the $S = 1$ spin state. If the singlet and triplet states of a diradical are thermally activated, a similar effect can be studied by measuring the temperature dependent magnetic susceptibility. The product (χT) of magnetic susceptibility (χ) and T will decrease when J is negative and will increase for a positive J value. The value of J and $\Delta E_{\text{singlet–triplet}}$ by fitting the χT *vs.* T plot by two interacting $S = 1/2$ spin models. The effect will not be clearly reflected on the χT *vs.* T plot if the population–depopulation effect is negligible. The EPR is more informative than magnetic susceptibility measurements when the electronic interactions at the fine levels are concerned.

For a monoradical one set of EPR resonance [due to allowed ($\Delta m_s = \pm 1$) transition only (Fig. 1a)] is obtained while two sets of EPR signals are a triplet diradical [due to both allowed ($\Delta m_s = \pm 1$; $m_s = -1 \rightarrow 0$ and $0 \rightarrow +1$) and forbidden ($\Delta m_s = \pm 2$; $m_s = +1 \rightarrow -1$ and $m_s = -1 \rightarrow +1$) transitions] (Fig. 1b). When three energy levels are degenerate under zero applied magnetic field, two resonances (Fig. 1b) are observed for a triplet diradical.

The dipolar coupling between two electronic spins in triplet diradicals produces an internal magnetic field which splits the energy level into three levels under zero applied magnetic fields. Three resonance absorptions are obtained for triplet states in a rigid solid state (Fig. 1c; m). Two resonances (signal-1 and signal-2; Fig. 1c) are observed due to $\Delta m_s = \pm 1$ transition while third resonance (signal-3; Fig. 1c) is originated due to $\Delta m_s = \pm 2$ transition (half-field signal). This suggests that the three energy levels (as shown in Fig. 1c) are not energetically degenerate even when the external magnetic field is switched off.

The features of the EPR signal are changed if zero-field splitting (zfs) parameters D and E are introduced in the system. The two zero-field splitting parameters are determined from triplet EPR signals (Fig. 1c; n, p). Two allowed transitions are expected to originate as six lines for a genuine triplet species because of the three magnetic axes of x, y, and z (Fig. 1c; n).

The zero-field splitting is derived from the dipole–dipole interaction and D is related to the distance r between the two unpaired electrons. The value of D can be used to calculate the

average distance r between the two unpaired electrons by the point-dipole approximation;[14c,d] $D = 1.39 \times 10^4 (G/r^3)$. D is given in Gauss (G), and r is in angstroms (Å). The distance (<10 Å) between two spins can be determined from the above mentioned relation and can be correlated with the experimental distance. When the distance between the two spin centers is greater than 10 Å, the signal intensity corresponding to the forbidden transition ($\Delta m_s = \pm 2$) becomes extremely weak or vanishes. The resonance signal of $\Delta m_s = \pm 2$ might be absent when the D value is small ($D < 25$ G). Thus, detection of the EPR signal due to forbidden transition ($\Delta m_s = \pm 2$) can confirm the genuine triplet state of a diradical species.

The zfs parameter E is significantly related to the symmetry of two electrons in a triplet species. Two triplet sublevels of E_x and E_y are degenerate for a molecular structure with 3-fold or higher symmetry. Consequently, the EPR signal of the allowed transitions (signal-1 and signal-2) will look like as shown in Fig. 1c, p and the numerical value of D can be evaluated.

It also has been established that, at short distances or in delocalized systems, the validity of the point-dipole approximation is not good enough for correlating the D value with the inter spin–spin distance (r).[14e,f] When the two electronic spins have a large separation with a small D value, the half-field signal ($\Delta m_s = \pm 2$) might not be observed. Thus, it is not easy to unambiguously distinguish between triplet and doublet signals using continuous-wave (cw) EPR spectroscopy. In that case measurement of the two-dimensional electron spin transient nutation (2D-ESTN) utilizing a pulsed EPR spectrometer is a powerful tool for the determination of the spin multiplicity of high-spin molecules. The nutation frequency (ω_{NT}) depends on the spin-quantum number S by the equation $\omega_{NT} = [S(S+1) - m_s(m_s-)]^{1/2}\omega_1$, where ω_1 is the strength of the magnetic field of the microwave irradiation field.[14g]

Other than EPR, negative-ion photoelectron spectroscopy (NIPES) is a useful method for studying the physical properties of highly reactive intermediates. A beam of mass-selected negative ions (R−) is intersected with an intense laser beam in gas-phase experiments. When a photodetachement of an electron occurs, a neutral reactive intermediate is generated. The plot of the number of photodetached electrons as a function of electron binding energy gives the electron affinity and energies of the electronic states of the neutral intermediate. Additional quantum chemical calculations combined with experimental results gives important information on the structure and electronic configuration of the intermediate species. The photoelectron spectrum of the negative anion of an open-shell molecule provides valuable information on the $E_{singlet-triplet}$ energy gap. A radical anion yields both singlet and triplet states of the neutral open-shell molecules in the photoelectron spectrum and hence the $E_{singlet-triplet}$ energy gap can be experimentally obtained.[14h]

Diradicaloid

When the electronic interactions between two radical centers within a molecule are very strong they are called diradicals. Singlet diradicals generally exhibit a relatively small energy gap between their lowest energy singlet and triplet states. The stability of diradicals is increased with the increasing HOMO–LUMO energy gap which leads to a larger singlet–triplet separation. When the value of occupation of the LUMO of the molecule reaches zero, they are rationalized as closed-shell molecules. Thus they are not referred to as diradicals or diradicaloids. However, the occupation of the LUMO is not negligible for diradicaloids[14i] due to the small HOMO–LUMO energy gap. Diradicaloids are comparatively more reactive than closed-shell molecules.[14j]

There are several theoretical methods[15] for computational studies of radicals, diradicals and diradicaloids. The $E_{singlet-triplet}$ can be also theoretically calculated. There are some limitations of different levels of theories. However, they are extremely helpful to study bond and spin density distribution of these species.

In this review, we will first discuss the effect of bulky organic ligands on the stabilization of several silicon centered stable radicals and radical ions and then we will focus on how π-accepting cyclic alkyl(amino) carbenes (cAACs) can be utilized as neutral mono-dentate ligands for the stabilization of radicals, radical ions, diradicals, and diradicaloid species. We will also highlight some of the radicals and radical ions which have been stabilized by σ-donating N-heterocyclic carbenes (NHCs). The stability and bonding of those compounds will also be discussed.

Results and discussion

Silicon being the sister element of carbon has attracted huge research interest for the past four decades. The syntheses and characterization of several silicon containing compounds have been reported so far.[15–30] However, radicals containing the silicon functional group are limited in number.[30] Silicon centered radicals known as silyl radicals are the open shell species bearing an unpaired electron on the silicon atom. They act as reactive intermediates in numerous organometallic transformations and their existence have long been speculated through spectroscopic characterization.[31] Although, persistent silyl radicals stabilized by bulky groups[32] have been reported almost three and a half decades ago, it was only in 2001 when stable and isolable silyl radicals were successfully synthesized for the first time by Sekiguchi *et al.*[33] (Scheme 1, top). In their report, initially the precursor cyclotetrasilenylium cation ($\mathbf{1}^+$) was synthesized by reacting tetrakis[di-*tert*-butyl-(methyl)silyl]cyclotrisilene with $[Et_3Si(benzene)]^+TPFPB^-$ (TPFPB$^-$ = tetrakis(pentafluorophenyl) borate).[34] The successive one electron reduction of $\mathbf{1}^+$ at room temperature (rt) with a bulky trialkylsilylsodium reagent $^tBu_3SiNa$ in diethyl ether resulted in the formation of the first stable cyclotetrasilenyl radical ($\mathbf{1}^\bullet$) in 67% yield.[33]

The same product is also obtained by using KC_8 as the reducing agent with a much increased yield of 83%. X-ray single crystal analysis of $\mathbf{1}^\bullet$ reveals that the four-membered ring in $\mathbf{1}^\bullet$ is nearly planar with a very small dihedral angle of 4.7° between the Si1–Si2–Si3 and Si1–Si4–Si3 planes. This is in marked contrast with the cationic precursor $\mathbf{1}^+$ which has a large corresponding dihedral angle of 46.6°. Although $\mathbf{1}^\bullet$ is best represented as an allyl type radical, the Si1, Si2, and Si3 atoms in it are not exactly symmetrical. While Si1 and Si2 have a planar geometry,

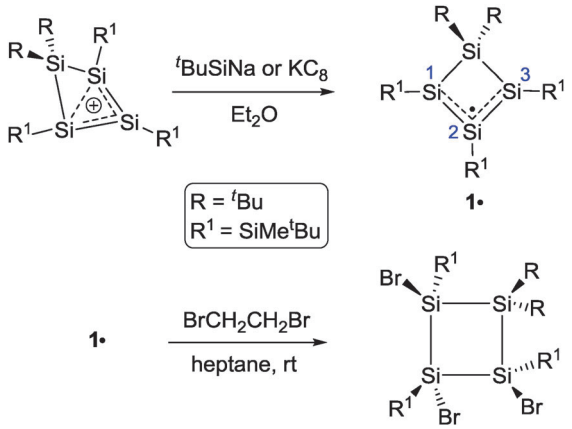

Scheme 1 Synthesis and reactivity of the cyclotetrasilenyl radical (**1•**) (top) and its reaction with $BrCH_2CH_2Br$ (bottom).

the Si3 atom has slightly pyramidal geometry. A similar trend is also observed in the case of the bond lengths. Si1–Si2 [2.226(1) Å] is found to be slightly shorter than Si2–Si3 [2.263(1) Å] and are in-between the Si=Si double bond [2.174(4) Å] and the Si–Si single bond [2.349(4)–2.450(4) Å] found in the previously reported four-membered ring of hexakis-(*tert*-butyldimethylsilyl)cyclotetrasilene.[35] The inter-atomic distance between Si1 and Si3 is found to be [3.225(2) Å] indicating the absence of any 1,3-orbital interaction. The radical character of **1•** is confirmed by the EPR resonances observed both in the solid state and in a dilute *n*-heptane solution of **1•**. The crystalline sample of **1•** exhibits an intense EPR signal with a comparable *g* value of 2.0058 found in the case of the typical tris(trialkylsilyl)silyl radicals (2.0053–2.0063).[31,32] The typical allylic nature of the cyclotetrasilenyl radical is concluded by assigning the larger hyperfine coupling constants (at 40.7 and 37.4 G) to the coupling of the radical electron with the terminal ^{29}Si1 and ^{29}Si3 nuclei and the relatively smaller hyperfine coupling constant (at 15.5 G) to the coupling with the central ^{29}Si2 nucleus. This in turn supports the typical delocalization of the unpaired electron in the allylic radical **1•** over the two terminal silicon atoms. The reactivity of this unprecedented silyl radical is also studied by treating **1•** with 1,2-dibromoethane. The tribrominated product of **1•** is obtained in 79% yield (Scheme 1, bottom).

Soon after the synthesis report of the first silyl radical stabilized by delocalization, the first air stable silyl radical without any π-conjugation is prepared by the same research group.[36] It is the first example of an air stable silyl radical. The straightforward synthesis of this air stable silyl radical follows three consecutive steps. In the first step bis[di-*tert*-butyl-(methyl)-silyl]dibromosilane is reacted with di-*tert*-butyl(methyl)silylsodium in di-ethyl ether at room temperature to *in situ* generate the corresponding intermediate carbene species $[(R^1)_2Si:]$. This upon treatment with another equiv. of the reducing agent produces the corresponding sodium salt of tris[di-*tert*-butyl(methyl)silyl]silyl anion $\mathbf{2^-Na^+}$. The one electron oxidation of the *in situ* generated anion $\mathbf{2^-}$ with germanium(II)dichloride–dioxane complex at room temperature results in the formation of the stable tris[di-*tert*-butyl(methyl)silyl]silyl radical **2•** (Scheme 2) in 44% yield.[36]

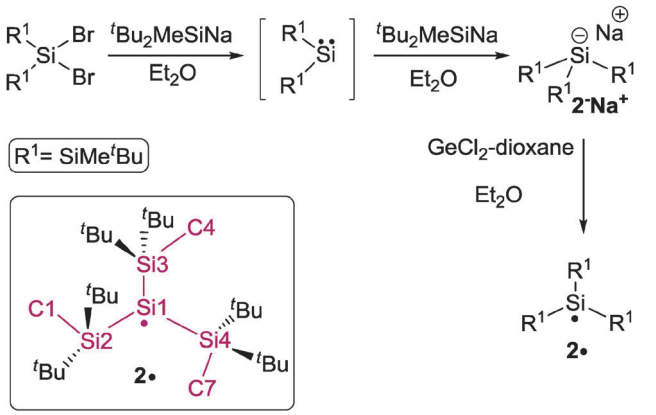

Scheme 2 Synthesis of the tris[di-*tert*-butyl(methyl)silyl]silyl radical (**2•**).

The single crystal X-ray analysis of **2•** reveals that Si1 adopts planar geometry and is surrounded by three bulky electropositive per-silyl substituents (Scheme 2, bottom). The presence of the bulky and electropositive substituents leads to the lowering of the inversion barrier at the Si1 radical center resulting in a planar geometry. All the methyl groups present at Si1–Si4 are found to be arranged in a "gear"-type fashion where the C_{Me} atoms are located in the same plane of Si1–Si2–Si3–Si4 (Scheme 2 and Fig. 2) which could effectively minimize the steric strain of the molecule. This special arrangement without any doubt contributed extra stability by the delocalization of the radical electron over the σ* orbitals of the planar Si–C bonds. The EPR spectroscopy reveals that this specific planar arrangement of radical **2•** is also present in solution.[36] The EPR spectrum of an *n*-hexane solution of **2•** at room temperature exhibits a strong signal with the *g* value of 2.0056 which is comparable to that of a typical persilyl-substituted Si-centered radical (2.0050–2.0063).[32] The two pairs of satellites observed in the EPR spectrum can be attributed to the coupling of the radical electron with the two different sets of ^{29}Si nuclei ($I = 1/2$). The satellites with a larger value of the hyperfine coupling constant [$\alpha(^{29}Si) = 58.0$ G] could be assigned to the coupling of

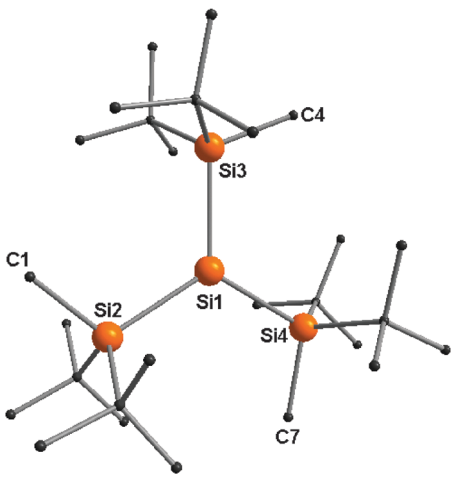

Fig. 2 Molecular structure of the tris[di-*tert*-butyl(methyl)silyl]silyl radical (**2•**).

the radical electron with the central Si1 nucleus, and the satellites with a much smaller hyperfine coupling constant [$\alpha(^{29}Si)$ = 7.9 G] could be assigned to that with the Si atoms of the three substituents (Si2, Si3, and Si4). The small value of the hyperfine coupling constants observed for **2•** signifies that the radical electron resides in an orbital with a higher degree of p-character, predominantly indicating a planar sp^2 hybridized Si-centered π-radical. The highly reactive tris[di-*tert*-butyl(methyl)-silyl]silyl radical (**2•**) produces the corresponding halogenated products in almost quantitative yields upon treatment with carbon tetrachloride, 1,2-dibromoethane, and benzyl bromide.[36]

The *para*- and *meta*-quinodimethane derivatives are well known in the literature as the carbon centered radicals, where the *para*-isomer possesses a singlet ground state with a closed-shell quinoid form[37] and the *meta*-isomer possesses a triplet ground state.[38] The syntheses of the higher analogues of these group 14 compounds with two or more radical centers has been elusive until Sekiguchi *et al.* reported the syntheses and characterization of the isomeric *para*- and *meta*-disilaquinodimethanes in 2011 (Scheme 3).[39]

When the 1,4-bis(bromosilyl)benzene derivative (**3-Br$_2$**) is treated with two equiv. of KC_8 in THF at −78 °C a dark purple solution of 3,6-bis[bis(di-*tert*-butylmethylsilyl)silylidene]cyclohexa-1,4-diene (**3**) is produced (Scheme 3) in 23% yield.

The X-ray single crystal diffraction shows that the Si1 center of **3** adopts a trigonal planar geometry (Fig. 3, top). The co-planarity of the 3p orbital of Si and the 2p orbital C atom of the six-membered aromatic ring suggests an effective π-conjugation between these two orbitals ensuring a closed-shell quinoid structure. The Si1–C1 bond [1.8174(14) Å] is found to be shorter than the typical Si–C_{sp^2} single bond (1.879 Å), but longer than the Si=C bonds (1.702–1.775 Å). The ^{29}Si NMR spectrum of **3** shows the resonances at 91.1 ppm. The bond parameters suggest that **3** features two silicon–carbon double bonds. Compound **3** has a 1,4-quinoid structure with a smaller contribution of a singlet bis(silyl radical) character. The UV-vis absorption band is of **3** observed at 555 nm.

Similarly, when the 1,3-bis(iodosilyl)benzene derivative (**4-I$_2$**) is treated with two equiv. of KC_8 under the comparable reaction condition as employed for the *para*-analogue, light yellow crystals of 1,3-bis[bis(di-*tert*-butylmethylsilyl)silyl]benzene-1′,1″-diyl (**4**) are

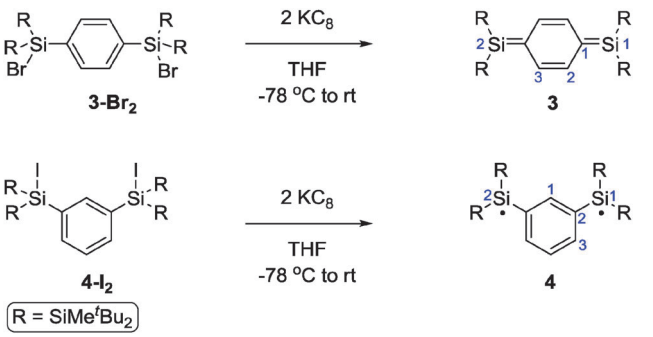

Scheme 3 Synthesis route of disilaquinodimethane (**3**) and bis (silyl radical) (**4**).

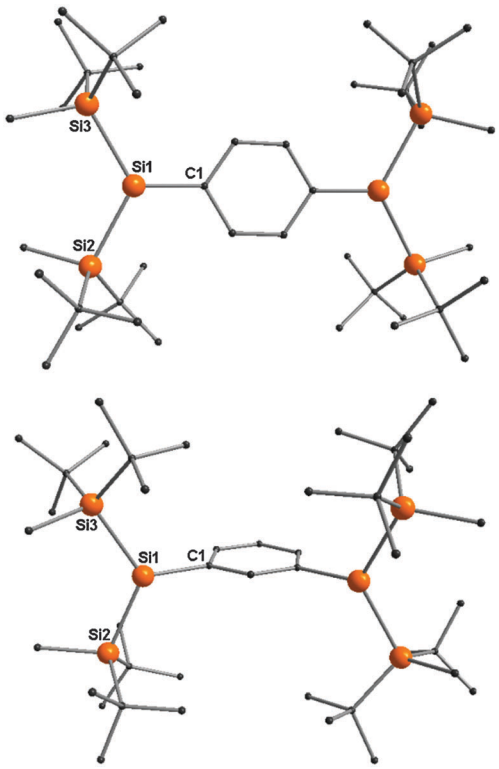

Fig. 3 Molecular structures of the diradicaloid (**3**) (top) and the diradical (**4**) (bottom).

obtained (Scheme 3) in 29% yield. The UV-vis absorption bands are observed at 433 and 413 nm. The single crystal X-ray diffraction of **4** reveals that although the Si1 and Si2 centers attain a near trigonal planar geometry, the Si-3p and C_{aryl}-2p orbitals are orthogonal to each other, hence preventing their overlap. The Si1–C2 and Si2–C2′ bond lengths are found to be 1.9108(19) Å, showing a normal Si–C single bond. The C–C bond distances within the six-membered ring also indicate a typical aromatic ring structure. According to these experimentally obtained bond parameters and the theoretically obtained results, it can be easily concluded that **4** is a *meta*-phenylene bridged bis(silyl radical) (Fig. 3, bottom). Computational studies reveal that the triplet ground state is energetically more favourable than the singlet state by 20 kcal mol^{-1} energy. The EPR spectrum of a solution of **4** in 3-methylpentane at 80 K exhibits the characteristic signal with six hyperfine lines at 3352 G (g = 2.0034) due to allowed ($\Delta m_s = \pm 1$) transition. The zero field splitting parameters are found to be D = 6.4 × 10^{-3} cm^{-1} (at 138 G) and E = 0.80 × 10^{-3} cm^{-1} (at 17.2 G). Considering the point dipole approximation, the calculated distance between the unpaired electrons in **4** is found to be 5.89 Å, which is close to the value (5.72 Å) obtained from the X-ray crystal structure. These values prove that the two unpaired electrons in **4** reside mainly on the two silicon atoms. Another weak signal which appears exactly at the half field 1674 G confirms the triplet diradical ground state of **4** due to forbidden ($\Delta m_s = \pm 2$) transition.

These major structural differences in **3** and **4** are also reflected in their reactivity patterns (Scheme 4). While **3** reacts with both

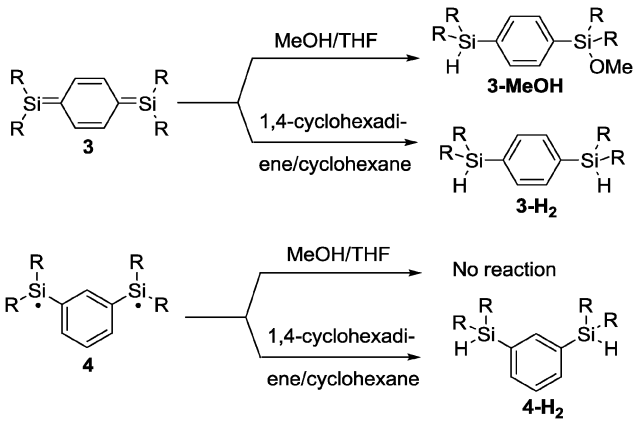

Scheme 4 Reactivity of *para*- and *meta*-[(^{t}Bu$_2$MeSi)$_2$Si]$_2$C$_6$H$_4$ (**3** and **4**) towards MeOH and 1,4-cyclohexadiene.

MeOH, and 1,4-cyclohexadiene to produce quantitatively the desired 1,6-adduct **3-MeOH** and the hydrogen-abstraction product **3-H$_2$**, respectively; **4** fails to react with MeOH which is known as a typical reagent for silence. However, **4** reacts quantitatively with the hydrogen donor 1,4-cyclohexadiene to produce the *m*-bis(hydrosilyl)-benzene **4-H$_2$** indicating its bis(silyl radical) nature.

Disilene and disilyne radical anions

In 2004, Sekiguchi *et al.* reported the synthesis and characterization of a red colored disilene radical anion **5**$^{\bullet-}$ in the form of its lithium salt *via* the one-electron reduction of the dark blue colored tetrakis(di-*tert*-butylmethylsilyl)disilene **5** by ^{t}BuLi (1.2 equiv.) in THF (Scheme 5).[40a]

The X-ray crystal structure analysis of **5**$^{\bullet-}$ reveals a near orthogonal arrangement along the Si1–Si2 bond. The EPR spectrum of a solution of **5**$^{\bullet-}$ in 2-methyltetrahydrofuran is measured at room temperature which exhibits a strong signal (g = 2.0061). Additionally, the pair of satellites observed is corroborated to the coupling of the unpaired electron with the ^{29}Si nuclei having the hyperfine coupling constant of $\alpha(^{29}\mathrm{Si})$ = 24.5 G. This value is half of that observed in the case of the tris(di-*tert*-butylmethylsilyl)silyl radical (58.0 G).[36] Based on these observations, it is assumed that a rapid spin exchange occurs between Si1 and Si2 atoms in the solution. The EPR spectrum measured in the solid state at 120 K exhibits a pair of satellites with a coupling constant of 45 G indicating the suppression of the spin exchange at lower temperature.[40b]

The radical cation **5**$^{\bullet+}$ is obtained *via* abstraction of one electron from compound **5** by trityl cation (Ph_3C^+) in toluene (Scheme 5, bottom). The disilene radical cation **5**$^{\bullet+}$ is isolated as air and moisture sensitive borate [$(C_6F_5)_4B^-$] salt in 65% yield.[40c] It has been characterized by X-ray single crystal diffraction (Fig. 4). The central Si–Si bond length and its twisting angle of neutral **5** are 2.2598(18) Å and 54.5°, respectively while the corresponding values of cation **5**$^{\bullet+}$ are 2.307(2) Å and 64.9°, respectively. This suggests that the Si–Si bond distance increases after one-electron oxidation. The geometry around the Si1 and

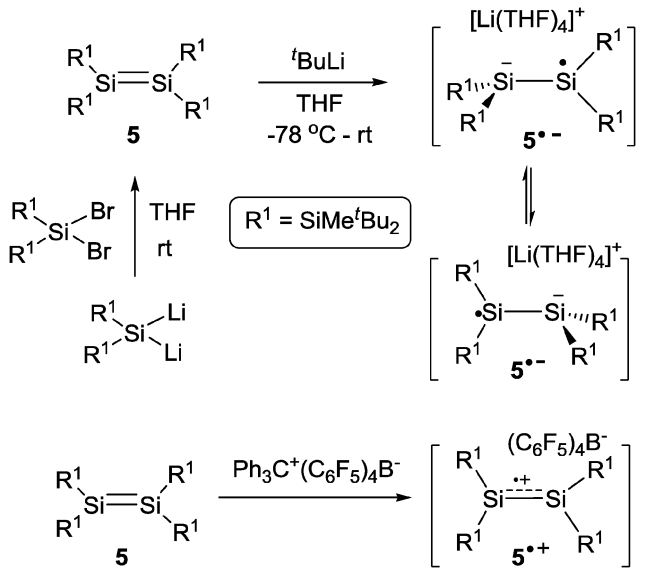

Scheme 5 Synthesis strategy of the tetrakis(di-*tert*-butylmethylsilyl)disilene radical anion (**5**$^{\bullet-}$) (top) and cation (**5**$^{\bullet+}$) (bottom).

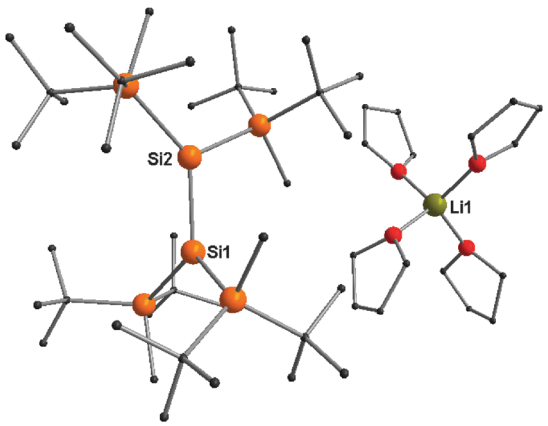

Fig. 4 Molecular structure of the disilene radical anion **[5**$^{\bullet-}$**][Li(OTHF)$_4$]**$^+$.

Si1′ atoms of **5**$^{\bullet+}$ is nearly planar. This is in significant contrast with the disilene radical anion **5**$^{\bullet-}$ with a twisting angle of 88° and the Si–Si bond distance of 2.341(5) Å. The unpaired electron and negative charge in **5**$^{\bullet-}$ cause the bond rotation around the central Si–Si bond (Scheme 4).

The EPR spectrum of **5**$^{\bullet+}$ measured[40c] in the range of 298 to 200 K in fluorobenzene exhibited a resonance at g = 2.0049, having a pair of satellite signals (23.0 G) due to coupling of the unpaired electron with the central ^{29}Si nuclei. This coupling constant is less than half that of the similar (^{t}Bu$_2$MeSi)$_3$Si$^\bullet$ (58.0 G), suggesting the radical electron is delocalized over two silicon centers. In contrast, the radical electron of **5**$^{\bullet-}$[40a] shows a rapid spin exchange between the two central Si atoms on the EPR time scale, featuring a sp^3-silyl anion and a sp^2-silyl radical.

Following a comparable synthesis strategy to that of **5**$^{\bullet-}$, the disilyne radical anion **6**$^{\bullet-}$ with the potassium counter cation[40d] is prepared and characterized by X-ray crystallography and EPR measurements in 2007 (Scheme 6 and Fig. 5).

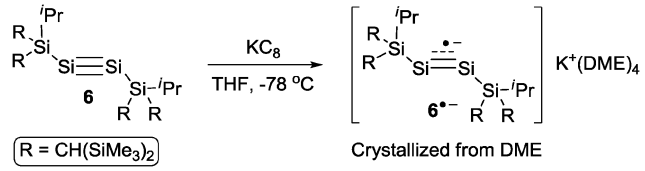

Scheme 6 Synthesis strategy of the disilyne radical anion (**6**$^{\bullet-}$).

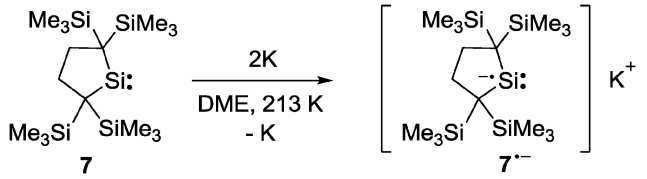

Scheme 7 Generation of the persistent dialkylsilylene radical anion **7**$^{\bullet-}$.

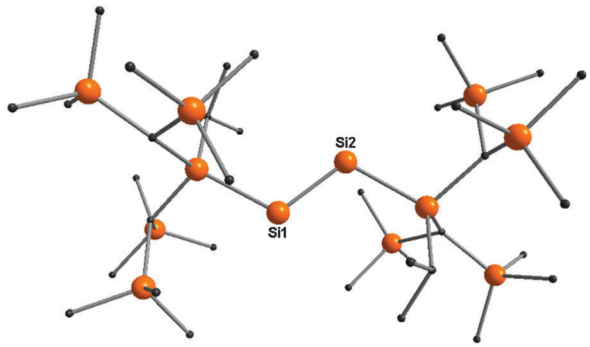

Fig. 5 Molecular structure of the disilyne radical anion **[6**$^{\bullet-}$**][K(DME)$_4$]$^+$**. The cation **[K(DME)$_4$]$^+$** is omitted for clarity.

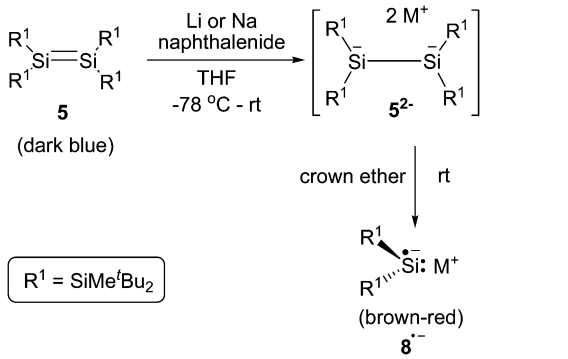

Scheme 8 Generation of the persistent dialkylsilylene radical anion (**8**$^{\bullet-}$).

The reaction of disilyne **6**[30b] containing two bulky substituents, Si^{i}Pr[CH(SiMe$_3$)$_2$]$_2$ groups at the triply bonded silicon atoms with one equiv. of KC_8 in THF at −78 °C results in the formation of the corresponding disilyne radical anion **6**$^{\bullet-}$. It is crystallized from pentane and 1,2-dimethoxyethane (DME) as dark brown crystals in 63% yield. The EPR spectrum of **6**$^{\bullet-}$ exhibits a triplet resonance with two pairs of satellites arising from the coupling with ^{29}Si. The experimentally obtained g value (g = 1.99962) is found to be the smallest for any reported silicon centered radicals till now.[31b]

Silylene radical anions and radical cations

Since early 1970s, the radical ions of carbenes and their analogues have been suggested as the reactive intermediates in redox reactions of diazo compounds both in the liquid and in the gas phases.[41] In recent years, the heavier group 14 analogues of carbenes known as the metallylenes and their corresponding radical ions have attracted huge interest of the scientific community. The isolation and structural characterization of the metallylene radical ions are highly challenging due to their very high reactivity. Although the existence of several group 14 element-centered radical anions R$_2$E:$^{\bullet-}$ (E = Ge, Sn) have been long ago synthesized and characterized by EPR spectroscopy.[42] The characterization of silylene radical anions in solution has not been reported until Kira *et al.* published the synthesis of persistent dialkylsilylene radical anion **7**$^{\bullet-}$ *via* the one electron reduction of 1,2-dilithiodisilane 7 using two equiv. of KC_8 in THF at 213 K (Scheme 7).[43] The EPR spectrum of the *in situ* generated radical anion is recorded at 213 K which reveals its unique structural characteristics. Radical anion **7**$^{\bullet-}$ is stable at −70 °C in DME but decomposes rapidly at room temperature with a half-life time of 20 min.[43]

The first isolable silylene radical anion (**8**$^{\bullet-}$) is reported in 2007[44] by reacting disilene **5** (dark blue) with 2.2 equiv. of lithium naphthalenide in THF at −78 °C and treating the resultant dark red solution with 4.3 equiv. of 12-crown-4 (Scheme 8).

The air and moisture sensitive red crystals of bis(di-*tert*-butylmethylsilyl) silylene radical anion **8**$^{\bullet-}$ are isolated as the corresponding lithium salt in 56% yield (Scheme 8). Mechanistically, the reaction is proposed to proceed *via* the initial formation of the 1,2-dianionic species (^{t}Bu$_2$MeSi)$_2$Si(Li)-Si(Li)-(SiMe^{t}Bu$_2$)$_2$ upon reduction which undergoes dissociation upon further treatment with the crown ether to produce the corresponding radical anion **8**$^{\bullet-}$.[44] The formation of the 1,2-dianionic species can be also established by NMR spectroscopy. The structure of **8**$^{\bullet-}$**Li**$^+$ in the solid state is characterized by X-ray single crystal diffraction. The EPR spectrum of a dilute solution of **8**$^{\bullet-}$**Li**$^+$ in THF shows signals (g = 2.0074) with two sets of satellites due to the coupling with ^{29}Si nuclei. No hyperfine coupling with the lithium atom was observed suggesting the formation of a metal-free silylene radical anion. However, the EPR spectrum of the sodium salt of the radical anion (**8**$^{\bullet-}$**Na**$^+$) in toluene at rt exhibits a well resolved quartet (g = 2.0074) which could be attributed to the coupling with ^{23}Na nucleus (I = 3/2) with a hyperfine coupling constant of $\alpha(^{23}\text{Na})$ = 1.9 G. This indicates the presence of a Si–Na bond in the case of **8**$^{\bullet-}$**Na**$^+$. The two sets of satellite signals observed are due to coupling with the ^{29}Si nuclei. When the EPR spectrum of **8**$^{\bullet-}$**Na**$^+$ is recorded in polar solvents like THF, the quartet signal disappears. This indicates that a shift from the contact ion pair structure to the solvent separated ion-pair structure has occurred due to the polarity of the particular solvent. Detection of a radical cation (diphenylcarbene radical cation) in solution by EPR spectroscopy

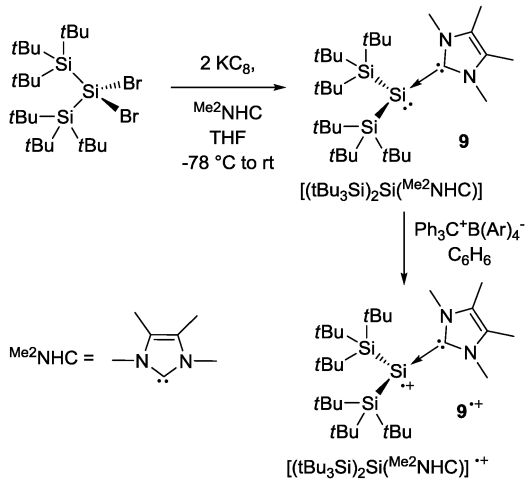

Scheme 9 Synthesis routes of $[(^{t}Bu_3Si)_2Si(^{Me2}NHC)]^{\bullet+}B(Ar)_4^{-}$ ($9^{\bullet+}B(Ar)_4^{-}$).

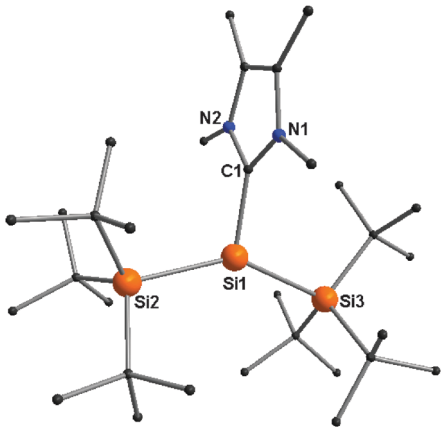

Fig. 6 Molecular structure of $[(^{t}Bu_3Si)_2Si(^{Me2}NHC)]^{\bullet+}B(Ar)_4^{-}$. H-atoms and the $B(Ar)_4^{-}$ group are omitted for clarity.

was first accomplished in 1993.[45] Both the radical anions $7^{\bullet-}$ and $8^{\bullet-}$ are not characterized by X-ray single crystal diffraction due to short lifetimes of former and poor crystalline nature of the later.

The silylene radical cations are rarely characterized. Silylene radical cation $H_2Si^{\bullet+}\cdots H_2$ can be considered as a hydrogen complex of the parent $H_2Si^{\bullet+}$ species.[46] It is generated under neon matrix deposition at 4 K by the photoionization of SiH_4.

In 2012 Sekiguchi *et al.* reported the synthesis of NHC stabilized silylene radical cation $[(^{t}Bu_3Si)_2Si \leftarrow {}^{Me2}NHC]^{\bullet+}(Ar_4B)^{-}$ ($9^{\bullet+}$)(Ar_4B)$^{-}$ (Scheme 9).[47] The dibromosilane $(^{t}Bu_3Si)_2SiBr_2$ is treated with two equiv. of KC_8 in the presence of ^{Me2}NHC in THF. The orange crystals of the silyl substituted silylene–NHC complex $(^{t}Bu_3Si)_2Si: \leftarrow {}^{Me2}NHC$ (**9**) is obtained in 43% yield. When a mixture of **9** and one equiv. of $Ph_3C^{+}Ar_4B^{-}$ (Ar_4B^{-} = tetrakis[4-(*tert*-butyldimethylsilyl)-2,3,5,6-tetrafluorophenyl]-borate) have been reacted stable radical cation $9^{\bullet+}$ is formed in 83% yield.

Cation $9^{\bullet+}$ is structurally characterized by the single crystal X-ray analysis (Fig. 6). The central silicon atom of $9^{\bullet+}$ adopts a planar three coordinate geometry. The five-membered NHC ring and the Si2–Si1–Si3 plane are found to be nearly perpendicular to each other. The Si1–C_{NHC} bond length in $9^{\bullet+}$ is 1.915(3) Å which is slightly shorter than that in precursor **9** [1.933(4) Å]. This indicates an increase in the s character of the Si1–C_{NHC} bond resulting from the change in hybridization of the central silicon atom. The comparatively larger Si1–Si2 and Si1–Si3 bond lengths in $9^{\bullet+}$ [2.4664(11) and 2.4659(10) Å, respectively] than those in **9** [2.4542(15) and 2.4419(14) Å, respectively] can be explained by the steric repulsion between the two extremely bulky $^{t}Bu_3Si$ groups which suppress any bond shortening. The NBO analysis at the level of (U)B3LYP/6-31G(d) for compounds **9** and $9^{\bullet+}$ suggests that an electron is removed from the lone pair of silylene **9** upon oxidation resulting in a change in geometry from the pyramidal to a planar structure in $9^{\bullet+}$. This also shows that the spin density in $9^{\bullet+}$ is mainly located on the tricoordinate silicon atom. The EPR spectrum of a benzene solution of $9^{\bullet+}$ recorded at room temperature exhibits a quintet with a *g* value of 2.00466. The nature of this spectrum can easily be attributed to the coupling of the radical electron with two ^{14}N nuclei ($I = 1$) of the NHC with a hyperfine coupling constant of $\alpha(^{14}N)$ = 2.6 G. The satellite signals with a hyperfine coupling constant of $\alpha(^{29}Si)$ = 71.6 G are observed due to the coupling of the radical electron with the central Si1 nucleus.

Diradicaloids

The organic diradicals are very often too unstable to be isolated.[48a,c] However, there are some examples of stable organic diradicals.[48] Although the heavier congeners of the group 14 element centered diradicals are reported by Lappert[49] and Power[50] in 2004, the syntheses of the analogous silicon compounds remain challenging until 2011. The dark purple colored singlet diradicaloid species RSi(μ-NAr)$_2$SiR (**10**) was first synthesized in 58% yield when the disilyne **6** slowly reacts with *trans*-3,3′,5,5′-tetramethylazobenzene in THF at room temperature under light-shielded conditions. The reaction is faster (complete in 5 min) and the same compound is isolated when **6** is reacted with *cis*-3,3′,5,5′-tetramethylazobenzene. The chemical shift value of the skeletal silicon has been observed at 19.4 ppm. The UV-vis absorption band at 529 nm in *n*-hexane corresponds to its blue color (HOMO−1 → LUMO, HOMO → LUMO). Compound **10** possesses a perfectly planar centrosymmetric four-membered Si_2N_2 ring with both the silicon atoms having a pyramidal geometry (Fig. 7, top). The Si–Si bond length of the Si_2N_2 ring is 2.6380(9) Å which is significantly longer than a normal Si–Si single bond length (2.341 Å). Theoretical calculations show that compound **10** has a singlet diradicaloid spin ground state. The singlet–triplet energy gap is 12.8 kcal mol^{-1}. The calculated frontier orbitals of **10** include the four π-orbitals with six π-electrons in the cyclic Si_2N_2 ring corresponding to 6π-aromatic character. The HOMO is generated by a non-bonding combination of silicon centered radical electrons. The HOMO−1 and LUMO correspond to the bonding and antibonding π-orbitals, respectively of the four-membered Si_2N_2 ring.

Carbon tetrachloride is well known as a silyl radical scavenger. Compound **10** also reacts with CCl_4 to give the colorless dichlorinated *trans*-product **10-Cl$_2$** in 55% yield. **10** also reacts with

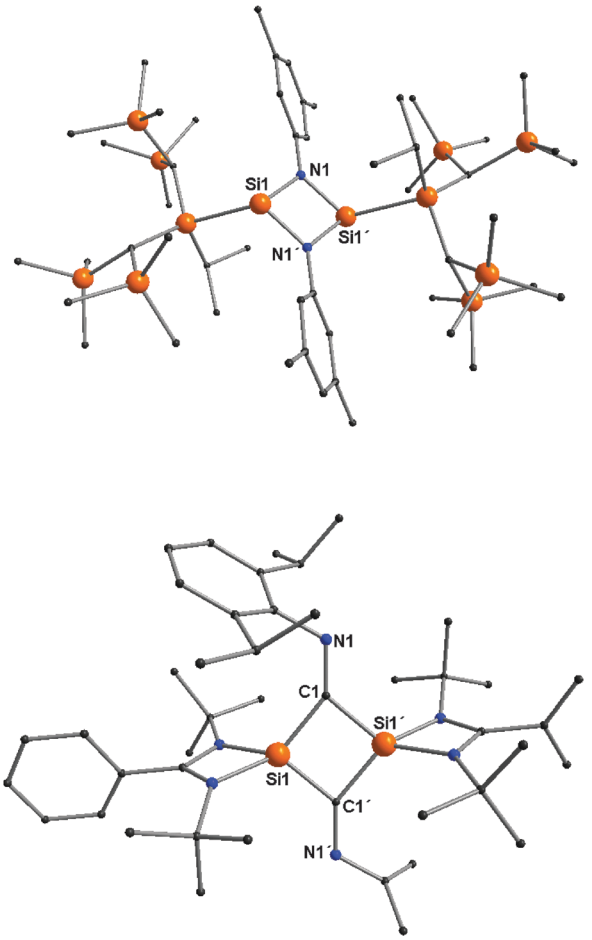

Fig. 7 Molecular structures of diradicaloid **10** (top) and LSi{μ-C(N-Dipp)}$_2$SiL (**11**) (bottom).

methanol to produce the corresponding *cis*-product **10-MeOH** in 65% yield (Scheme 10). Both of these reactions confirmed the 1,3-diradical character of **10**.[51]

The bis-silylene LSi–SiL [L = PhC(N-^{t}Bu)$_2$] reacts with Dipp-N=N-Dipp [Dipp = 2,6-diisopropylphenyl] to produce the yellow-brown crystals of diradical LSi{μ-C(N-Dipp)}$_2$SiL (**11**) in 25.7% yield (Scheme 11 and Fig. 7, top).

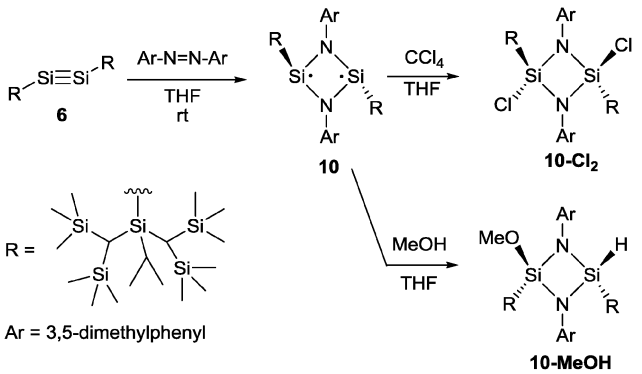

Scheme 10 Synthesis routes of diradicaloid **10** and its reaction with CCl_4 and MeOH.

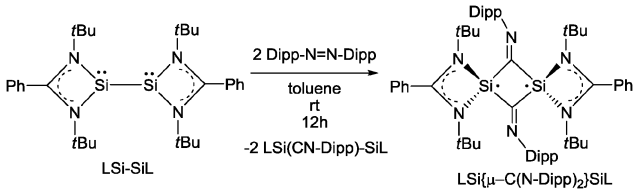

Scheme 11 Synthesis route of LSi{μ-C(N-Dipp)}$_2$SiL (**11**) from LSi-SiL.

The resonance of ^{29}Si NMR is observed as a singlet at −39.9 ppm. Theoretical calculations show that the singlet is the ground state of LSi{μ-C(N-Dipp)}$_2$SiL (**11**) while the triplet state is 30.1 kcal mol^{-1} higher in energy. The radical electrons are delocalized in the four-membered Si_2C_2 ring (Fig. 7, bottom) and additionally conjugated with two central exo-cyclic C=N double bonds. The Si–Si bond length is 2.553(2) Å which is significantly larger than that of the precursor LSi–SiL (2.413(2) Å).[52]

cAAC–silicon compounds

Stable singlet N-heterocyclic carbene (NHC)[26] has been synthesized and isolated as a storable crystalline solid in 1991. The strong σ-donor ability of NHCs as ligands was slowly realized by the chemists. The low coordinate $(Si)_2Cl_2$ and Si_2 species have been successfully trapped by two ^{IP}NHCs [^{IP}NHC = :C{N(2,6-i$Pr_2C_6H_3$)(CH)}$_2$].[27] ^{IP}NHC can also stabilize dichlorosilylene ($SiCl_2$) in the form of (^{IP}NHC)$SiCl_2$.[28] NHCs are employed as ligands for the stabilization of several unusual main group species in different oxidation states. Over the last two decades NHCs are utilized as efficient ligands in different areas of chemistry.[29]

Bertrand *et al.* have isolated cyclic alkyl(amino) carbenes (cAACs) in 2005.[53] The carbene carbon atom of NHC is bound to two σ-withdrawing and two π-donating N-atoms while one N-atom is replaced by one σ-donating quaternary C-atom in a cAAC. The HOMO of cAAC is little higher in energy and and the LUMO of cAACs is slightly lower in energy than those of NHCs. The HOMO–LUMO energy gap is smaller in cAAC when compared with that of NHC (Fig. 8).[54] As a result cAACs are stronger σ-donors and better π-acceptors than those of NHCs. This has been experimentally established by ^{31}PNMR chemical shifts[55] of carbene–phosphinidene adducts. cAACs are different in certain respects and thus can activate very strong bonds (*e.g.*, H–H, H–NH_2, *etc.*) which are not achievable when NHCs are employed instead of cAACs.[56] The cAAC has been utilized for the stabilization of several radical species of main group elements.[1g]

The unstable species dichlorosilylene ($SiCl_2$)[16a] is usually generated under the elimination of HCl from trichlorosilane ($HSiCl_3$) in the presence of a base (such as R_3N). It is stable in the monomeric form at low temperatures (< −50 °C). However, $SiCl_2$ cannot be isolated and stored at room temperature in its monomeric form, since it undergoes polymerization to produce polychlorosilane on increasing the temperature of the solution. ^{IP}NHC [^{IP}NHC = :C{N(2,6-^{i}$Pr_2C_6H_3$)(CH)}$_2$] behaves as a strong σ-donor ligand and a base as well. ^{IP}NHC reacts with $HSiCl_3$ in a 1 : 1 molar ratio to generate $SiCl_2$ species under the elimination of ^{IP}NHC·HCl. The light yellow crystalline powder of ^{IP}NHC

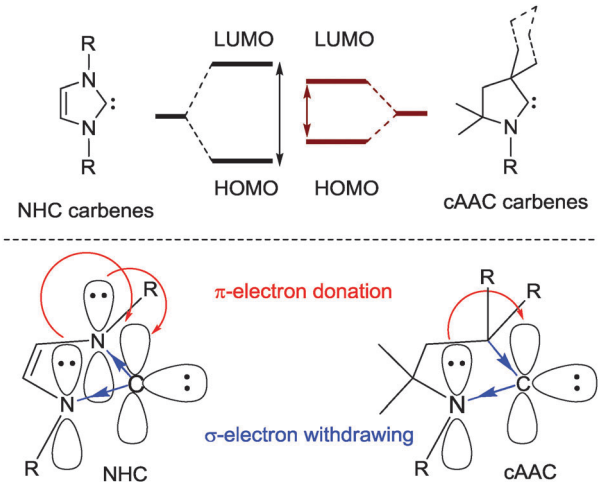

Fig. 8 Comparison between NHC (left) and cAAC (right) carbenes.

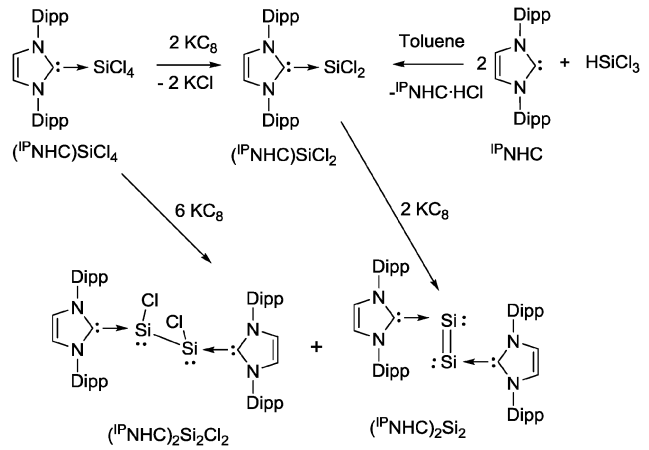

Scheme 12 Synthesis routes of (^{IP}NHC)SiCl$_2$, (^{IP}NHC)$_2$Si$_2$Cl$_2$ and (^{IP}NHC)$_2$Si$_2$.

anchored (^{IP}NHC)SiCl$_2$[28] (Scheme 12) is isolated as the air and moisture sensitive compound in 75% yield if the reaction of ^{IP}NHC and HSiCl$_3$ is carried out in a 2 : 1 molar ratio in toluene. (^{IP}NHC)SiCl$_2$ is completely soluble in toluene but partially soluble in *n*-hexane and tetrahydrofuran (THF).

The cyclic alkyl amino carbene (cAAC) is expected to substitute ^{IP}NHC from (^{IP}NHC)SiCl$_2$ since cAAC is a slightly stronger σ-donor and considerably a better π-acceptor. A dark blue solution is obtained on addition of THF to the 1 : 1 molar mixture of cAAC and (^{IP}NHC)SiCl$_2$ at rt. The X-ray single crystal diffraction on the dark blue blocks, reveals the composition of the compound as (cAAC$^{\bullet}$)$_2$SiCl$_2$ (Scheme 13).[57] The yield of (cAAC$^{\bullet}$)$_2$SiCl$_2$ is increased from 35% to 78% and 91% when the molar ratio of cAAC and (^{IP}NHC)SiCl$_2$ is increased to 2 : 1 and 3 : 1, respectively. The third equivalent of cAAC is required to form (cAACH)(^{IP}NHC) carbene as a side product under C–H functionalization of the five-membered ring of ^{IP}NHC.

(Me$_2$-cAAC$^{\bullet}$)$_2$SiCl$_2$ exists in two polymorphs (-I and -II). The polymorph-II is experimentally found to be the major conformer.[57]

Both the polymorphs are characterized by X-ray structural analysis and showed only small differences (Fig. 9, bottom).

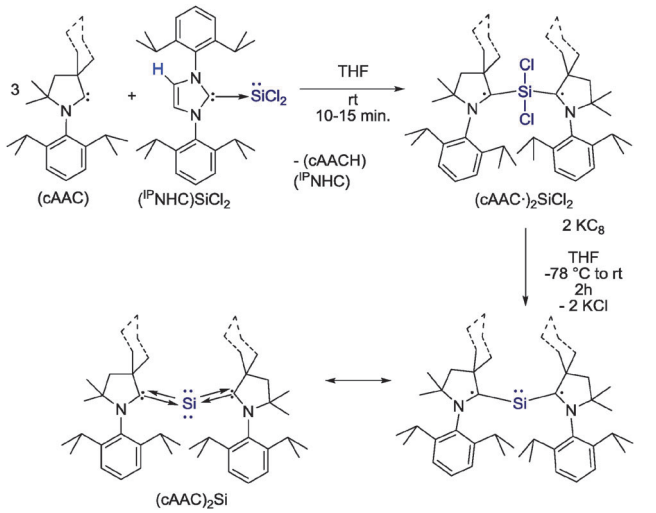

Scheme 13 Synthesis routes of (cAAC$^{\bullet}$)$_2$SiCl$_2$ and (cAAC)$_2$Si. [cAAC = Me$_2$-cAAC and Cy-cAAC].

The central silicon atom of (Me$_2$-cAAC$^{\bullet}$)$_2$SiCl$_2$ is bound to two chlorine atoms and two carbene carbon atoms to adopt a near tetrahedral coordination geometry (Fig. 9).[57] In contrast, the silicon atom of (^{IP}NHC)SiCl$_2$ features trigonal pyramidal geometry at the three-fold coordinate silicon atom.[28] The silicon atom of (^{IP}NHC)SiCl$_2$ possesses a lone pair of electrons which is

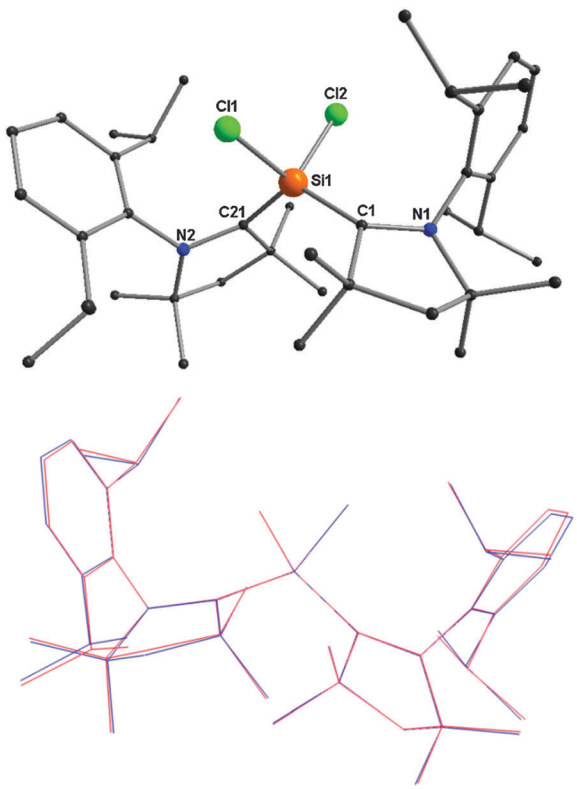

Fig. 9 Molecular structure of polymorph-I of (Me$_2$-cAACμ)$_2$SiCl$_2$ (top). An overlap picture (bottom) of polymorph-I and polymorph-II. Reproduced from ref. 57 with permission of John Wiley and Sons. Color version courtesy of Prof. G. Frenking.

available for the coordination to acceptors.[16a] The C_{cAAC}–Si bond lengths (~1.8455(16)–184.82(17) Å) in $(Me_2\text{-cAAC}^{\bullet})_2SiCl_2$ are shorter by 0.14 Å when compared to that of $(^{IP}NHC)SiCl_2$ (1.985(4) Å).[28] The Si–C bonds in $(Me_2\text{-cAAC})_2SiCl_2$ are even shorter than Si–C_{aryl} single bonds (1.879 Å)[25] but slightly longer than Si–C bonds (1.8174(14) Å) of 3,6-bis[bis(di-*tert*-butylmethylsilyl)silylidene]cyclohexa-1,4-diene and much longer than Si=C double bonds (1.702–1.775 Å).[25] The C_{cAAC}–N bond distances are 1.3994(19) and 1.395(2) Å, respectively and larger than those found in the similar free carbenes (~1.315 Å).[53] Combined valence bond electron count and coordination geometry of the central silicon atom of $(cAAC^{\bullet})_2SiCl_2$ leads to an initial impression that it might be a diradical with one unpaired electron on each carbene carbon atom of cAAC.

Theoretical calculations show that the distributions of spin density of the unpaired electrons are mainly located at the C_{cAAC} of Me_2-cAAC ligands and to a minor extent at the nitrogen atoms and to a negligible extent at the central silicon atom. The bonding situations in $(Me_2\text{-cAAC}^{\bullet})_2SiCl_2$[57] and $(^{IP}NHC)SiCl_2$[28] are quite different. The C→Si bond in the NHC complex $(^{IP}NHC)SiCl_2$ comes from the donation of the carbene lone-pair orbital into the vacant acceptor orbital of $SiCl_2$ (Scheme 14). In contrast, the C–Si bonds in $(Me_2\text{-cAAC}^{\bullet})_2SiCl_2$ are electron-sharing bonds between the triplet states of $SiCl_2$ and the ligands Me_2-cAAC where the unpaired electrons in the singly occupied σ orbitals of the carbene carbon atoms couple with the unpaired electrons of $SiCl_2$ (Scheme 14).[57] There remains one unpaired electron at each of the carbene carbon atoms of the ligand Me_2-cAAC, which couples with the nitrogen lone pair orbital. This explains why there is some spin density at nitrogen as well.[57]

The singlet–triplet energy difference in $(Me_2\text{-cAAC}^{\bullet})_2SiCl_2$ has been computed to be different in magnitude and is dependent on the level of theory employed. It is approximately 2.5 to 4.5 kcal mol^{-1}. The singlet diradical ground state of $(Me_2\text{-cAAC}^{\bullet})_2SiCl_2$ is more stable than the triplet diradical state. The optimized geometry of $(Me_2\text{-cAAC}^{\bullet})_2SiCl_2$ in the singlet state at the CASSCF(2,2)/SVP level and the wave function shows that the compound is an open-shell singlet species (Fig. 10). The coefficients for the three singlet components are 0.80 (2/0), −0.60 (1/1), and 0.0 (0.2). The preference for singlet diradical ground state suggests that the interactions between the two radical electrons of $(Me_2\text{-cAAC}^{\bullet})_2SiCl_2$ through bond/space is slightly dominant over each other (through-bond and through-space communication).[57]

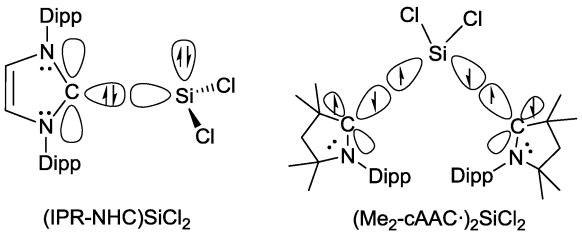

Scheme 14 Schematic representation of donor-acceptor bonding in the precursor $(^{IP}NHC)SiCl_2$ (left) and electron-sharing bonding in the product $(Me_2\text{-cAAC}^{\bullet})_2SiCl_2$ (right).

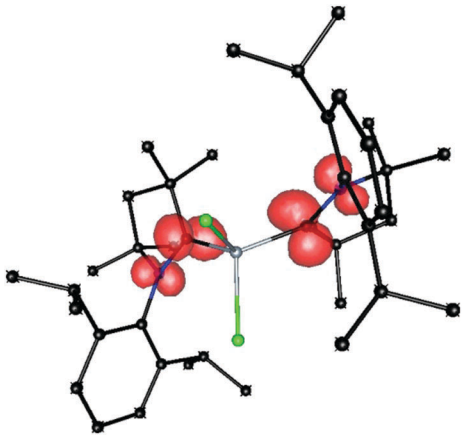

Fig. 10 Calculated (M05-2x/SVP) spin density of $(Me_2\text{-cAAC}^{\bullet})_2SiCl_2$. Reproduced from ref. 57 with permission of John Wiley and Sons. Color version courtesy of Prof. G. Frenking.

The magnetic susceptibility measurements on a polymorph-I rich solid sample of $(Me_2\text{-cAAC}^{\bullet})_2SiCl_2$ show ~16% of paramagnetic contribution and remaining 84% is diamagnetic polymorph-II.[57]

The origin of the EPR signal of polymorph-II of $(Me_2\text{-cAAC}^{\bullet})_2SiCl_2$ is expected from a small percentage of polymorph-I as a minor component, since diamagnetic polymorph-II must be EPR silent. However, a diluted C_6D_6 solution of $(Me_2\text{-cAAC}^{\bullet})_2SiCl_2$ shows six hyperfine lines at room temperature.[57] This pattern suggests that the splitting is due to the coupling with two ^{14}N nuclei ($I = 1$) *via* a dipole–dipole interaction of two coupled radicals and their hyperfine interaction with the closest ^{14}N neighbour nuclei, respectively. The data of the EPR spectrum of polymorph I of $(Me_2\text{-cAAC}^{\bullet})_2SiCl_2$ given in Fig. 11 is fitted with the use of the Easy Spin simulation package considering two different models. Firstly, the EPR spectrum could be simulated as two weakly coupled electrons (two $S_{eff} = 1/2$); each electron interacts with the closest ^{14}N nucleus. Secondly, the effective electronic spin $S_{eff} = 1$ (2 coupled electrons) interacts with two N nuclei. The half field $\Delta m_s = \pm 2$ forbidden transition is not observed either in the solid state or in solution of polymorph-I of $(Me_2\text{-cAAC}^{\bullet})_2SiCl_2$, which excludes a genuine triplet state of polymorph-I which might be due to weak magnetic interactions. Roques *et al.* reported[48b] the exchange in silole-bridged diradicals and most of the compounds

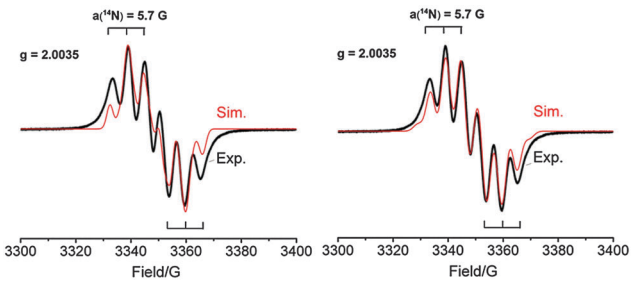

Fig. 11 Experimental EPR spectra (black lines) of C_6D_6 solution of polymorph-I of $(Me_2\text{-cAAC}^{\bullet})_2SiCl_2$. Simulated spectra (red lines); models with two $S_{eff} = 1/2$; (left) and $S_{eff} = 1$ (right). Reproduced from ref. 57 with permission of John Wiley and Sons.

showed $\Delta m_s = \pm 2$ forbidden transitions (characteristic of the triplet). The half-field signal is not observed for the two diradicals of their report even when large signal amplification and high concentrations are used. The magnetic susceptibility measurements showed that more than 50% of molecules[48b] of those diradicals are in their singlet ground states. A similar situation is faced for polymorph I of $(Me_2\text{-cAAC}^{\bullet})_2SiCl_2$.[57]

^{29}Si NMR of $(Me_2\text{-cAAC}^{\bullet})_2SiCl_2$ appears in very low intensity and shows a resonance at 4.13 ppm which is shifted to a high field, when compared with that of the precursor (^{IP}NHC)$SiCl_2$ (19.06 ppm).[57]

The crystalline powders of polymorph-II are isolated in 98.5% yield with a small content of polymorph-I ($\sim$1.5%).[57] It is concluded from the X-ray single crystal diffractions on several batches of the crystals of polymorph-I of $(Me_2\text{-cAAC}^{\bullet})_2SiCl_2$. Blue powders of $(Me_2cAAC^{\bullet})_2SiCl_2$ are stable for more than two years under an inert atmosphere without any decomposition. We have observed that $(Me_2cAAC^{\bullet})_2SiCl_2$ retains its color even when dipping the crystalline powder in a base bath or water for several days. The surface of blue blocks of $(Me_2cAAC^{\bullet})_2SiCl_2$ slowly turns to colorless after 3–4 days and needs more than a week to completely lose the blue color. Similarly, the $(Cy\text{-cAAC}^{\bullet})_2SiCl_2$ compound with comparable bonding and stability has been prepared.[58]

Having $(cAAC^{\bullet})_2SiCl_2$ in hand we envisioned that it could be converted to the corresponding dechlorinated analogue, a siladicarbene $(cAAC)_2Si$. Previously, theoretical calculations on various $(NHC)_2Si$ compounds, coined as silylones, suggested that the synthesis of this class of compounds is experimentally feasible. $(cAAC^{\bullet})_2SiCl_2$ is reduced with two equiv. of KC_8 in THF to obtain a dark blue solution of $(cAAC)_2Si$ (Scheme 13) which separated out from the mixture of KCl and $(cAAC)_2Si$ by extraction with *n*-hexane in 95% yield.[59] When $(cAAC^{\bullet})_2SiCl_2$ is treated with two equiv. of R–Li (R = Ph, ^{t}Bu) in THF, $(cAAC)_2Si$ is isolated instead of the functionalized hypothetical product $(cAAC^{\bullet})_2SiPh_2$ under the reductive elimination of Ph–Ph. $(cAAC^{\bullet})_2SiPh_2$ (Scheme 15)[59] is believed to be the intermediate species. $(Me_2\text{-cAAC})_2Si$ has a singlet spin ground state which has been confirmed by magnetic susceptibility and EPR measurements.

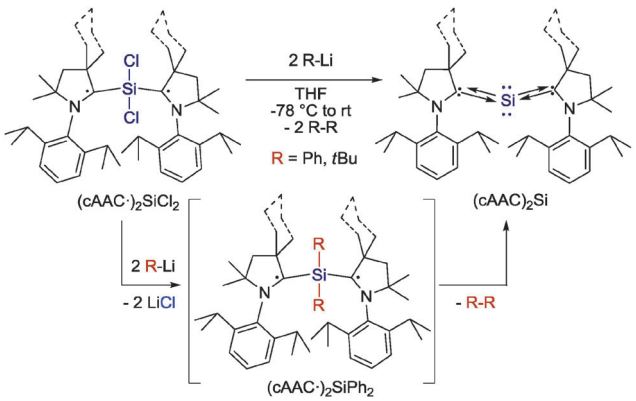

Scheme 15 Synthesis route of $(cAAC)_2Si$ from $(cAAC^{\bullet})_2SiCl_2$ [cAAC = Me_2-cAAC and Cy-cAAC] with R-Li.

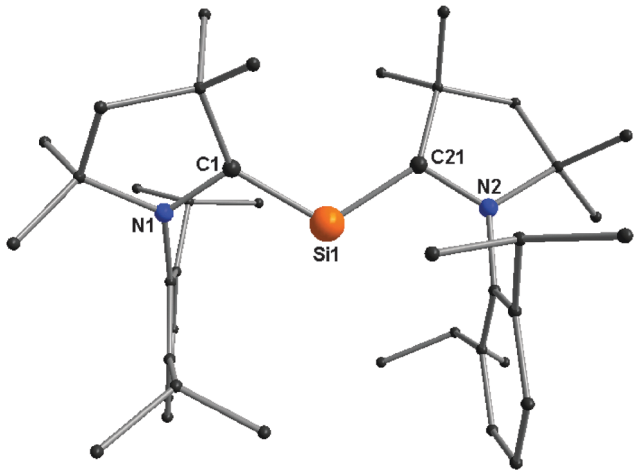

Fig. 12 Molecular structure of $(Me_2\text{-cAAC})_2Si$.

The ^{29}Si NMR spectrum of $(Me_2\text{-cAAC})_2Si$ exhibits a singlet at 66.71 ppm which is downfield shifted when compared with that of the precursor $(Me_2\text{-cAAC}^{\bullet})_2SiCl_2$ (4.13 ppm). The physical appearance of $(cAAC^{\bullet})_2SiCl_2$ (λ_{ab} = 569 nm) and $(cAAC)_2Si$ (λ_{ab} = 570, 611 nm) is similar from the point of view of their color. The latter one is darker blue in color while the former is bright blue.

The molecular structure of $(Me_2\text{-cAAC})_2Si$ consists of a two coordinate silicon atom (Fig. 12) at the center.[59] It is bound to two carbene carbon atoms of the two Me_2-cAAC ligands. The central silicon atom adopts a two coordinate bent geometry. The C_{cAAC}–Si–C_{cAAC} bond angles of the two symmetry independent molecules are more acute by $\sim 5^\circ$ compared with that of $(Me_2\text{-cAAC}^{\bullet})_2SiCl_2$.[59]

The sum of angles around the C_{cAAC} of $(Me_2\text{-cAAC})_2Si$[59] are on average 357.7° (358.1°, $(Me_2\text{-cAAC}^{\bullet})_2SiCl_2$) suggesting slight deviation from the trigonal planar geometry. The C_{cAAC}–Si bond distances of $(Me_2\text{-cAAC})_2Si$ are 1.8411(18) Å and 1.8417(17) Å which are very close to those of $(Me_2\text{-cAAC}^{\bullet})_2SiCl_2$ (1.8455(16) and 1.8482(17) Å).[57]

The optimized geometry of $(Me_2\text{-cAAC})_2Si$ is in very good agreement with the experimental one rather than that of the triplet state. The triplet state is between 17.2–17.6 kcal mol^{-1} higher in energy than the singlet state. The HOMO−1 is a σ lone-pair orbital at the Si atom, while the HOMO is a π-type orbital which has the largest extension at the Si but exhibits significant Si–C π bonding (Fig. 13). This is the typical feature of a silylone.[59]

The NBO analysis of $(Me_2\text{-cAAC})_2Si$ shows that the central silicon atom possesses two pairs of electrons. One σ lone-pair orbital resides on the silicon atom and the second pair of electrons forms a three-center C–Si–C π-bond. The numerical values for the distribution of the second pair of electrons are 40% at Si and 30% at each of the C_{cAAC}. Theoretically calculated first and second proton affinities are (PAs) 272.2 kcal mol^{-1} and 186.7 kcal mol^{-1}, respectively. The very large value for the second proton affinity clearly supports the assignment that $(Me_2\text{-cAAC})_2Si$ is genuinely a silylone.

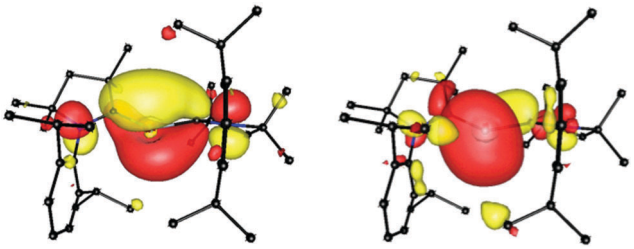

Fig. 13 Plots of the HOMO (left) and HOMO−1 (right) of $(Me_2\text{-cAAC})_2Si$. Reproduced from ref. 59 with permission of John Wiley and Sons. Color version courtesy of Prof. G. Frenking.

Further calculations reveal that it has a 54% of singlet diradical character. The calculation gives coefficients of 0.96 for the closed-shell 2,0 configuration, −0.28 for the 1,1 configuration and 0.0 for the 0,2 configuration. The closed-shell singlet configuration of $(Me_2\text{-cAAC})_2Si$ has a non-negligible contribution from the singly excited state which possesses some diradicaloid character (as shown in Scheme 13) and low electronic excitation energy.[59]

The experimental charge density calculations have confirmed that there are two pairs of electrons on the silicon atom in silylone. NBO calculations show accumulation of the positive partial charge at Si which agrees with the electronegativities of silicon and carbon. This indicates that the Si → C_{cAAC} π-back donation is larger than the Si ← C_{cAAC} σ-donation. This typical bonding scenario results in the reasonably stronger Si–C_{cAAC} bonds in silylone which is crucial for such a high stability of this compound. The dark blue crystals of $(cAAC)_2Si$ are found to be stable over two years at room temperature in an inert atmosphere without any decomposition.[60] $(cAAC)_2Si$ is also characterized by EI mass spectrometry. $(cAAC)_2Si$ is thermally stable up to 195 °C and decomposes above 220 °C to a yellow liquid. NMR studies show that $(cAAC)_2Si$ is chemically inert when it is reacted with molecular hydrogen, ammonia, and carbon dioxide at room temperature. The cyclic voltammetry (CV) studies on $(cAAC)_2Si$ in 0.1 M $[n\text{-}Bu_4N]PF_6$ THF solution suggest that $(cAAC)_2Si$ is quasi-reversibly reduced to its corresponding radical anion $(cAAC)_2Si^{\bullet-}$ at $E_{1/2} = -1.55$ V (against the reference $Cp^*_2Fe/Cp^*_2Fe^+$) (Fig. 14).[60] The radical anion intermediate $(cAAC)_2Si^{\bullet-}$ has been further confirmed by the EPR spectroscopy. The reaction mixture of $(Me_2\text{-CAAC})_2Si$ is stirred

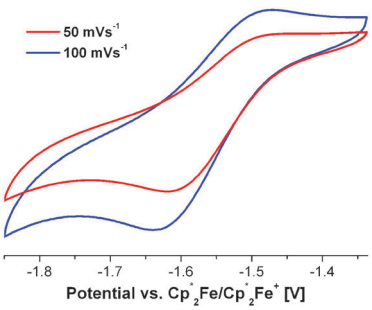

Fig. 14 Cyclic voltammogram (CV) of $(Cy\text{-cAAC})_2Si$ in THF solution (0.1 M $[n\text{-}Bu_4N]PF_6$) at indicated scan rates (potential *versus* $Cp^*_2Fe/Cp^*_2Fe^+$).

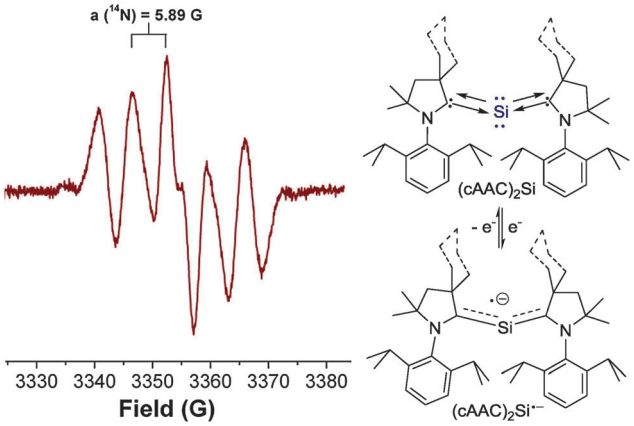

Fig. 15 X-band EPR spectrum of *in situ* generated $(Me_2\text{-cAAC})_2Si^{\bullet-}$ in THF at 298 K (left). Formation of $(cAAC)_2Si^{\bullet-}$ from of $(cAAC)_2Si$ (right). [cAAC = Me_2-cAAC and Cy-cAAC]. Reproduced with permission from ref. 60.

in the presence of potassium metal for 30 min to *in situ* generate the radical anion $(Me_2\text{-CAAC})_2Si^{\bullet-}$ in THF at 298 K.[60] The EPR spectrum (Fig. 15) of $(Me_2\text{-CAAC})_2Si^{\bullet-}$ produces five hyperfine lines at $g = 2.0058$ due to the coupling of a radical electron with two nitrogen nuclei ($\alpha(^{14}N) = 5.89$ G; $I = 1$). Two satellites ($\alpha(^{13}C) = 40$ G; $I = 1/2$) are originated due to coupling with C_{cAAC} atoms suggesting that the radical electron is delocalized in the C–Si–C back bone of $(Me_2\text{-CAAC})_2Si^{\bullet-}$. The radical electron resides on the p orbitals of the carbene carbon atoms (see the LUMO (Fig. 16) of $(cAAC)_2Si$ and SOMO ($(cAAC)_2Si)^{\bullet-}$).[60] The Mulliken spin density plot of the radical anion shows that the unpaired electron is delocalized (Fig. 17) between the two carbene carbon atoms *via* the vacant d-orbital of the silicon atom.

Potassium metal is an electro-positive metal and it has a high tendency to donate electrons to the low lying antibonding orbitals. Potassium metal is chosen as an electron donor and THF as the preferred solvent due to its high polarity and electron transport ability. Accordingly, we set up a reaction by adding THF to a 1 : 1 molar mixture of $(cAAC)_2Si$ and metallic potassium.[60] The resultant dark blue color of the reaction solution is changed to a greenish yellow color after 35 min of

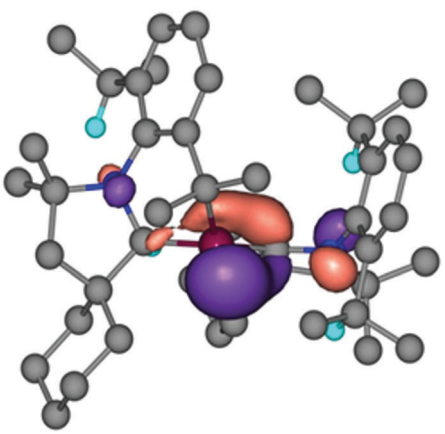

Fig. 16 LUMO of $(Cy\text{-cAAC})_2Si$. Reproduced with permission from ref. 60.

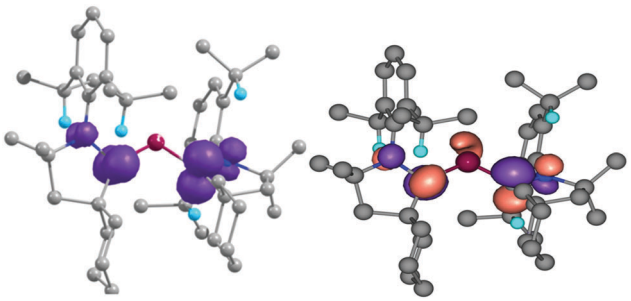

Fig. 17 Mulliken spin density plot (left) and SUMO (right) of $(Cy\text{-}cAAC)_2Si^{\bullet -}$. Reproduced with permission from ref. 60.

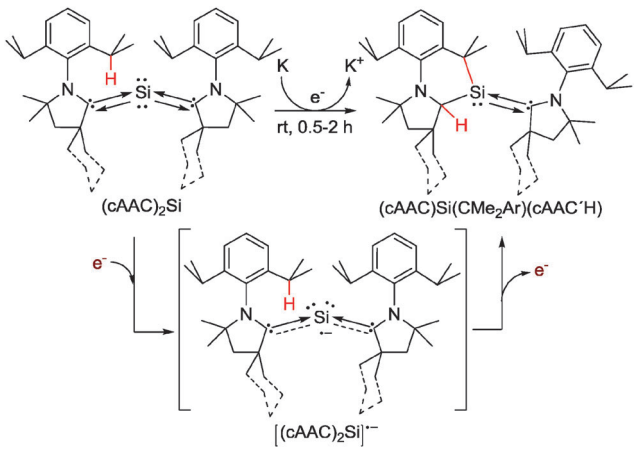

Scheme 16 Conversion of $(cAAC)_2Si$ with two coordinate silicon to $(cAAC)Si(CMe_2Ar)(cAAC'H)$ with three coordinate silicon [cAAC = Me_2-cAAC and Cy-cAAC].

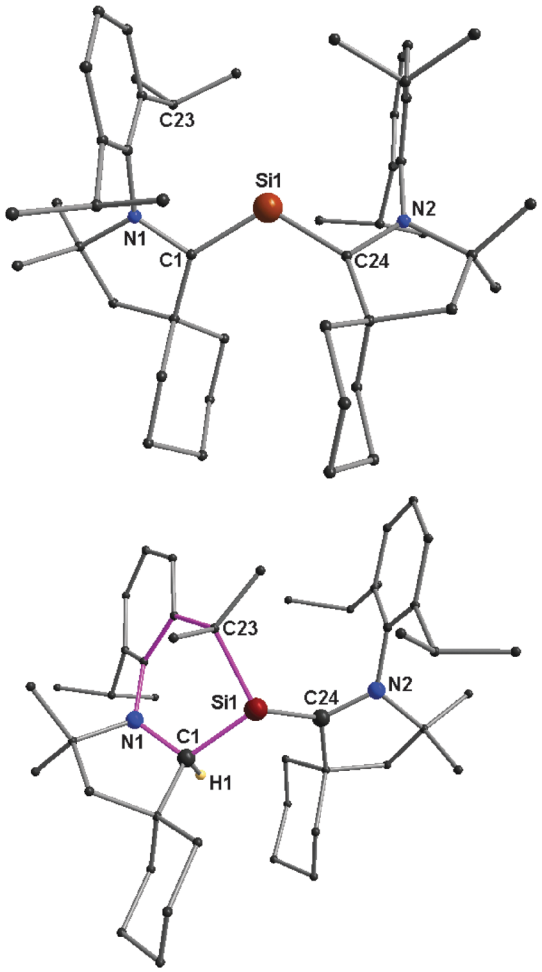

Fig. 18 Molecular structure of $(Me_2\text{-}cAAC)_2Si$ (top) and $(Cy\text{-}cAAC)Si(CMe_2Ar)$-$(Cy\text{-}cAAC'H)$ (bottom). Reproduced with permission from ref. 60.

vigorous stirring. Afterwards the solution was filtered to separate out the unreacted potassium metal. The concentrated THF solution is stored at −32 °C in a freezer to form yellow blocks of $(cAAC)Si(CMe_2Ar)(cAAC'H)$ (Scheme 16) in reasonable (Me_2-cAAC) to high yields (Cy-cAAC).[60]

X-ray single crystal diffraction reveals the formation of a six-membered cyclic silylene $(cAAC)Si(CMe_2Ar)(cAAC'H)$ with a three coordinate silicon atom in the center (Scheme 16 and Fig. 18).[60]

The recovery of the 67% of unreacted potassium metal reveals that 33% of the metal had been consumed during the reaction course (Scheme 16). This means that only a sub-stoichiometric amount of the metal atom can successfully induce the reaction of the apparently unreactive silylone $(cAAC)_2Si$ to its structural isomer $(cAAC)Si(CMe_2Ar)(cAAC'H)$ in an atom economical fashion. In this respect it is important to mention that stirring of the reaction solution for a longer time leads to the further rearrangement of $(cAAC)Si(CMe_2Ar)(cAAC'H)$ to different products which could not be isolated. The crystals of $(cAAC)Si(CMe_2Ar)(cAAC'H)$ are stable at room temperature for more than one month in an inert atmosphere and they melt above 211 °C. $(cAAC)Si(CMe_2Ar)(cAAC'H)$ is stable enough to be further characterized by EI mass spectrometry.[60] The ^{29}Si NMR spectrum of $(cAAC)Si(CMe_2Ar)(cAAC'H)$ exhibits resonances at 55.98 (cAAC = Cy-cAAC) and 54.55 ppm (cAAC = Me_2-cAAC), which are upfield-shifted when compared to those of $(cAAC)_2Si$ (71.15 and 66.71 ppm, respectively). The ^{13}C NMR spectrum of $(cAAC)Si(CMe_2Ar)(cAAC'H)$ shows resonances at 69.4(CH)/173.5(C:) and 66.2(CH)/172.1(C:) ppm, respectively, which are upfield-shifted when compared to those of $(cAAC)Si(CMe_2Ar)(cAAC')$ (210.8 and 210.9 ppm, respectively).

A detailed investigation of the reaction mechanism reveals that the formation of $(cAAC)Si(CMe_2Ar)(cAAC'H)$ from $(cAAC)_2Si$ could be rationalized as the activation of the C–H bond of one of the two $CHMe_2$ groups of $(cAAC)_2Si$ which has selectively reacted (Scheme 16) with one C_{cAAC}–Si bond, producing the H–C_{cAAC}–$Si(CMe_2)$ moiety in $(cAAC)Si(CMe_2Ar)(cAAC'H)$.

The formation of the silylone radical anion intermediate $(cAAC)_2Si^{\bullet -}$ is assumed to be the key step for the activation of the very strong C–H bond. This could finally help to overcome the challenge behind the so far elusive reactivity of the highly stable silylone $(cAAC)_2Si$ to produce the corresponding six-membered silylene $(cAAC)Si(CMe_2Ar)(cAAC')$.[60]

The closed-shell singlet electronic state of $(Cy\text{-}cAAC)Si(CMe_2Ar)(Cy\text{-}cAAC')$ is lower in energy by 16.8 kcal mol^{-1} than its triplet form. Geometry optimization with broken symmetry formalism reveals that the diradical singlet state again is higher

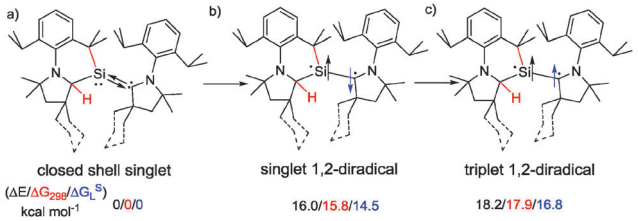

Fig. 19 Calculated energy values of the (a) singlet (left), (b) singlet 1,2-diradical (middle) and (c) triplet 1,2-diradical (right) species implying the preference for the singlet ground state (left) of (cAAC)Si(CMe_2Ar)(cAAC′).

in energy than the closed-shell singlet state by 14.5 kcal mol^{-1} (ΔG_L^S).[60] The optimized geometrical parameters of the singlet state are in much better agreement to the X-ray crystal structure of (Cy-cAAC)Si(CMe_2Ar)(Cy-cAAC′) than its diradical singlet or triplet states (Fig. 19).[60]

The detail structural investigations (Fig. 18) of (Cy-cAAC)Si(CMe_2Ar)(Cy-cAAC′H) show that one carbene carbon atom (C_{cAAC}) contains one proton and the silicon atom is further bound to the CMe_2 group (C23) of one of the former isopropyl groups ($CHMe_2$; C23–Si1 = 1.961(2) Å).[60] The C_{cAAC}–Si and C_{cAAC}–N bonds of (Cy-cAAC)Si(CMe_2Ar)(Cy-cAAC′H) are elongated from 1.8404(11) to 1.952(2) and 1.3827(15) to 1.461(3) Å, respectively. The C24(C_{cAAC})–Si1 and C24–N2 bond distances are very close to the values (C_{cAAC}–Si = 1.8535(12) Å, C24–N2 = 1.3724(14) Å) of silylone (Cy-cAAC)$_2$Si. A newly formed six-membered ring containing two heteroatoms is shown in purple color in Fig. 18.[60]

Unlike carbon, silicon has vacant d orbitals and hence silicon can form higher coordinate compounds *via* the mixing of s and p with d orbitals. As a result, a five coordinate (cAAC)$SiCl_4$ adduct (Scheme 17) is formed in high yield (97–98%) when cAAC is reacted with $SiCl_4$ in a 1 : 1 molar ratio in THF.[61] (cAAC)$SiCl_4$ is very polar in nature and soluble in polar solvent THF. The ^{29}Si chemical shift value of (Me_2-cAAC)$SiCl_4$ is −103.5 ppm. It is also partially soluble in non-polar solvents like *n*-hexane, benzene and toluene. The colorless crystals of (cAAC)$SiCl_4$ decompose above 123 °C. They are also prone to decomposition in THF if the solution of (cAAC)$SiCl_4$ is stored for a longer time (several days). This simple looking higher coordinate adduct (cAAC)$SiCl_4$ has been eventually found to be a very important precursor for the syntheses of several low coordinate cAAC-silicon compounds. (cAAC)$SiCl_4$ is believed to have zwitterionic character based on bond parameters. The bond between a carbene carbon atom (C_{cAAC}) and a silicon atom is a coordinate bond (C_{cAAC} → Si; 1.944(2) Å), while the C_{cAAC}–N has a partial double bond character (1.3040(2) Å) which is close to that of a free carbene (1.315 Å).[61]

The LUMO of the cAAC is lower lying when compared with that of NHC. The LUMO of the carbene is located at π_{C-N^*} of cAAC. It can be argued that both the HOMO and LUMO of cAAC are further lower due to donation of electron pairs on the carbene carbon atom to the silicon atom of (cAAC)$SiCl_4$. Thus, reducing agents, like KC_8 are very much effective to eliminate the chlorine atoms from (cAAC)$SiCl_4$. We have observed that the reduction of (cAAC)$SiCl_4$ with KC_8 even starts at very low temperature (< −78 °C) in polar solvents, like THF. Non-polar solvents like *n*-hexane are effective for the selective reduction of (cAAC)$SiCl_4$ to (cAAC$^\bullet$)$SiCl_3$ at room temperature. The temperature of the reaction must be kept very low (< −78 °C) for the controlled reduction of (cAAC)$SiCl_4$ to (cAAC$^\bullet$)$SiCl_3$ in THF. The electron transfer from KC_8 to (cAAC)$SiCl_4$ is very slow in non-polar solvents. The electron transfer from KC_8 to (cAAC)$SiCl_4$ possibly occurs *via* THF solvated electron transport and hence the kinetics of the reduction is very fast.[61]

We believe that KC_8 donates the electron to the LUMO of (π_{C-N}* of cAAC) of (cAAC)$SiCl_4$ to form a radical anion intermediate [(cAAC)$SiCl_4$]$^{\bullet-}$ which then eliminates a chloride anion with the formation of KCl and (cAAC$^\bullet$)$SiCl_3$ (Scheme 18).[61] The bond parameters obtained from the X-ray single crystal diffraction of (cAAC$^\bullet$)$SiCl_3$ lead to the conclusion that the bond between a carbene carbon atom (C_{cAAC}) and a silicon atom is an electron sharing covalent single bond (C_{cAAC}–Si; 1.8152(12) Å) with an elongated C_{cAAC}–N bond (137.79(14) Å). The synthesis of a carbene centered stable radical *via* the transformation of a C_{cAAC} → Si coordinate bond to an electron sharing covalent single bond C_{cAAC}–Si is unique.[61]

The fluorescent yellow plates/needles of (cAAC$^\bullet$)$SiCl_3$ are isolated either at room temperature from a concentrated solution or a dilute solution at 0 °C from a refrigerator. They are highly soluble

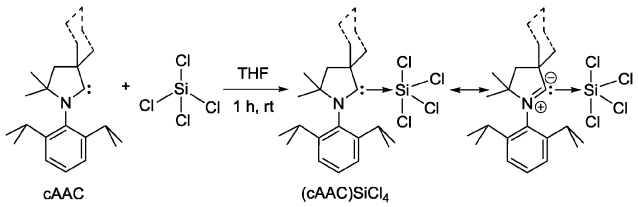

Scheme 17 Synthesis of (cAAC)$SiCl_4$. [cAAC = Me_2-cAAC and Cy-cAAC].

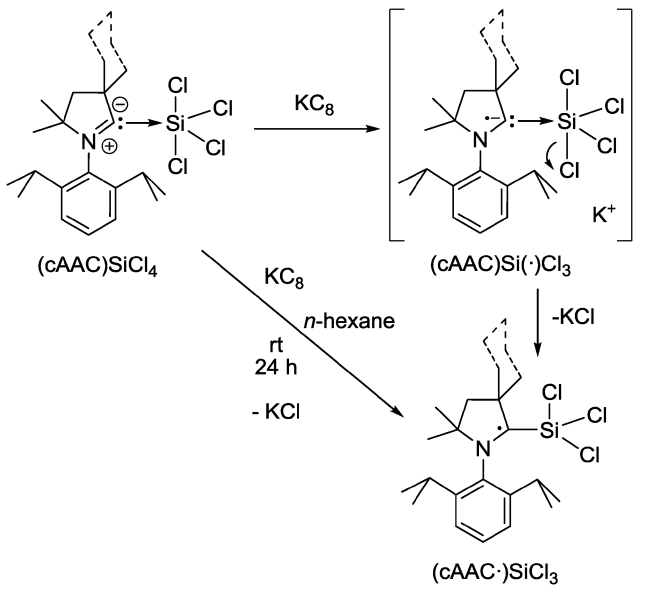

Scheme 18 Reduction of (cAAC)$SiCl_4$ to (cAAC$^\bullet$)$SiCl_3$ by KC_8. [cAAC = Me_2-cAAC and Cy-cAAC].

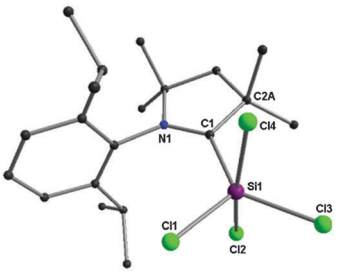

Fig. 20 Molecular structures of $(Me_2\text{-cAAC})_2SiCl_4$.

in both polar and non-polar solvents. They melt at around 115 °C. They can be characterized by electron ionization (EI) mass spectrometry. They are stable for more than a year under an inert atmosphere at room temperature.[61]

The silicon atom in the $(Me_2\text{-cAAC})SiCl_4$ adduct adopts a trigonal bipyramidal coordination geometry. The important structural feature of $(Me_2\text{-cAAC})SiCl_4$ is that the axial Si–Cl bond distances (~2.18 Å) are significantly longer than those of equatorial Si–Cl bonds (~2.04 Å) (Fig. 20). The $C_{carbene}$–Si and $C_{carbene}$–N bond distances are 1.944(2) Å and 1.3040(2) Å, respectively.[61]

The silicon atom of compound $(cAAC^{\bullet})SiCl_3$ [cAAC = Me_2-cAAC and Cy-cAAC] is bound to three chlorine atoms and one carbene carbon atom. The silicon atom adopts a near-tetrahedral geometry (Fig. 21).[61] The $C_{carbene}$–Si bond distances in $(Me_2\text{-cAAC}^{\bullet})SiCl_3$ and $(Cy\text{-cAAC}^{\bullet})SiCl_3$ are 1.8152(12) and 1.8193(8) Å, respectively. The $C_{carbene}$–Si bond distance in $(cAAC^{\bullet})SiCl_3$ is slightly shorter than that of the electron sharing Si–C single bond distances of $(cAAC^{\bullet})_2SiCl_2$ (1.8455(16) and 1.8482(17) Å) but significantly shorter than that of the precursor $(cAAC)SiCl_4$ (1.944(2) Å). The $C_{carbene}$–N bond lengths are 1.3779(14)–138.27(10) Å which are close to those (1.3994(19)–1.400(2) Å)[57] obtained for the diradical $(cAAC^{\bullet})_2SiCl_2$ but it is shorter by 0.07 Å when compared with that of the precursor $(cAAC)SiCl_4$ (1.3040(2) Å). All the bond parameters of $(cAAC^{\bullet})SiCl_3$ suggest that $C_{carbene}$–Si is an electron sharing Si–C single bond while the same one is a $C_{cAAC} \rightarrow Si$ coordinate σ-bond in $(cAAC)SiCl_4$.[61]

DFT calculations concerning the bonding and electron density distribution have been carried out on $(cAAC^{\bullet})SiCl_3$.[61] The calculations show that the unpaired electron (Fig. 23) is

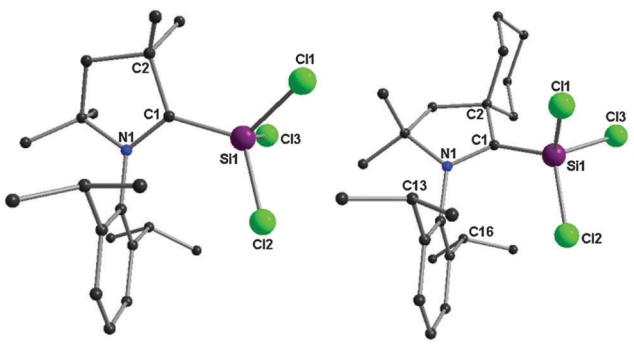

Fig. 21 Molecular structure of $(Me_2\text{-cAAC}^{\bullet})SiCl_3$ (left) and $(Cy\text{-cAAC}^{\bullet})SiCl_3$ (right).

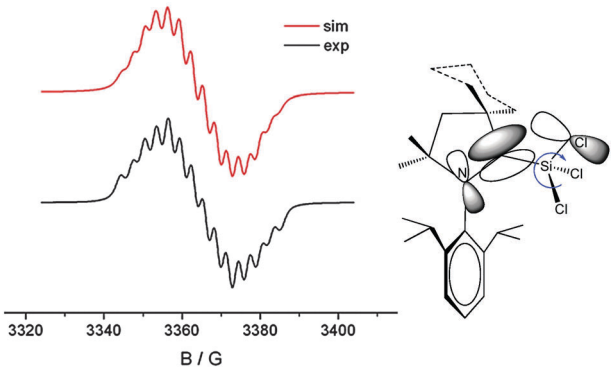

Fig. 22 Experimental and simulated X-band EPR spectrum of a C_6D_6 solution of $(Cy\text{-cAAC}^{\bullet})SiCl_3$ at 298 K. Reproduced from ref. 61 with permission of John Wiley and Sons. Color version courtesy of Dr D. Koley.

mainly located on the carbene carbon of cAAC (*ca.* 52%), with a smaller contribution from the N1 atom (23%) and the remaining 25% of the electron density is scattered over the Dipp/cAAC units and one of the Cl atoms (oriented parallel to the p_z orbital of C_{cAAC} atom). The EPR spectrum of $(cAAC^{\bullet})SiCl_3$ [cAAC = Me_2-cAAC and Cy-cAAC] is recorded in C_6D_6 which shows multiple hyperfine lines. The EPR spectrum of $(Cy\text{-cAAC}^{\bullet})SiCl_3$ is better resolved than that of $(Me_2\text{-cAAC}^{\bullet})SiCl_3$. The simulation considering the electronic coupling of one radical electron with one ^{14}N ($I = 1$) and one $^{35/37}Cl$ ($I = 3/2$) nuclei does not reproduce the experimental pattern suggesting that the free rotation of the $SiCl_3$ group around the carbon–silicon bond (C_{cAAC}–Si) might be possible.[61]

The simulation of the experimental EPR spectrum (Fig. 22) of $(Cy\text{-cAAC}^{\bullet})SiCl_3$ reveals a ^{14}N coupling constant (I = 1) of 6.4 G, and smaller couplings of about 3.4 G (1 Cl) and 2.7 G (2 Cl), with three Cl atoms (I = 3/2, gyromagnetic ratio = 1.20). The relatively intensified outermost lines suggest the non-equivalence of the chlorine couplings. This also suggests a partially hindered rotation of the $SiCl_3$ group.[61]

It is important to mention that highly reactive trichlorosilane radical $^{\bullet}SiCl_3$ is frequently generated by flash photolysis. It is an active radical intermediate in many photochemical transformations such as chemical vapour deposition (CVD) and is a product in chlorine plasma etching of silicon. The $(cAAC^{\bullet})SiCl_3$ can be considered as the cAAC stabilized stable radical of $^{\bullet}SiCl_3$.[61]

When three equivalents of PhLi is added drop by drop to the fluorescent yellow colored solution of $(Cy\text{-cAAC}^{\bullet})SiCl_3$ in THF at −78 °C and the temperature of the reaction solution is slowly increased to rt, a dark red solution of $(Cy\text{-cAAC}^{\bullet})SiPh_3$ (Scheme 19) is obtained in 90% yield.[62] The crystals $(Cy\text{-cAAC}^{\bullet})SiPh_3$ melt in the temperature range of 148–149 °C. The compound $(Cy\text{-cAAC}^{\bullet})SiPh_3$ is further characterized by EI mass spectrometry like its precursor.[62]

The molecular structure of $(Cy\text{-cAAC}^{\bullet})SiPh_3$ is unambiguously established (Fig. 24) by the X-ray single crystal structure determination. This reveals that the central silicon atom is bound to three phenyl groups and one carbon atom of the Cy-cAAC ligand with a coordination number of four. The silicon atom

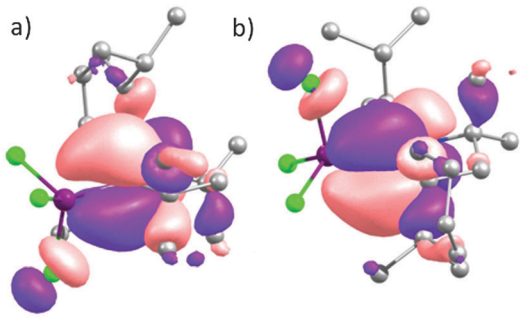

Fig. 23 The KS-SOMO (a) (Me_2-cAAC•)$SiCl_3$ and (b) (Cy-cAAC•)$SiCl_3$ at the UM05-2X/TZVP//UM05-2X/SVP level. Reproduced from ref. 61 with permission of John Wiley and Sons. Color version courtesy of Dr D. Koley.

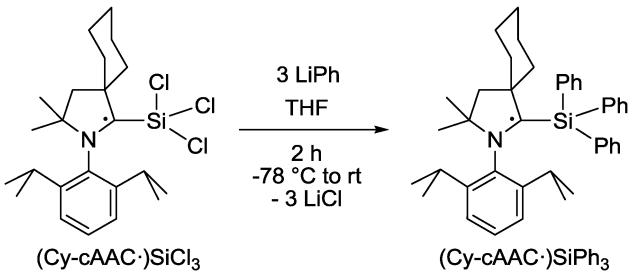

Scheme 19 Synthesis of (Cy-cAAC•)$SiPh_3$ from (Cy-cAAC•)$SiCl_3$.

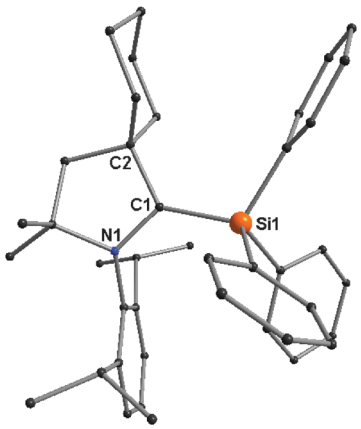

Fig. 24 The molecular structure of compound (Cy-cAAC•)$SiPh_3$.

adopts a slightly distorted geometry due to the asymmetric steric crowding around it.[62]

The Si–C_{cAAC} bond length (1.8704(17) Å)[62] of (Cy-cAAC•)$SiPh_3$ is slightly longer than that of its precursor (Cy-cAAC•)$SiCl_3$ (1.8193(8) Å).[61] This is possibly due to the substitution of all the three electron-withdrawing chlorine atoms by electron-donating phenyl groups at silicon. Theoretical calculations (Fig. 25) on (Cy-cAAC•)$SiPh_3$ show that 55% of the electron density (unpaired) is primarily located on C_{cAAC} with 21% contribution from the adjacent nitrogen atom. The remaining 24% of the electron density is delocalized over the Dipp group of the cAAC unit and the C_{ipso} atom in one of the phenyl groups.[62]

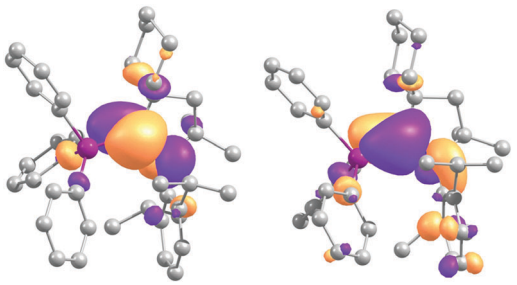

Fig. 25 The KS-HOMO (left) and KS-LUMO (right) of (Cy-cAAC•)$SiPh_3$ at the UM05-2X/TZVP//UM05-2X/SVP level. Reproduced with permission from ref. 62.

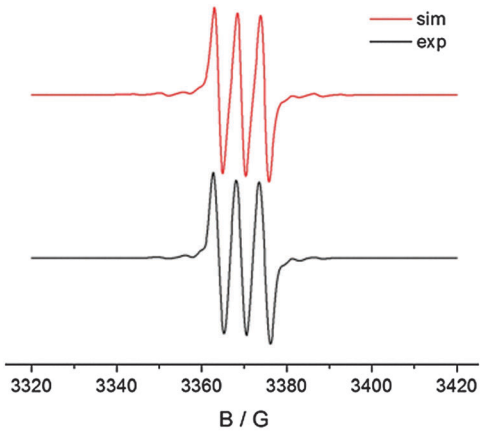

Fig. 26 Experimental and simulated X-band EPR spectra of C_6D_6 solution of (Cy-cAAC•)$SiPh_3$. Reproduced with permission from ref. 62.

The X-band EPR spectrum (Fig. 26) of (Cy-cAAC•)$SiPh_3$ exhibits three hyperfine lines at g = 2.0019 due to the coupling (5.4 G) with one ^{14}N (I = 1) nucleus. The satellites from ^{29}Si (8.0 G; ^{29}Si: I = 1/2, 4.7% natural abundance), and three carbon atoms (25 G), are tentatively identified through simulation of the EPR spectrum and theoretically calculated hyperfine coupling constants. Two γ carbons at the cyclohexyl ring of Cy-cAAC ligand transfer spin *via* hyperconjugation. One carbon atom from a Si-phenyl group (38.0 G) causes the broadening of hyperfine lines. Thus, (Cy-cAAC•)$SiPh_3$ is identified as the predominantly spin-bearing carbene carbon centered p radical. The hyperfine coupling constants of ^1H are calculated to be very small and are not observed experimentally.[62]

It has been mentioned before that (^{IP}NHC)$SiCl_2$ is exclusively obtained from the reaction of $HSiCl_3$ with two equiv. of NHC under the elimination of ^{IP}NHC·HCl.[16a] Alternatively, (^{IP}NHC)$SiCl_2$ is also prepared *via* the reduction of the (^{IP}NHC)-$SiCl_4$ adduct with two equiv. of KC_8 under the elimination of KCl (Scheme 12). Both the NHC and cAAC stabilized (L)ECl_2 (L = NHC, for E = Si, Ge, Sn; L = cAAC for Ge, Sn) have been reported.[16a,17]

The dechlorination reaction is regarded to be an important technical process, due to the formation of $SiCl_4$ as a side product during the reduction of $HSiCl_3$ to Si with hydrogen gas. It has been observed that dichlorosilylene ($SiCl_2$) is generated from

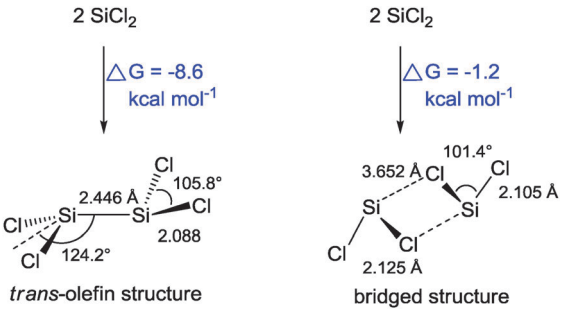

Scheme 20 Calculated dimerization energies and bond parameters of Si_2Cl_4.

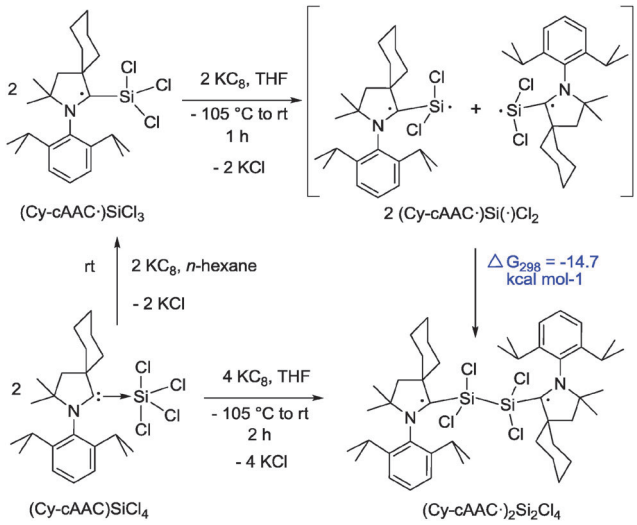

Scheme 21 Synthesis route of (Cy-cAAC•)$_2$Si$_2$Cl$_4$.

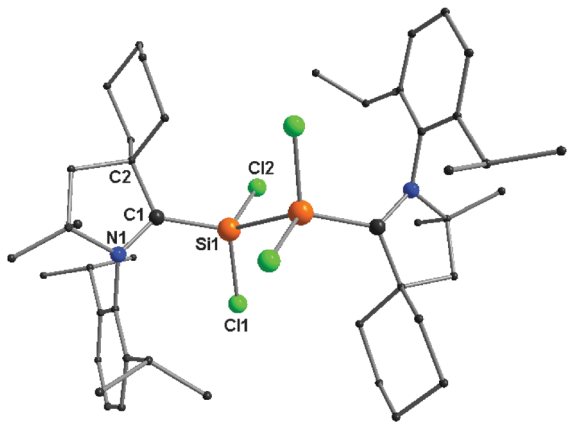

Fig. 27 The molecular structure of (Cy-cAAC•)$_2$Si$_2$Cl$_4$.

trichlorosilane ($HSiCl_3$) in the presence of a base. It can be trapped as (NHC)$SiCl_2$ by NHC.[16a,28] In the presence of triethylamine, the dimer Si_2Cl_6 produces $SiCl_4$ and Si_6Cl_{14}. The exact mechanism has not been established yet. Hexachlorodisilane (Si_2Cl_6) undergoes disproportionation to produce $SiCl_4$ and $SiCl_2$, both of which have been trapped by NHC too.[16a] $SiCl_2$ could also be generated from Si_3Cl_8 in the presence of tertiary amine. Gaseous $SiCl_2$ is known for a long time but it condenses to polymeric $(SiCl_2)_n$.[16a] The stabilization of the dimer (Si_2Cl_4) of $SiCl_2$ has not been even suggested previously before our report. In 2003, Boganov *et al.* suggested that the dimerization of $2SiCl_2 \rightarrow Si_2Cl_4$ is energetically favorable over complexation between $SiCl_2$ and molecular N_2.[63a] This has been concluded from the quantum chemical calculations and experiments at low temperature by an argon–nitrogen matrix isolation of the pyrolysis product (N_2-$SiCl_2$) from Si_2Cl_6. The Si_2Cl_4 is predicted to exist in two forms (*trans*-olefin and bridged structure; Scheme 20). The calculated dimerization energy ($2SiCl_2 \rightarrow Si_2Cl_4$) is evaluated to be -8.6 kcal mol^{-1} for the *trans*-olefin structure and -1.2 kcal mol^{-1} for the bridged structure.[63]

Having (cAAC•)$SiCl_3$ in hand,[61] the possibility of studying the dimerization of (cAAC)$_2SiCl_2$ seems to be elusive.[64] The NHC analogue (NHC•)$SiCl_3$ is still not isolated. Note that (^{IP}NHC)$SiCl_2$ is stable in the monomeric form at room temperature for months under an inert atmosphere and does not undergo any sort of dimerization/polymerization.[28] cAAC reacts with (NHC)$SiCl_2$ to exclusively produce (cAAC•)$_2SiCl_2$.[57] To attempt the synthesis of Si_2Cl_4, stabilized by carbenes, compound (Cy-cAAC•)$SiCl_3$ has been chosen as the precursor instead of (NHC)$SiCl_2$, because treatment of the latter with cAAC resulted exclusively in the formation of (cAAC•)$_2SiCl_2$.[57]

(Cy-cAAC•)$SiCl_3$ is thus treated with one equiv. of KC_8 in THF at low temperature to generate the desired species (Cy-cAAC)$_2Si_2Cl_4$ (Scheme 21).[64] Green crystals of (Cy-cAAC•)$_2Si_2Cl_4$ are isolated from a concentrated solution stored at -32 °C in a freezer in 85% yield. The same product is obtained when the (cAAC)$SiCl_4$ adduct is reduced with two equiv. of KC_8 (Scheme 21). The green crystals of (Cy-cAAC•)$_2Si_2Cl_4$ decompose above 93 °C and are stable at -32 °C for several months but slowly decompose at higher temperature. The ^{29}Si chemical shift value of (Cy-cAAC•)$_2Si_2Cl_4$ is 3.3 ppm.[64]

Both the silicon atoms of (Cy-cAAC•)$_2Si_2Cl_4$ adopt a near-tetrahedral geometry and each of them is bound to one carbene carbon atom, two chlorines and one silicon atom (Fig. 27). The bond parameters are in good agreement with those of the previously calculated values for a *trans*-olefin structure of the optimized discrete Si_2Cl_4 molecule (Scheme 20).[63,64] The Si_2Cl_4 unit of (Cy-cAAC•)$_2Si_2Cl_4$ adopts a *trans*-olefin like configuration as predicted by Swihart *et al.* and Boganov *et al.*[63] The Si–Si bond distance in (Cy-cAAC•)$_2Si_2Cl_4$ is 2.454(3) Å which is close to that of the hypothetical Si_2Cl_4 (2.446 Å, Scheme 20). The average Si–Si single bond distances are close to the value of 2.35 Å. The Si–Si single bond distance of 2.424(8) Å has been reported for the polymeric perchloropolysilane $(SiCl_2)_n$.[65] The carbenes of (Cy-cAAC•)$_2Si_2Cl_4$ are oriented in a *trans*-position with respect to the central Si_2Cl_4 unit with a C–Si–Si–C torsion angle of 180°. Hence, (Cy-cAAC•)$_2Si_2Cl_4$ can be considered as a Si_2Cl_4 bridged carbon centered 1,4-diradical.[64]

Theoretical calculations using the broken symmetry formalism reveals that the diradical singlet state is 2.8 kcal mol^{-1} lower in energy than the triplet state. The CASSCF(2,2)/SVP method has been employed for the optimization of the geometry of (Cy-cAAC•)$_2Si_2Cl_4$ in the singlet state. The coefficient values for

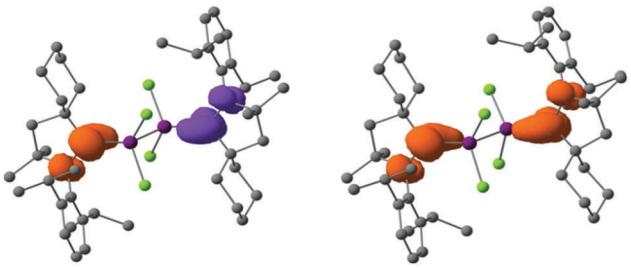

Fig. 28 Computed Mulliken spin density plots (isosurface = 0.006 au) of (Cy-cAAC•)$_2$Si$_2$Cl$_4$ in the diradical singlet (left) and triplet state (right). Reproduced with permission from ref. 64.

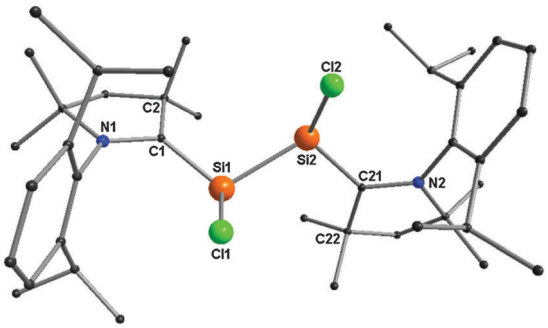

Fig. 29 The molecular structure of (Me-cAAC)$_2$Si$_2$Cl$_2$.

the three singlet components are 0.80(2/0), −0.60(0/2), and 0.0(1/1) and the diagonal elements of the final one electron symbolic density matrix are 1.3 and 0.7, respectively, suggesting that the singlet form of (Cy-cAAC•)$_2$Si$_2$Cl$_4$ possesses two unpaired electrons with an opposite sign.[64] The unpaired electrons are stabilized by coupling with the neighboring lone-pairs of the nitrogen atoms in cAAC.

The Mulliken spin density distribution plot of the singlet diradical and the triplet (Fig. 28) form entails that the two unpaired electrons are localized at the C_{cAAC} of the Cy-cAAC.[64] It has been concluded from the theoretical investigations that the radical intermediate (Cy-cAAC•)Si(•)Cl$_2$ formed[64] from the reaction of (Cy-cAAC•)SiCl$_3$ and KC$_8$ depicted in Scheme 21 possesses a singlet ground state (Cy-cAAC•↑)Si(•↓)Cl$_2$. Dimerization of two such species to form the 1,4-diradical (Cy-cAAC•)$_2$Si$_2$Cl$_4$ is found to be favorable with an exothermicity of −30.9 kcal mol^{-1} (ΔG_{298} = −14.7 kcal mol^{-1}, Fig. 27, Scheme 21).[64]

The dark green solution of (cAAC•)$_2$Si$_2$Cl$_4$ is reduced with two equiv. of KC$_8$ with the goal of isolation of the hypothetical 1,2,3,4-tetra radical (cAAC•)$_2$Si(•)$_2$Cl$_2$. A dark green solution of composition (cAAC)$_2$Si$_2$Cl$_2$ is obtained. The molecular structure has been confirmed by X-ray single crystal diffraction (Fig. 29). The ^{29}Si NMR spectrum of (Me$_2$-cAAC)$_2$Si$_2$Cl$_2$ exhibits[66] a singlet at 25.62 ppm which is downfield shifted when compared to that of (Me$_2$-cAAC)SiCl$_4$ (−103.5 ppm). The same compound (Me$_2$-cAAC)$_2$Si$_2$Cl$_2$ can be directly synthesized from the reduction of the (Me$_2$-cAAC)SiCl$_4$ adduct with three equiv. of KC$_8$ in THF (Scheme 22).[66]

The C_{cAAC}–Si bond distances of (Me$_2$-cAAC)$_2$Si$_2$Cl$_2$ (1.823(3)–1.826(3) Å) are slightly shorter when compared with that of (Cy-cAAC•)$_2$Si$_2$Cl$_4$ (1.846(5) Å). The Si–Si bond distances of (Me$_2$-cAAC)$_2$Si$_2$Cl$_2$[66] and (Cy-cAAC•)$_2$Si$_2$Cl$_4$[64] are 2.3058(13) Å and 2.454(3) Å, respectively, suggesting significant shortening of the Si–Si bond length in the former species.

However, the theoretical calculation reveals[66] that four electrons of (Me$_2$-cAAC)$_2$Si$_2$Cl$_2$ are involved in weak π-bonding and hence it should be termed a 1,4-diarylamino-2,3-disiladichlorobutadiene (C_{AAC}═Si(Cl)–Si(Cl)═C_{cAAC}) derivative (Scheme 22 and Fig. 29)[66] rather than a hypothetical 1,2,3,4-tetra radical (cAAC•)$_2$Si(•)$_2$Cl$_2$. The C_{cAAC}–Si and Si–Si bonds are shorter due to delocalized π-bonding which is extended to the delocalized C–Si–Si–C backbone. It has a singlet ground state which is stable by 27.9 kcal mol^{-1}, when compared with that of the triplet state.[66]

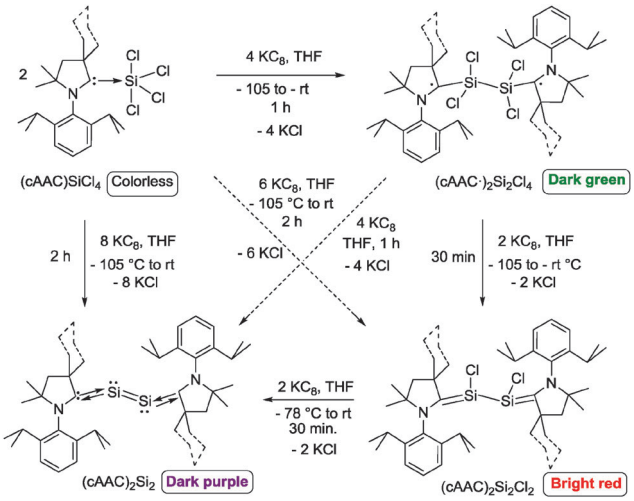

Scheme 22 Synthesis strategy of (cAAC•)$_2$Si$_2$Cl$_4$, (cAAC)$_2$Si$_2$Cl$_2$, and (cAAC)$_2$Si$_2$ from (cAAC)SiCl$_4$ with KC$_8$ [cAAC = Me$_2$-cAAC and Cy-cAAC].

The 2,3-disiladicarbene (cAAC)$_2$Si$_2$ is isolated in 47–48% yield when (cAAC)SiCl$_4$ is reduced with four equiv. of KC$_8$ in THF (Scheme 22). Compound (cAAC)$_2$Si$_2$[67] is isolated as dark purple needles. They are stable for months under an inert atmosphere without any decomposition. (Cy-cAAC)$_2$Si$_2$ melts in the range of 188–190 °C and has been further characterized by EI mass spectrometry. The ^{29}Si NMR spectrum of (Cy-cAAC)$_2$Si$_2$ shows a singlet resonance at 249.1 ppm in C$_6$D$_6$.[67]

X-ray single crystal diffraction exhibits that each silicon atom is bound to one Cy-cAAC ligand and one silicon atom (Fig. 30). The C_{cAAC}–Si bond lengths of (Cy-cAAC)$_2$Si$_2$ are 1.849(4) to 1.876(4) Å.

The cyclic voltammogram of (Cy-cAAC)$_2$Si$_2$ has been studied in THF containing 0.1 M *n*-Bu$_4$NPF$_6$ as an electrolyte. The CV shows a quasi-reversible reduction at $E_{1/2}$ = −1.40 V *versus* Cp*$_2$Fe/Cp*$_2$Fe$^+$ indicating the possible formation of a radical anion (Cy-cAAC)$_2$Si$_2^{\bullet-}$ (Fig. 31).[67]

The purple color of the THF solution gradually changes to red when (Cy-cAAC)$_2$Si$_2$ is treated with metallic potassium at room temperature for 16 h.[67] The formation of a pale yellow colored solution is easily visible around the surface of the piece of potassium. Pale yellow rods are isolated when the concentrated THF solution of the reaction mixture is stored at −32 °C.

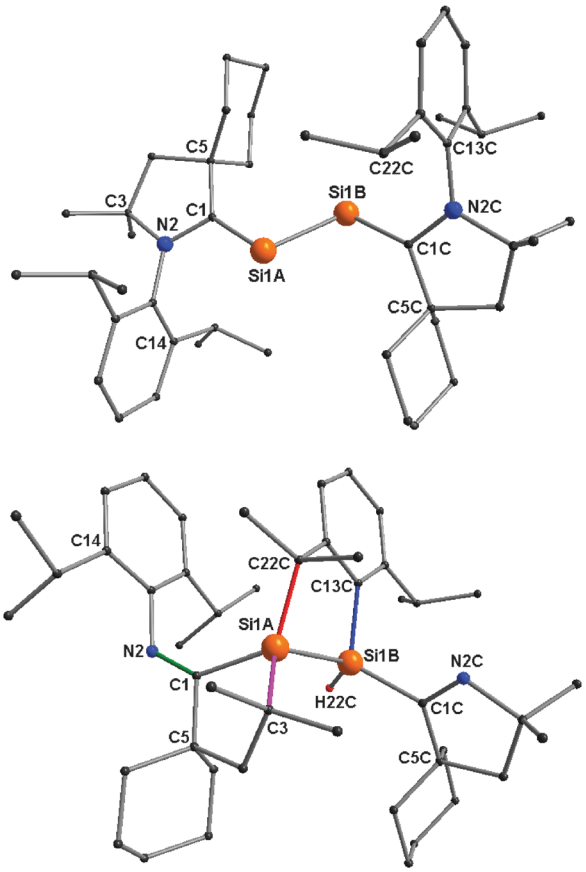

Fig. 30 The molecular structures of $(Cy\text{-}cAAC)_2Si_2$ (top) and its rearranged product $R^1{}_3Si{-}SiHR^2{}_2$ (bottom).

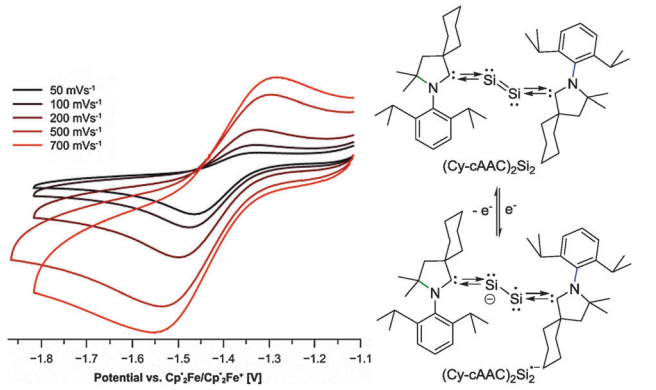

Fig. 31 CV of $(Cy\text{-}cAAC)_2Si^{\bullet-}$ in THF (left) (potential *versus* $Cp^*{}_2Fe/Cp^*{}_2Fe^+$). Formation of $(Cy\text{-}cAAC)_2Si_2^{\bullet-}$ from $(Cy\text{-}cAAC)_2Si_2$ (right). Reproduced with permission from ref. 67.

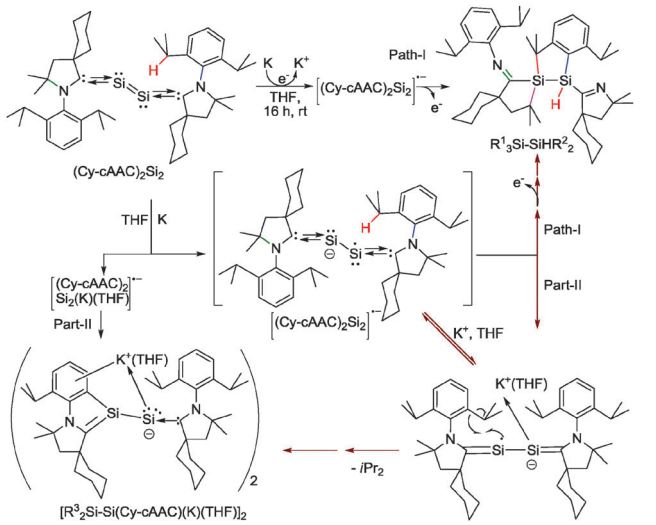

Scheme 23 One electron mediated rearrangement of $(Cy\text{-}cAAC)_2Si_2$.

X-ray single crystal diffraction reveals a rearranged structure of $R^1{}_3Si{-}SiHR^2{}_2$ which is shown in Scheme 23. Compound $R^1{}_3Si{-}SiHR^2{}_2$ (Fig. 30) can be considered as an isomer of $(Cy\text{-}cAAC)_2Si_2$. After the separation of $(Cy\text{-}cAAC)_2Si_2$ some red rods of $[R^3{}_2Si{-}Si(Cy\text{-}cAAC)(K)(THF)]_2$ are isolated (Fig. 32).[67]

X-ray single crystal diffraction (Fig. 30) reveals that $R^1{}_3Si{-}SiHR^2{}_2$ underwent multiple structural rearrangements when compared with $(Cy\text{-}cAAC)_2Si_2$.[67] Both the silicon atoms of $R^1{}_3Si{-}SiHR^2{}_2$ (Fig. 30) maintain a slightly distorted tetrahedral geometry in the formal oxidation state four. The Si1A center is bound to three carbons (C1, C3, C22C) and one silicon (Si1B) atom. The second silicon atom (Si1B) is bound to two carbons (C1C, C13C), one hydrogen (H22C) and one silicon (Si1A) atom. All the four Si–C/H bonds are electron sharing covalent single bonds. The structural features of $R^1{}_3Si{-}SiHR^2{}_2$ are unique. It possesses one exo-cyclic (C1–N2) and one endo-cyclic (C1C–N2C) double bonds with two five-membered spiro rings (Fig. 30).[67]

The CV suggests the formation of the radical anion $(Cy\text{-}cAAC)_2Si_2^{\bullet-}$ (Fig. 31)[67] *via* a quasi-reversible electron transfer process between $(Cy\text{-}cAAC)_2Si_2$ and metallic potassium. Intermediate $(Cy\text{-}cAAC)_2Si_2^{\bullet-}$ might not be stable enough as indicated by CV, it undergoes numerous bond activations followed by rearrangements. Theoretical calculation shows that $(Cy\text{-}cAAC)_2Si_2^{\bullet-}$ can take two pathways (path-I and path-II) and both of them are energetically favorable (Scheme 24). The path-I is suggested to proceed *via* the intermediates IM1, IM2, and IM3 finally giving rise to the rearranged product $R^1{}_3Si{-}SiHR^2{}_2$. The path-II involves the coordination of the lone pair of electrons to potassium ions to produce $(Cy\text{-}cAAC)_2Si_2(K)(THF)^{\bullet-}$ which loses an isopropyl radical to give a THF coordinated dimeric $[R^3{}_2Si{-}Si(Cy\text{-}cAAC)(K)(THF)]_2$ salt.[67] In general, several stable radical anions or radical cations are often generated for the isolation and characterization *via* electron addition or electron snatching processes from some compounds if those species have long life-time. Scheme 23 shows a classic example that illustrates what might be possibly occur if a radical intermediate is not stable enough.[67]

Carbene centered radicals and radical anions bearing a unique diphenyl-phosphino-dichlorosilane group

NHCs favor the formation of the NHC → PCl_3 adduct with trichlorophosphine (PCl_3).[68] NHC → PCl_3 has been reduced to bisphosphinedene $(NHC \rightarrow P)_2$ by six equiv. of KC_8. The cAAC

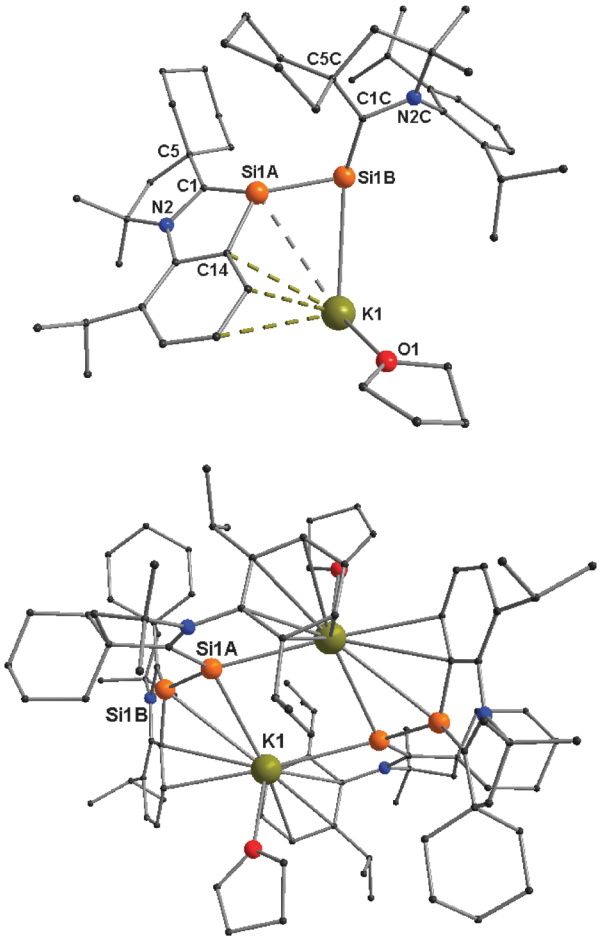

Fig. 32 The monomeric (top) and dimeric (bottom) views of $[R^3{}_2Si\text{-}Si(Cy\text{-}cAAC)(K)(THF)]_2$.

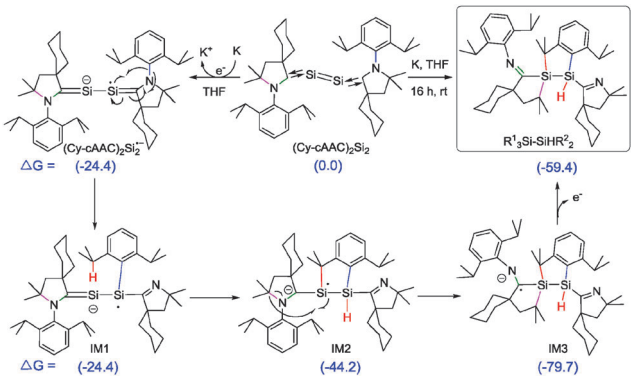

Scheme 24 Proposed reaction pathway (path-I) for the formation of $R^1{}_3Si\text{-}SiHR^2{}_2$ from $(Cy\text{-}cAAC)_2Si_2$. Relative free energies ΔG at BP86/SVP are given in kcal mol^{-1}.

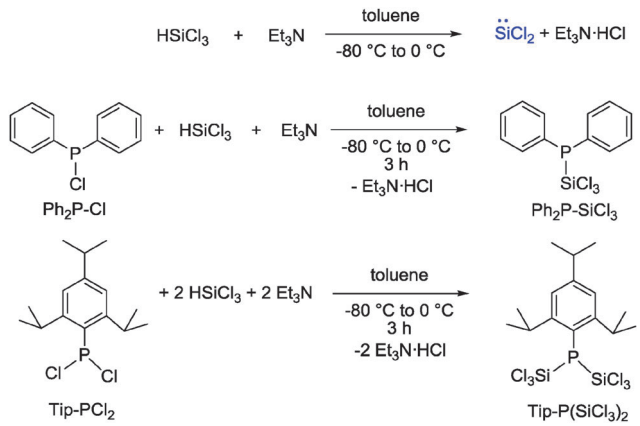

Scheme 25 Synthesis strategy of $Ph_2P\text{-}SiCl_3$ and $Tip\text{-}P(SiCl_3)_2$.

analogue of $(NHC \rightarrow P)_2$ is suggested to have a $C_{cAAC}{=}P$ double bond in $(cAAC{=}P)_2$ rather than a coordinate single bond like in $(NHC \rightarrow P)_2$. So far, the comparative carbene affinity of silicon and phosphorus centers when present in the same compound is only rarely studied. Two decades ago du Mont *et al.* developed the first synthesis route of phosphine substituted chlorosilanes.[69] We realized that the chemistry of carbene/phosphino-chlorosilane follows a significantly diverse path when compared to that of carbene/$SiCl_4$ and carbene/PCl_3.[70]

An attempt is made to synthesize a hypothetical stable radical species incorporating two different neutral compounds, *viz.* cAAC and phosphinochlorosilane. Initially, the intermediate species $SiCl_2$ is *in situ* generated by reacting $HSiCl_3$ with Et_3N in toluene in the 1 : 1.1 molar ratio below −80 °C and subsequently reacted with Ph_2PCl and $Tip\text{-}PCl_2$ [Tip = 2,4-6-triisopropylphenyl] in 1 : 1 and 2 : 1 molar ratios, respectively (Scheme 25).

A one pot reaction of $Ph_2P\text{–}SiCl_3$, cAAC and KC_8 in the 1 : 1 : 1 molar ratio in THF always resulted in the formation of the yellow blocks of $[(cAAC)PPh_2]^+Cl^-$ as the major product.

To avoid the formation of $[(cAAC)PPh_2]^+Cl^-$, a 1 : 1 molar mixture of cAAC and KC_8 and one equiv. of $Ph_2P\text{–}SiCl_3$ are placed separately in two different Schlenk flasks. Both the flasks are cooled utilizing liquid nitrogen baths.[70] Pre-cooled THF (∼−100 °C) is added to the flask containing $Ph_2P\text{–}SiCl_3$ through a canula. The solution of $Ph_2P\text{–}SiCl_3$ is then passed into the other flask containing cAAC and KC_8 (∼−105 °C) with continuing stirring for 5 min at the same temperature. The temperature of the reaction solution is slowly increased to produce a greenish-red solution.

The red needles of compound $(cAAC^{\bullet})Si(Cl_2)(PPh_2)$ [cAAC = Me_2-cAAC, Et_2-cAAC] (Scheme 26) are isolated in 22–25% yield.[70] For comparison, when a similar reaction is carried out with an equivalent amount of NHC instead of cAAC, $NHC \rightarrow SiCl_2$[28] is isolated instead of $(NHC)Si(Cl_2)(PPh_2)$.

The above mentioned protocol is mandatory for the synthesis and isolation of the compound $(cAAC^{\bullet})Si(Cl_2)(PPh_2)$ in a pure form.[70] If the reaction is initiated at −78 °C using a frozen solvent bath and the temperature of the reaction slurry is slowly increased, a dark blue solution of the previously reported $(cAAC^{\bullet})_2SiCl_2$ is obtained as the major product with a much decreased amount of the desired $(cAAC^{\bullet})Si(Cl_2)(PPh_2)$.[70] This suggests that further cleavage of the $Si\text{–}PPh_2$ bond of $(cAAC^{\bullet})Si(Cl_2)(PPh_2)$ occurs in the absence of proper temperature control followed by the anchoring of another cAAC which leads to the formation of the undesired compound $(cAAC^{\bullet})_2SiCl_2$. The isolation of $(cAAC^{\bullet})Si(Cl_2)(PPh_2)$ from this mixture *via* partial

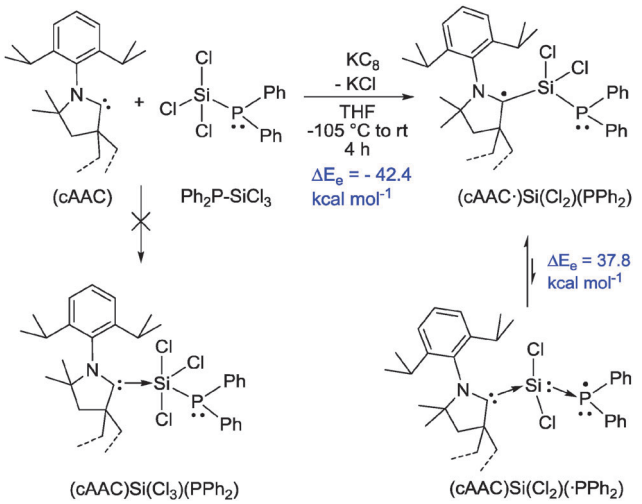

Scheme 26 Synthesis strategy of (cAAC•)Si(Cl_2)(PPh_2) [cAAC = Me_2-cAAC and Et_2-cAAC].

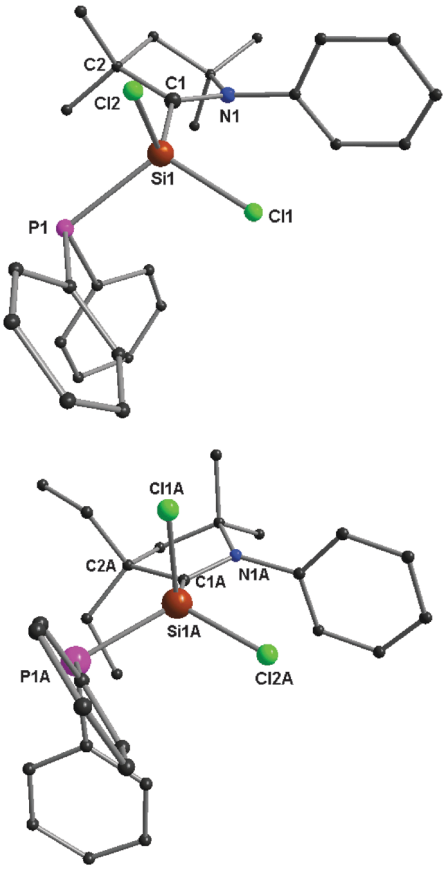

Fig. 33 Molecular structures of (Me_2-cAAC•)Si(Cl_2)(PPh_2) (top) and (Et_2-cAAC•)Si(Cl_2)(PPh_2) (bottom). H-atoms and isopropyl groups from Dipp are omitted for clarity.

crystallization is not fruitful since the presence of (cAAC•)$_2$$SiCl_2$ hinders the crystallization of (cAAC•)Si(Cl_2)(PPh_2) in its pure form. The previously mentioned protocol minimizes the formation of (cAAC•)$_2$$SiCl_2$ and increases the yield of (cAAC•)Si(Cl_2)(PPh_2) to a large extent.[70]

The central silicon atom in (cAAC•)Si(Cl_2)(PPh_2) adopts a near-tetrahedral coordination geometry and is bound to one phosphorus, one carbene carbon, and two chlorine atoms (Fig. 33). The Si–C_{cAAC} bond distance in (cAAC•)Si(Cl_2)(PPh_2) [cAAC = Me_2-cAAC and Et_2-cAAC] is 1.826(3)–1.839(2) Å which is longer (~0.12 Å) than the C_{cAAC} → Si coordinate bond of (cAAC)$SiCl_4$ but close to the covalent electron sharing Si–C single bond of (cAAC•)$SiCl_3$. One chlorine atom tries to orient perpendicular to the C2C1N1 plane (the angle between C2C1N1 and C1Si1Cl2 is 66.85°).[70]

As mentioned previously that the compound [(Me_2-cAAC)-PPh_2]$^+$$Cl^-$ is obtained as a major product when Ph_2P–$SiCl_3$ is directly reacted with Me_2-cAAC in 1 : 1 molar ratio suggesting that Me_2-cAAC prefers to bind at the phosphorus center with the elimination of $SiCl_2$. The reaction of Ph_2P–$SiCl_3$ with KC_8 is very slow in THF at room temperature and thus the unreacted Ph_2P–$SiCl_3$ is recovered from the reaction mixture even after two days suggesting that the formation of Ph_2P–Si(•)Cl_2 is not facile. Based on the experimental observations a possible mechanism for the formation of (Me_2-cAAC•)Si(Cl_2)(PPh_2) is proposed in Scheme 27 and the energetics are calculated for (Me_2-cAAC•)Si(Cl_2)(PPh_2). The *in situ* formation of a carbene radical anion (cAAC•$^-$) intermediate is favorable since Me_2-cAAC has a lower lying LUMO. cAAC•$^-$$K^+$ knocks out one chloride from Ph_2P–$SiCl_3$ to produce (Me_2-cAAC•)Si(Cl_2)(PPh_2) with the formation of KCl. All the steps of the reaction are energetically favorable. Theoretical calculations further suggest that (Me_2-cAAC•)Si-(Cl_2)(PPh_2) (carbene centered radical form) is more stable by an energy of −37.8 kcal mol^{-1} than (Me_2-cAAC)Si(Cl_2)(•PPh_2) (phosphorus centered radical form). The formation of (Me_2-cAAC•)$_2$$SiCl_2$ from the reaction of (Me_2-cAAC)Si(Cl_2)(•PPh_2) with Me_2-cAAC/KC_8 is energetically preferred. This might be the reason why the temperature of the reaction has to be controlled so minutely to minimize the formation of (cAAC•)$_2$$SiCl_2$ and maximize the yield of (cAAC•)Si-(Cl_2)(PPh_2). We also have observed that the undesired product (cAAC•)$_2$$SiCl_2$ is produced in good yield if a mixture of Ph_2P–$SiCl_3$, cAAC, and KC_8 is reacted in the 1 : 2 : 2 molar ratio at −78 °C to room temperature in THF for 2–3 h.[70]

Importantly, the C_{cAAC} atom has contributed ~73% electron density to the C_{cAAC}–Si bond indicating polar character.[70] The calculated Mulliken spin density plots, for Me_2-cAAC and Et_2-cAAC analogues shown in Fig. 34 (top), suggest that the unpaired electron is mostly located on the carbene carbon (75–76%), with a comparatively lower contribution from the N1 atom (18–20%) present in the cAAC fragment. Moreover, the unpaired electron exhibits some finite occupancy over one chlorine atom (1%) and the phosphorus (~3%) atom.

The EPR spectra of (Me_2-cAAC•)Si(Cl_2)(PPh_2) and (Et_2-cAAC•)Si-(Cl_2)(PPh_2) are recorded in toluene (Fig. 35 and 36). Compound (Me_2-cAAC•)Si(Cl_2)(PPh_2) exhibits a partially resolved EPR spectrum which could be simulated with data according to the DFT calculated hyperfine coupling: a(^{31}P) 15.6 G (calc. 20.5 G), a(^{14}N) 6.5 G (calc. 4.2 G), a(^{35}Cl) 4.1 G (calc. 3.1 G).

The spin density is mostly concentrated at the carbene carbon atom (*ca.* 75%), and the adjacent nitrogen atom (19%).

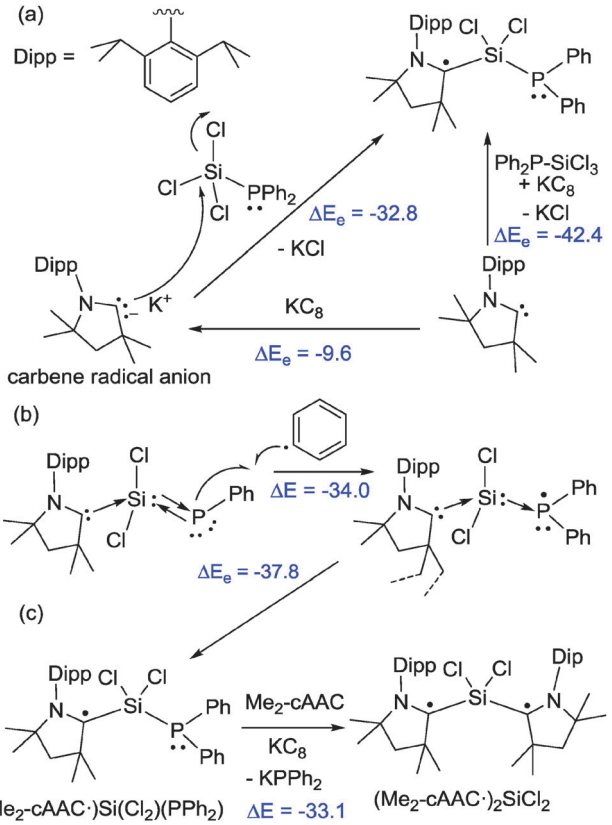

Scheme 27 (a) The proposed mechanism for the formation of (cAAC•)Si-$(Cl_2)(PPh_2)$, (b) energetics for hypothetical reaction of (cAAC)Si(Cl_2)(P-Ph) to (cAAC)Si(Cl_2)(•PPh_2) and (cAAC•)Si$(Cl_2)(PPh_2)$ and (c) (cAAC•)Si$(Cl_2)(PPh_2)$ to (cAAC•)$_2$SiCl_2. ΔE in kcal mol^{-1}. [cAAC = Me_2-cAAC].

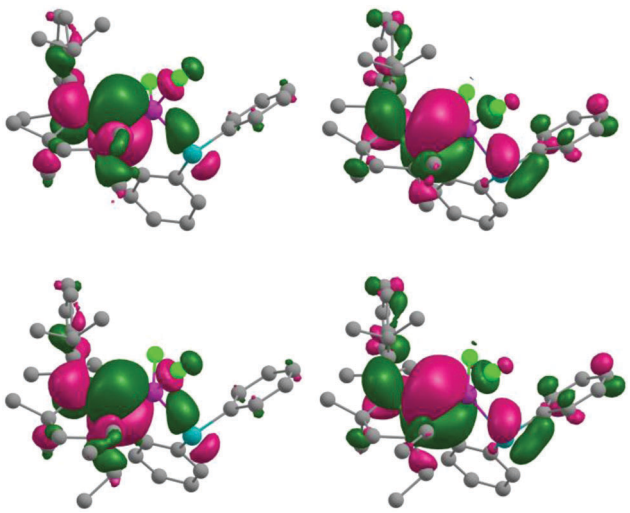

Fig. 34 KS-MO (frontier MO; SUMO (left) and LUMO (right)) for (cAAC•)Si-$(Cl_2)(PPh_2)$ [cAAC = Me_2-cAAC (top) and Et_2-cAAC (bottom)], (isodensity = 0.03 electron bohr^{-3}). Reproduced with permission from ref. 70.

Accordingly, the g factors for both (Me_2-cAAC•)Si$(Cl_2)(PPh_2)$ (2.0027) and (Et_2-cAAC•)Si$(Cl_2)(PPh_2)$ (2.0024) are very close to that of the free electron (2.0023). The heteroatom ^{31}P and one of the chlorine atoms in the β-position exhibit detectable hyperfine coupling despite

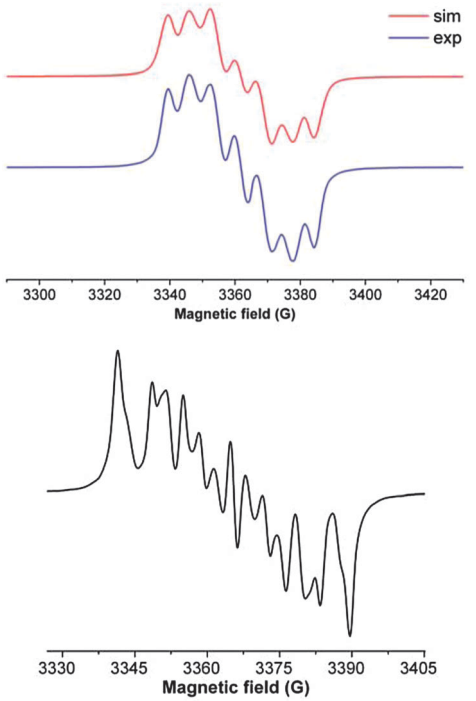

Fig. 35 Experimental and simulated EPR spectra of (Me_2-cAAC•)Si$(Cl_2)(PPh_2)$ at 298 K (top) and experimental EPR of (Et_2-cAAC•)Si$(Cl_2)(PPh_2)$ at 299 K (bottom). Reproduced with permission from ref. 70.

rather small spin densities $<5\%$. A ^{29}Si satellite coupling (4.7% nat. abundance, $I = 1/2$) could be observed for (Et_2-cAAC•)-Si$(Cl_2)(PPh_2)$ at about 10 G (calc. 13.4 G; 3.6% spin density).[70]

The ethyl substituents of Et_2-cAAC at (Et_2-cAAC•)Si$(Cl_2)(PPh_2)$ are labile. The Si$(Cl_2)(PPh_2)$ group can rotate around the Si–C_{cAAC} bond depending upon the substitutions at the C2 atom which is clearly observed when the molecules in (Me_2-cAAC•)Si$(Cl_2)(PPh_2)$ and (Et_2-cAAC•)Si$(Cl_2)(PPh_2)$ are viewed along the Si–C_{cAAC} bond (Fig. 33). Moreover, the five-membered rings of the carbene part adopt different conformations. One chlorine atom Cl2 of (Me_2-cAAC•)Si$(Cl_2)(PPh_2)$ and Cl1A of (Et_2-cAAC•)Si$(Cl_2)(PPh_2)$ is differently oriented with respect to the p_z-orbital of carbene carbon atoms which exerts hyperfine interaction of different strengths in (Me_2-cAAC•)Si$(Cl_2)(PPh_2)$ and (Et_2-cAAC•)Si$(Cl_2)(PPh_2)$. It is noteworthy that there are two molecules present in the asymmetric unit of (Et_2-cAAC•)Si$(Cl_2)(PPh_2)$ with slightly different bond parameters. This leads to the superposition of EPR signals from the two conformers (Fig. 35 and 36) leading to a complicated EPR signal, the signature of which changes dramatically when the temperature is varied (Fig. 36). As a consequence, the temperature dependent EPR spectra between 183 and 340 K show variable line widths. Thus simulation could not be achieved within the accessible temperature range for (Et_2-cAAC•)Si$(Cl_2)(PPh_2)$.[70]

The redox property is also investigated for (cAAC•)Si$(Cl_2)(PPh_2)$ by cyclic voltammetry measurements [Fig. 37; (Me_2-cAAC•)Si$(Cl_2)(PPh_2)$] in THF solution. The CV shows one electron quasi-reversible process at $E_{1/2} = -0.86$ V against $Cp^*_2Fe/Cp^*_2Fe^+$, suggesting the formation of the anion (cAAC•)Si$(Cl_2)(PPh_2)^-$.

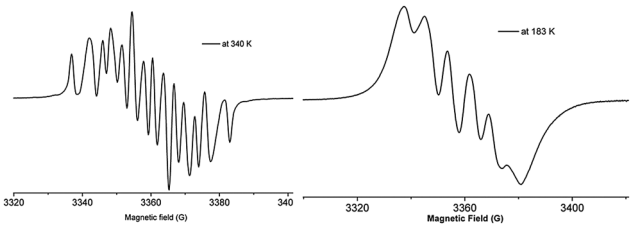

Fig. 36 Experimental EPR spectra of $(Et_2\text{-cAAC}^{\bullet})Si(Cl_2)(PPh_2)$ at 340 K (left) and 183 K (right). Reproduced with permission from ref. 70.

In analogy with $(cAAC^{\bullet})_2SiCl_2$,[57] we hypothesized the synthesis of a novel carbene (cAAC)/phosphinidine (P-Ar, Ar = 2,4,6-triisopropylphenyl) stabilized dichlorosilylene $(cAAC^{\bullet})SiCl_2(^{\bullet}P\text{-Ar})$ as a stable diradical (Scheme 28). When a precooled THF is added at −78 °C to a 2 : 1 : 2 molar mixture of cAAC, Tip-P($SiCl_3$)$_2$, and KC_8, an immediate color change is observed from colorless to green and then to dark blue. The dark blue blocks of (cAAC)-($SiCl_2$)(P-Tip) are obtained in 45% yield (Scheme 28).[71] When ^{IP}NHC [:C{N(2,6-i$Pr_2C_6H_3$)(CH)}$_2$] is employed instead of cAAC, the analogous compound (^{IP}NHC)($SiCl_2$)(P-Tip) is obtained as a bright red crystalline solid in 90% yield.

The ^{29}Si NMR spectra of (Cy-cAAC)($SiCl_2$)(P-Tip), (^{IP}NHC)-($SiCl_2$)(P-Tip) exhibit doublets at −6.56 (J_{Si-P} = 198.4 Hz), and −19.12 (J_{Si-P} = 197.7 Hz) ppm, respectively, which are upfield shifted when compared with that of $(Me_2\text{-cAAC}^{\bullet})_2SiCl_2$ (+4.13 ppm).[71] The ^{13}C NMR resonances of (Cy-cAAC)($SiCl_2$)(P-Tip), and (^{IP}NHC)($SiCl_2$)(P-Tip) (for $C_{carbene}$) are observed at 208.05, and 211.44 ppm, respectively which are again upfield shifted when compared with that of the free carbene (309.4 ppm for Cy-cAAC) but close to that of Cy-cAAC → $SiCl_4$ (207.0 ppm), and $(cAAC)_2Si$ (210 ppm). The UV-vis spectrum of (Cy-cAAC)($SiCl_2$)(P-Tip) is recorded in THF which shows a broad (500–900 nm) absorption band at 665 nm, while the corresponding (400–600 nm) value for compound (^{IP}NHC)($SiCl_2$)(P-Tip) is observed at 475 nm.[71]

The compounds (carbene)($SiCl_2$)(P-Tip) are characterized by single crystal X-ray structure determinations. The molecular structure of (Cy-cAAC)($SiCl_2$)(P-Tip) shows (Fig. 38) that the central $SiCl_2$ unit is bound to one carbene (Cy-cAAC) and one phosphorus atom of the P-Tip group. The silicon atom adopts a distorted tetrahedral geometry while the phosphorus atom

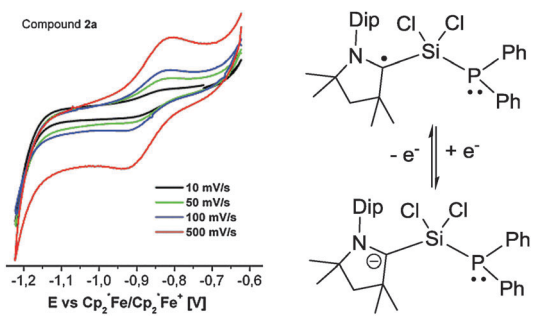

Fig. 37 Cyclic voltammogram of a THF solution of $(Me_2\text{-cAAC}^{\bullet})Si(Cl_2)(PPh_2)$ at indicated scan rates (potential *versus* $Cp^*_2Fe/Cp^*_2Fe^+$), containing 0.1 M [*n*-$Bu_4N]ClO_4$ as an electrolyte (left) suggesting that $(cAAC^{\bullet})Si(Cl_2)(P\text{-}Ph_2)$ converts to $(cAAC)Si(Cl_2)(PPh_2)^-$. Reproduced with permission from ref. 70.

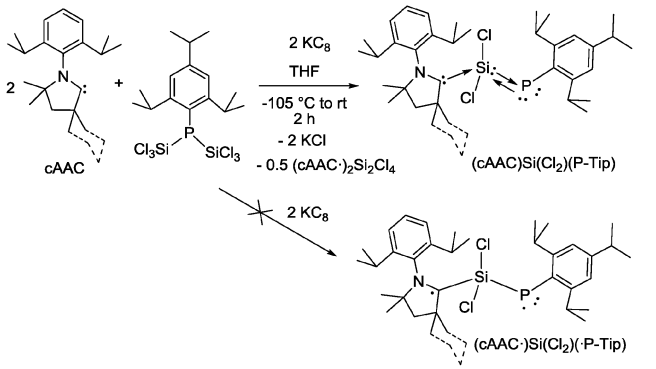

Scheme 28 Synthesis strategy of (cAAC)$Si(Cl_2)$(P-Tip) [cAAC = Me_2-cAAC, Et_2-cAAC and Cy-cAAC].

attends a bent geometry. The phosphorus atom is bound to one silicon (Si1–P1 2.1225(9) Å) and one carbon atom (P1–C24 1.874(2) Å) of the Tip group. The C_{cAAC}–Si and C_{cAAC}–N bond distances were found to be 1.945(2) and 1.308(3) Å, respectively, which are close to those values (1.944(2) and 1.303(2) Å), found in Me_2-cAAC → $SiCl_4$. The aforementioned bond parameters of (Cy-cAAC)($SiCl_2$)(P-Tip) suggest that the bond between the carbene carbon atom and the silicon atom is a coordinate bond (C → Si) rather than an electron sharing single bond (which is supposed to be ∼1.84 Å). To elucidate the exact bonding situations in the compounds cAAC → $SiCl_2$ → P-Tip, and ^{IP}NHC → $SiCl_2$ → P-Tip, detailed theoretical calculations have been carried out on the model compounds **2M**, and **3M**, respectively, where the Dipp groups at the cAAC and NHC donor moieties and the iPr groups at P-Tip are replaced by the methyl groups. NBO analysis reveals that the bonding scenario of these molecules could be best represented in terms of the donor–acceptor interactions D → $SiCl_2$ → P-Tip (D = cAAC, NHC). As a result, we can say that the $DSiCl_2$ moiety as a whole forms a coordinate bond (DCl_2Si → P) with the phosphorus atom of the P-Tip group leaving two pairs of electrons on the phosphorus atom with σ

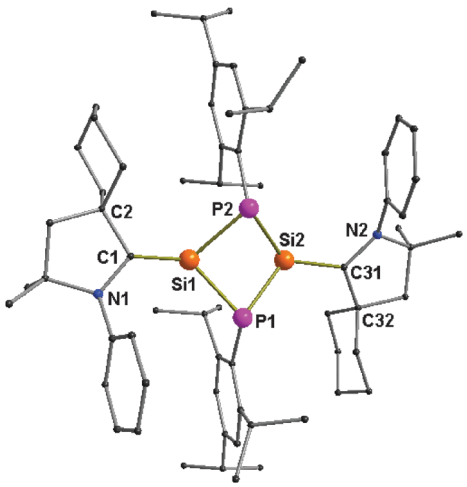

Fig. 38 Molecular structure of (Cy-cAAC)($SiCl_2$)(P-Tip). All H-atoms and iPR groups of Dipp are omitted for clarity.

and π symmetry where the latter is engaged in some π-backdonation to the Si. Hence, in reality there is no diradical character found in the dark blue colored cAAC → $SiCl_2$ → P-Tip as hypothesized previously in comparison with $(cAAC^{\bullet})_2SiCl_2$. The HOMO of cAAC → $SiCl_2$ → P-Tip is located on the $\pi_{Si=P}$ bond while the LUMO is located on the carbene moiety (cAAC or NHC). The characteristic dark blue color of cAAC → $SiCl_2$ → P-Tip is originated from the strong intramolecular charge transfer transition (ICT) from $\pi_{Si=P} \rightarrow \pi^*_{carbene}$. The dramatic change in color from red (^{IP}-NHC → $SiCl_2$ → P-Tip) to blue (cAAC → $SiCl_2$ → P-Tip) is attributed to the lower lying LUMO of cAAC.[71]

We have seen before that $(Cy\text{-}cAAC^{\bullet})SiCl_2$ has a singlet diradical spin ground state $[(Cy\text{-}cAAC^{\bullet})Si(^{\bullet})Cl_2]$ and as a consequence, dimeric 1,4-diradical $(Cy\text{-}cAAC^{\bullet})_2Si_2Cl_4$[64] is eventually isolated (Scheme 21). Thus, it has been intriguing what might be the electronic structure of the dechlorinated product of (Cy-cAAC → $SiCl_2$ → P-Tip). The employment of KC_8 as the reducing agent for this purpose has not been successful. However, (Cy-cAAC → $SiCl_2$ → P-Tip) is successfully reduced with two equiv. of sodium napthalenide ($NaC_{10}H_8$) in THF at room temperature to obtain the dark purple colored monomeric compound (Cy-cAAC)Si(P-Tip) (Scheme 29).[72] It is stable for several hours at room temperature. The ^{29}Si and ^{31}P chemical shift values of (Cy-cAAC)Si(P-Tip) are observed at 288.3 ppm and 309.6 ppm (J_{Si-P} = 163 Hz), respectively. Theoretical calculation concerning the nature of the ground state reveals that (Cy-cAAC)-Si(P-Tip) does not possess a singlet diradical ground state. c_{cAAC}–Si and Si–P are found to be the donor acceptor type partial double bond (C_{cAAC} → Si) and the double bond (Si=P), respectively. The Si=P double bond becomes weak due to the donation of one lone pair of electrons on the silicon atom to the π* of the Si=P double bond. Thus, this monomer undergoes dimerization to produce the thermodynamically more stable (−50.7 kcal mol^{-1}) and isolable compound $[(Cy\text{-}cAAC)Si(P\text{-}Tip)]_2$ (Scheme 29)[72] It is characterized by X-ray single crystal diffraction. In $[(Cy\text{-}cAAC)Si(P\text{-}Tip)]_2$ each phosphorus atom is bound to a Tip group and each silicon atom to a carbene (Cy-cAAC). The P-Tip groups are oriented in *cis* conformation with respect to the Si_2P_2 ring. The aromatic rings of Tip groups are arranged perpendicular to the Si_2P_2 ring,

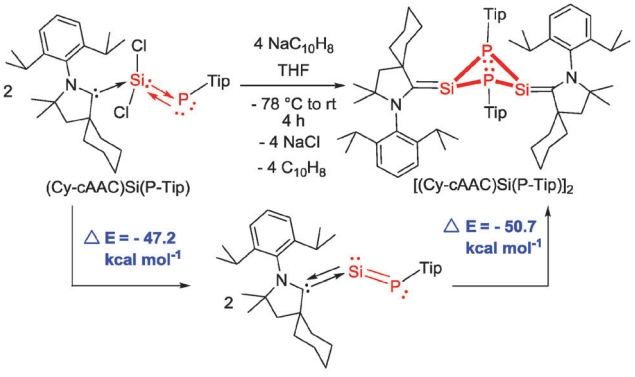

Scheme 29 Synthesis strategy of monomeric (Cy-cAAC)Si(P-Tip) and dimeric $[(Cy\text{-}cAAC)Si(P\text{-}Tip)]_2$.

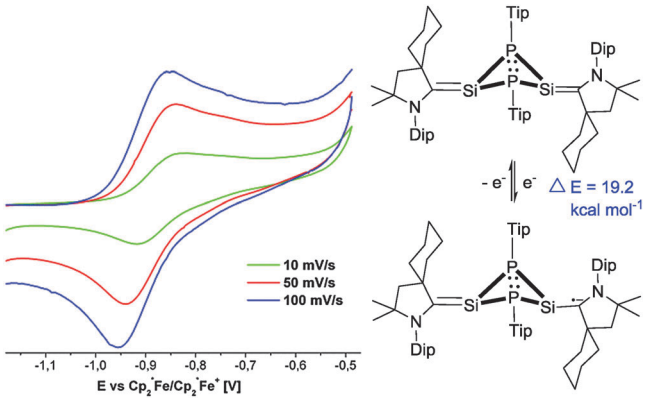

Fig. 39 Cyclic voltammogram of THF solution of $[(Cy\text{-}cAAC)Si(P\text{-}Tip)]_2$, containing 0.1 M $[n\text{-}Bu_4N]ClO_4$ as the electrolyte (potential *versus* $Cp^*_2Fe/Cp^*_2Fe^+$). Reproduced with permission from ref. 72.

while the five-membered carbene rings of Cy-cAAC are parallel to the average plane of the Si_2P_2 ring.[72]

The ^{31}P NMR spectrum of $[(Cy\text{-}cAAC)Si(P\text{-}Tip)]_2$ in THF-d_8 solution exhibits a singlet at −113.4 ppm, flanked by a pair of ^{29}Si satellites (J_{Si-P} = 44 Hz).[72] It is downfield shifted when compared with that of the precursor $(Cy\text{-}cAAC)(SiCl_2)(P\text{-}Tip)$ (−123.0 ppm; J_{Si-P} = 198 Hz). A triplet signal at 37.1 ppm with the same coupling constant (J_{Si-P} = 44 Hz) is observed in the ^{29}Si NMR spectrum. Theoretical calculations on an optimized geometry of both the singlet and triplet states of $[(Cy\text{-}cAAC)Si(P\text{-}Tip)]_2$ shows that the former is the electronic ground state with an energy difference ($\Delta E_{S\rightarrow T}$) of 14.2 kcal mol^{-1}.

The diamagnetic spin ground state of $[(Cy\text{-}cAAC)Si(P\text{-}Tip)]_2$ is confirmed by magnetic susceptibility measurements.[72] The CV shows a one electron quasi-reversible process at $E_{1/2}$ = −0.87 V against $Cp^*_2Fe/Cp^*_2Fe^+$, suggesting the formation of the radical anion $[(Cy\text{-}cAAC)Si(P\text{-}Tip)]_2^{\bullet-}$ (Fig. 39).[72] $[(Cy\text{-}cAAC)Si(P\text{-}Tip)]_2^{\bullet-}$ could not be isolated. However, it is characterized by EPR spectroscopy and its bonding and electron density distribution are studied by theoretical calculations. The X-band EPR spectrum of the *in situ* generated radical anion (a typical S = 1/2 species) in toluene solution at 285 K consists of twelve well-resolved lines of equal intensity (Fig. 40).[72] The splitting pattern is reproduced by simulation (Fig. 40, top), which shows a doublet of doublets, where each component splits further into three equidistant lines. The latter splitting is assigned to the coupling of electron spin with one ^{14}N nucleus (I = 1) at 5.9 G. This value is in the range of values reported for cAAC centered radicals. The two larger doublet hyperfine splittings at 44.1 and 20.6 G are attributed to two inequivalent ^{31}P nuclei (I = 1/2).[72] EPR coupling constants of ^{31}P are frequently large due to the high nuclear magnetic moment, not necessarily reflecting very large spin densities. The inequivalence of the two ^{31}P nuclei in the EPR experiment is in good agreement with the calculated difference in orientation of the P-involving bonds with respect to the mainly spin-bearing p(z) orbital at the carbene carbon center. Accordingly, a ^{29}Si satellite isotope coupling (I = 1/2, 4.7% nat. abundance) with a typical value of about 11 G is also observed.

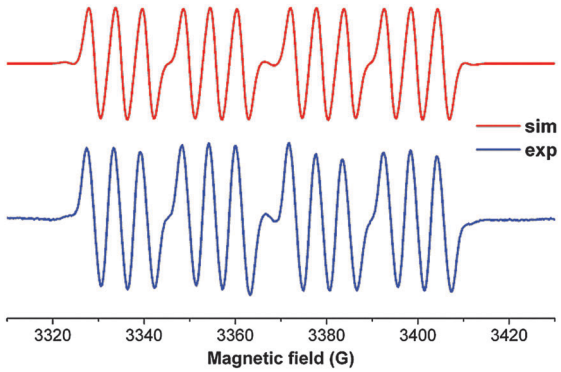

Fig. 40 Simulated and experimental EPR spectra of the radical anion $[(Cy\text{-}cAAC)Si(P\text{-}Tip)]_2^{\bullet -}$ in toluene at 285 K. Reproduced with permission from ref. 72.

One electron reduction of $[(Cy\text{-}cAAC)Si(P\text{-}Tip)]_2$ results in an increase of the electron density in its LUMO. Consequently, the C–N bond distances are elongated in $[(Cy\text{-}cAAC)Si(P\text{-}Tip)]_2^{\bullet -}$ (1.365/1.364 in $[(Cy\text{-}cAAC)Si(P\text{-}Tip)]_2$ *vs.* 1.405/1.413 in $[(Cy\text{-}cAAC)Si(P\text{-}Tip)]_2^{\bullet -}$).[72] The C_{cAAC}–Si bond lengths become unsymmetrical (1.778/1.896) in $[(Cy\text{-}cAAC)Si(P\text{-}Tip)]_2^{\bullet -}$, as the radical resides on the C_{cAAC} atom in α-HOMO (Fig. 41). The calculated spin density points unambiguously the position of the unpaired electron at the carbene carbon (C_{cAAC}), with a minor contribution from neighboring N and Si atoms of the other side.[72]

However, one electron oxidation is observed for monomeric compound (^{IP}NHC)Si(P-Mes*)[73] at −0.053 V suggesting formation of the corresponding radical cation which has neither been isolated nor characterized by EPR measurement.

Untill now, we have mostly discussed on the radicals and diradicals of cAAC-silicon chemistry. However, the group of G. Bertrand and others also have developed novel synthetic routes to the carbene (both cAAC and NHC) stabilized radicals and radical ions of main group elements.[74–89] The number of reports on cAAC stabilized radicals are higher than those of NHC due to the fact that cAAC is a better π-acceptor. Thus cAACs are comparatively more suitable for anchoring the radical species. It is important to mention that cAACs not only stabilize the radicals and radical-ions of main group elements, they also stabilize transition metals with two coordinate geometry, having radical electrons spanning over two carbene carbon atoms of $(cAAC)_2M$ [M = Au, Cu, Mn, Zn].[90–93]

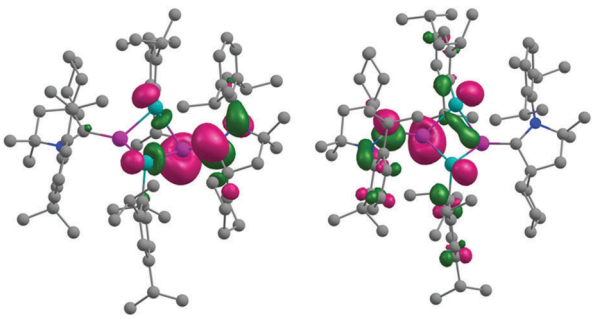

Fig. 41 KS-MOs [α(HOMO) left; and α(LUMO); middle] of $[(Cy\text{-}cAAC)Si(P\text{-}Tip)]_2^{\bullet -}$. Reproduced with permission from ref. 72.

Conclusions

In conclusion, we have summarized the syntheses and characterization of stable silyl radicals and silyl radical ions *via* the reduction or oxidation of suitable precursors under highly controlled synthesis conditions. Some of the synthesis routes are found to be unique. In a few cases the steric bulk of the adjacent ligands has played a significant role for the preparation of some of these species in unusual directions. The radical species are isolated and characterized by X-ray single crystal diffraction and studied by EPR. Similarly, disilene radical anions and cations are stabilized by bulky ligands. The structural and bonding aspects are illustrated by X-ray single crystal structure determination and theoretical calculations. The fine electronic interactions of these radicals with adjacent nuclei are investigated by EPR measurements. The silylene radical anion is characterized only in solution at low temperature while the carbene coordinated silylene radical cation is isolated in a stable form. The disilyne radical anion is also synthesized, isolated and characterized by X-ray single crystal diffraction and EPR measurements. The singlet 1,3-diradicaloid with a cyclic four-membered ring is synthesized by reaction of the Ar–N=N–Ar compound with silyne or bis-silylene. All these radicals, radical ions, diradicals, and diradicaloids are stabilized mostly by the steric effect of the ligands. The radical centers are well protected and prevented from undergoing dimerization or polymerization. However, it is found that the radical intermediates can also be stabilized by strong σ-donation of carbene. The NHC carbene is a poor π-acceptor and hence stabilizes the radical intermediate by σ-donation. The cAAC ligand is a significantly better π–acceptor and a strong σ-donor. cAAC can switch its nature of bonding with the bound silicon atom depending upon the accumulation of electron density around it. The mono radicals of $^{\bullet}SiCl_3$ and $^{\bullet}SiPh_3$ are stabilized by cAAC with the formation of the C_{cAAC}–Si single bond having the radical electron on the carbene carbon atom. The diradical of $SiCl_2$ is stabilized by two cAACs $[(cAAC^{\bullet})_2SiCl_2]$ while singlet $SiCl_2$ species is stabilized by one NHC in a non-radical monomeric form $(NHC)SiCl_2$. The cAAC analogue of the latter one undergoes dimerization to produce 1,4-diradical $(cAAC^{\bullet})_2Si_2Cl_4$ with a Si_2Cl_4 unit in the middle. Further two electrons reduction of $(cAAC^{\bullet})_2Si_2Cl_4$ does not produce a hypothetical tetra radical $(cAAC^{\bullet})_2Si(^{\bullet})_2Cl_2$ rather it can be termed 1,4-diamino-2,3-disilabutadiene derivative $(cAAC)_2Si_2Cl_2$ with the C_{cAAC}=Si(Cl)–Si(Cl)=C_{cAAC} unit in the center of the molecule. A disiladicarbene $(cAAC)_2Si_2$ is obtained from the reduction of $(cAAC)SiCl_4$, $(cAAC^{\bullet})_2Si_2Cl_4$, and $(cAAC^{\bullet})_2Si_2Cl_2$ with the required equiv. amounts of KC_8. Furthermore, diradical $(cAAC^{\bullet})_2SiCl_2$ is reduced to silylone $(cAAC)_2Si$ which possesses significant singlet diradicaloid character due to the small HOMO–LUMO energy gap. Moreover, the CV of $(cAAC)_2Si$ and $(cAAC)_2Si_2$ show that both of them can form radical anion intermediates in a quasi-reversible process.

These radical anions are very reactive and hence undergo one electron induced multiple bond activations leading to unforeseen intra molecular rearrangements.

The synthesis route for the stable carbene centered radical with silicon-phosphine functionalities are little different. The sequence of addition of reactants should be properly adjusted along with the temperature of reduction. Monoradical (cAAC$^{\bullet}$)$SiCl_2(PPh_2)$ is isolated and characterized by X-ray single crystal diffraction. The experimental and simulated EPR spectra show that the hyperfine coupling of the radical electron with chlorine and phosphorus nuclei depends upon their relative orientations with respect to the p_z orbital of the carbene carbon atom. The rotation of the $SiCl_2(PPh_2)$ group around the C_{cAAC}–Si bond of (cAAC$^{\bullet}$)$SiCl_2(PPh_2)$ is comparatively more restricted than that of $SiCl_3$ in (cAAC$^{\bullet}$)$SiCl_3$. The analysis of bonding and optical properties of the blue colored compound (cAAC)($SiCl_2$)(P-TiP) show that it is not like an open shell blue colored diradical species (cAAC$^{\bullet}$)$_2SiCl_2$. (cAAC)($SiCl_2$)(P-TiP) has a singlet ground state with (cAAC:) → (Cl_2Si:) → (P-TiP) type donation of electron pairs. The blue color originates from the intra molecular charge transfer from the silicon–phosphorus π-type orbital to the LUMO of the carbene. (cAAC)($SiCl_2$)(P-TiP) is further converted to the diamagnetic monomeric (cAAC)Si(P-TiP) and dimeric [(cAAC)Si(P-TiP)]$_2$ species having a low HOMO–LUMO energy gap. The later species is quasi-reversibly converted to its radical anion [(cAAC)Si(P-TiP)]$_2^{\bullet-}$ which has been characterized by EPR measurements. All of these compounds are further studied by theoretical calculations which show that cAAC can display a wide range of bonding interactions such as the C_{cAAC} → Si coordinate σ-bond, electron sharing covalent single bond C_{cAAC}–Si, donor acceptor partial double bond. The nature of these bonds has a measureable effect on the C_{cAAC}–N bond lengths.

Acknowledgements

H. W. R. thanks the Deutsche Forschungsgemeinschaft (DFG RO 224/64-I) for financial support.

References

1 (*a*) M. Gomberg, *J. Am. Chem. Soc.*, 1900, **22**, 757–771; (*b*) H. Jkkk, in *Stable Radicals: Fundamental and Applied Aspects of Odd-Electron Compounds*, ed. R. G. Hicks, Wiley, Chichester, 2010; (*c*) J. B. Gilroy, *The design, synthesis, and chemistry of stable verdazyl radicals and their precursors*, PhD thesis, University of Victoria, 2003; (*d*) A. Rajca, *Chem. Rev.*, 1994, **94**, 871–893; (*e*) R. G. Hicks, *Org. Biomol. Chem.*, 2007, **5**, 1321–1338; (*f*) P. P. Power, *Chem. Rev.*, 2003, **103**, 789–809; (*g*) C. D. Martin, M. Soleilhavoup and G. Bertrand, *Chem. Sci.*, 2013, **4**, 3020–3030; (*h*) M. Abe, *Chem. Rev.*, 2013, **113**, 7011–7088; (*i*) D. Astruc, *Electron Transfer and Radical Processes in Transition Metal Chemistry*, Wiley, New York, 1995.

2 (*a*) J. Fossey, D. Lefort and J. Serba, *Free Radicals in Organic Chemistry*, John Wiley and Sons, 1995; (*b*) P. Renaud and M. P. Sibi, *Radicals in Organic Synthesis*, Wiley-VCH, 2008; (*c*) C. Chatgilialoglu and A. Studer, *Encyclopedia of Radicals in Chemistry, Biology and Materials*, Wiley-VCH, 2012.

3 (*a*) J. A. Murphy, T. A. Khan, S. Z. Zhou, D. W. Thomson and M. Mahesh, *Angew. Chem., Int. Ed.*, 2005, **44**, 1356–1360 (*Angew. Chem.*, 2005, **117**, 1380–1384); (*b*) J. A. Murphy, S.-Z. Zhou, D. W. Thomson, F. Schoenebeck, M. Mohan, S. R. Park, T. Tuttle and L. E. A. Berlouis, *Angew. Chem., Int. Ed.*, 2007, **46**, 5178–5183 (*Angew. Chem.*, 2007, **119**, 5270–5275); (*c*) S. O′Sullivan, E. Doni, T. Tuttle and J. A. Murphy, *Angew. Chem., Int. Ed.*, 2014, **53**, 474–478 (*Angew. Chem.*, 2014, **126**, 484–488); (*d*) S. F. Nelsen, *Acc. Chem. Res.*, 1987, **20**, 269–276.

4 B. Halliwell and J. M. C. Gutteridge, *Free Radicals in Biology and Medicine*, Oxford University Press, 2007.

5 (*a*) D. Griller and K. U. Ingold, *Acc. Chem. Res.*, 1976, **9**, 13–19; (*b*) A. Sekiguchi, T. Tanaka, M. Ichinohe, K. Akiyama and S. Tero-Kubota, *J. Am. Chem. Soc.*, 2003, **125**, 4962–4963.

6 (*a*) O. Armet, J. Veciana, C. Rovira, J. Riera, J. Castaner, E. Molins, J. Rius, C. Miravitlles, S. Olivella and J. Brichfeus, *J. Phys. Chem.*, 1987, **91**, 5608–5616; (*b*) J. Carilla, L. Fajari, L. Julia, J. Riera and L. Viadel, *Tetrahedron Lett.*, 1994, **35**, 6529–6532.

7 C. J. Hawker, A. W. Bosman and E. Harth, *Chem. Rev.*, 2001, **101**, 3661–3688.

8 R. A. Sheldon, I. Arends, G. J. Ten Brink and A. Dijksman, *Acc. Chem. Res.*, 2002, **35**, 774–781.

9 K. Matyjaszewski, H.-J. Paik, D. A. Shipp, Y. Isobe and Y. Okamoto, *Macromolecules*, 2001, **34**, 3127–3129.

10 E. M. Fatila, M. Rouzières, M. C. Jennings, A. J. Lough, R. Clérac and K. E. Preuss, *J. Am. Chem. Soc.*, 2013, **135**, 9596–9599.

11 A. Caneschi, D. Gatteschi, N. Lalioti, C. Sangregorio, R. Sessoli, G. Venturi, A. Vindigni, A. Rettori, M. G. Pini and M. A. Novak, *Angew. Chem., Int. Ed.*, 2001, **40**, 1760–1763.

12 D. Gatteschi and R. Sessoli, *Angew. Chem., Int. Ed.*, 2003, **42**, 268–297.

13 (*a*) J. S. Wright, D. J. Carpenter, D. J. McKay and K. U. Ingold, *J. Am. Chem. Soc.*, 1997, **119**, 4245–4252; (*b*) J. S. Wright, E. R. Johnson and G. A. DiLabio, *J. Am. Chem. Soc.*, 2001, **123**, 1173–1183.

14 (*a*) *IUPAC Compendium of Chemical Terminology, release 2.3.2*, International Union of Pure and Applied Chemistry (IUPAC), Research Triangle Park, NC, 2012, p. 168; (*b*) *IUPAC Compendium of Chemical Terminology, release 2.3.2*, International Union of Pure and Applied Chemistry (IUPAC), Research Triangle Park, NC, 2012, p. 427; (*c*) S. S. Eaton, K. M. More, B. M. Sawant and G. R. Eaton, *J. Am. Chem. Soc.*, 1983, **105**, 6550; (*d*) H. Sato, V. Kathirvelu, G. Spagnol, S. Rajca, A. Rajca, S. S. Eaton and G. R. Eaton, *J. Phys. Chem. B*, 2008, **112**, 2818–2828; (*e*) P. Bertrand, C. More, B. Guigliarelli, A. Fournel, B. Bennett and B. Howes, *J. Am. Chem. Soc.*, 1994, **116**, 3078–3086; (*f*) C. Riplinger, J. P. Y. Kao, G. M. Rosen, V. Kathiervelu, G. R. Eaton, S. S. Eaton, A. Kutateladze and F. Neese, *J. Am. Chem. Soc.*, 2009, **131**, 10092–10106; (*g*) T. Sawai, K. Sato, T. Ise, D. Shiomi,

K. Toyota, Y. Morita and T. Takui, *Angew. Chem., Int. Ed.*, 2008, **47**, 3988–3990 (*Angew. Chem.*, 2008, **120**, 4052–4054); (*h*) M. S. Robinson, M. L. Polak, V. M. Bierbaum, C. H. DePu and W. C. Lineberger, *J. Am. Chem. Soc.*, 1995, **117**, 6766–6778; (*i*) M. J. S. Dewar and L. E. Wade, *J. Am. Chem. Soc.*, 1977, **99**, 4417–4424; (*j*) A. Hinz, A. Schulz and A. Villinger, *Angew. Chem., Int. Ed.*, 2015, **54**, 668–672 (*Angew. Chem.*, 2015, **127**, 678–682).

15 (*a*) L. Loodleman, *J. Chem. Phys.*, 1981, **74**, 5737–5743; (*b*) L. Noodleman and E. J. Baerends, *J. Am. Chem. Soc.*, 1984, **106**, 2316–2327; (*c*) K. Yamaguchi, F. Jensen, A. Dorigo and K. N. Houk, *Chem. Phys. Lett.*, 1988, **149**, 537–542; (*d*) K. Kitagawa, T. Saito, M. Itoh, M. Shoji, K. Koizumi, S. Yamanaka, T. Kawakami, M. Okumura and K. Yamaguchi, *Chem. Phys. Lett.*, 2007, **442**, 445–450; (*e*) T. Saito, S. Nishihara, Y. Kataoka, Y. Nakanishi, T. Matsui, Y. Kitagawa, T. Kawakami, M. Okumua and K. Yamaguchi, *Chem. Phys. Lett.*, 2009, **483**, 168–171; (*f*) D. H. Ess, E. R. Johnson, Z. Hu and W. Yang, *J. Phys. Chem. A*, 2011, **115**, 76–83.

16 (*a*) R. S. Ghadwal, S. Azhakar and H. W. Roesky, *Acc. Chem. Res.*, 2013, **46**, 444–456; (*b*) S. K. Mandal and H. W. Roesky, *Chem. Commun.*, 2010, **46**, 6016–6041; (*c*) S. S. Sen, S. Khan, S. Nagendran and H. W. Roesky, *Acc. Chem. Res.*, 2012, **45**, 578–587; (*d*) B. Bolm and M. Driess, in *Functional Molecular Silicon Compounds II*, ed. D. Scheschkewitz, Structure and Bonding, Springer, Berlin, 2014, vol. 156, pp. 85–123; (*e*) P. P. Power, *Chem. Rev.*, 1999, **99**, 3463–3503.

17 (*a*) Y. Wang and G. H. Robinson, *Dalton Trans.*, 2012, **41**, 337–345; (*b*) Y. Wang and G. H. Robinson, *Inorg. Chem.*, 2014, **53**, 11815–11832.

18 Y. Wang, M. Chen, Y. Xie, P. Wei, H. F. Schaefer III, P. V. R. Schleyer and G. H. Robinson, *Nat. Chem.*, 2015, **7**, 509–513.

19 C. Caltagirone, A. Bettoschi, A. Garau and R. Montis, *Chem. Soc. Rev.*, 2015, **44**, 4645–4671.

20 A. F. Holleman, E. Wiberg and N. Wiberg, *Lehrbuch der Anorganischen Chemie*, Walter de Gruyter & Co., Berlin, 1995.

21 W. Simmler, *Silicon Compounds, Inorganic*, Ullmann's Encyclopedia of Industrial Chemistry, Wiley-VCH, Weinheim, 2005, DOI: 10.1002/14356007.a24_001.

22 R. West, M. J. Fink and J. Michl, *Science*, 1981, **214**, 1343–1344.

23 M. Denk, R. Lennon, R. Hayashi, R. West, A. V. Belyakov, H. P. Verne, A. Haaland, M. Wagner and N. Metzler, *J. Am. Chem. Soc.*, 1994, **116**, 2691–2692.

24 M. Kira, *Chem. Commun.*, 2010, **46**, 2893–2903.

25 V. Ya. Lee and A. Sekiguchi, *Organometallic Compounds of Low-Coordinate Si, Ge, Sn and Pb: From Phantom Species to Stable Compounds*, Wiley, New York, 2010.

26 A. J. Arduengo III, R. L. Harlow and M. Kline, *J. Am. Chem. Soc.*, 1991, **113**, 361–363.

27 Y. Wang, Y. Xie, P. Wei, R. B. King, H. F. Schaefer III, P. V. R. Schleyer and G. H. Robinson, *Science*, 2008, **321**, 1069–1071.

28 R. S. Ghadwal, H. W. Roesky, S. Merkel, J. Henn and D. Stalke, *Angew. Chem., Int. Ed.*, 2009, **48**, 5683–5686 (*Angew. Chem.*, 2009, **121**, 5793–5796).

29 M. N. Hopkinson, C. Richter, M. Schedler and F. Glorius, *Nature*, 2014, **510**, 485–496.

30 (*a*) S. Ishida, T. Iwamoto, C. Kabuto and M. Kira, *Nature*, 2003, **421**, 725–727; (*b*) A. Sekiguchi, R. Kinjo and M. Ichinohe, *Science*, 2004, **305**, 1755–1757.

31 (*a*) H. Sakurai, in *Free Radicals*, ed. J. K. Kochi, John Wiley & Sons Ltd., New York, 1973, vol. 2; (*b*) C. Chatgilialoglu, *Chem. Rev.*, 1995, **95**, 1229–1251.

32 (*a*) A. Hudson, R. A. Jackson, C. J. Rhodes and A. L. D. Vecchio, *J. Organomet. Chem.*, 1985, **280**, 173–176; (*b*) M. J. S. Gynane, M. F. Lappert, P. I. Riley, P. Riviere and M. Riviere-Baudet, *J. Organomet. Chem.*, 1980, **202**, 5–12; (*c*) H. Sakurai, H. Umino and H. Sugiyama, *J. Am. Chem. Soc.*, 1980, **102**, 6837–6840; (*d*) A. J. Mckinley, T. Karatsu, G. M. Wallraff, D. P. Thompson, R. D. Miller and J. Michl, *J. Am. Chem. Soc.*, 1991, **113**, 2003–2010; (*e*) S. Kyushin, H. Sakurai, T. Betsuyaku and H. Matsumoto, *Organometallics*, 1997, **16**, 5386–5388.

33 A. Sekiguchi, T. Matsuno and M. Ichinohe, *J. Am. Chem. Soc.*, 2001, **123**, 12436–12437.

34 A. Sekiguchi, T. Matsuno and M. Ichinohe, *J. Am. Chem. Soc.*, 2000, **122**, 11250–11251.

35 (*a*) M. Kira, T. Iwamoto and C. Kabuto, *J. Am. Chem. Soc.*, 1996, **118**, 10303–10304; (*b*) N. Wiberg, H. Auer, H. Noth, J. Knizek and K. Polborn, *Angew. Chem., Int. Ed.*, 1998, **37**, 2869–2872.

36 A. Sekiguchi, T. Fukawa, M. Nakamoto, V. Ya. Lee and M. Ichinohe, *J. Am. Chem. Soc.*, 2002, **124**, 9865–9869.

37 (*a*) J. Thiele and H. Balhorn, *Chem. Ber.*, 1904, **37**, 1463–1470; (*b*) L. K. Montgomery, J. C. Huffman, E. A. Jurczak and M. P. Grendze, *J. Am. Chem. Soc.*, 1986, **108**, 6004–6011.

38 (*a*) W. Schlenk and M. Brauns, *Chem. Ber.*, 1915, **48**, 661–669; (*b*) J. J. Gajewski, M.-J. Chang, P.-J. Stang and T. E. Fisk, *J. Am. Chem. Soc.*, 1980, **102**, 2096–2097; (*c*) B. B. Wright and M. S. Platz, *J. Am. Chem. Soc.*, 1983, **105**, 628–630; (*d*) A. Rajca and S. Utamapanya, *J. Am. Chem. Soc.*, 1993, **115**, 2396–2401.

39 T. Nozawa, M. Nagata, M. Ichinohe and A. Sekiguchi, *J. Am. Chem. Soc.*, 2011, **133**, 5773–5775.

40 (*a*) A. Sekiguchi, S. Inoue, M. Ichinohe and Y. Arai, *J. Am. Chem. Soc.*, 2004, **126**, 9626–9629; (*b*) S. Inoue, M. Ichinohe and A. Sekiguchi, *Chem. Lett.*, 2005, **34**, 1564–1565; (*c*) S. Inoue, M. Ichinohe and A. Sekiguchi, *J. Am. Chem. Soc.*, 2008, **130**, 6078–6079; (*d*) R. Kinjo, M. Ichinohe and A. Sekiguchi, *J. Am. Chem. Soc.*, 2007, **129**, 26–27.

41 D. Bethell and V. D. Parker, *Acc. Chem. Res.*, 1988, **21**, 400–407.

42 L. R. Sita and I. Kinoshita, *J. Am. Chem. Soc.*, 1992, **114**, 7024–7029.

43 S. Ishida, T. Iwamoto and M. Kira, *J. Am. Chem. Soc.*, 2003, **125**, 3212–3213.

44 S. Inoue, M. Ichinohe and A. Sekiguchi, *J. Am. Chem. Soc.*, 2007, **129**, 6096–6097.

45 T. Bally, S. Matzinger, L. Truttman, M. S. Platz, A. Admasu, F. Gerson, A. Arnold and R. Schmidlin, *J. Am. Chem. Soc.*, 1993, **115**, 7007–7008.

46 L. B. Knight, M. Winiski, P. Kudelko and C. A. Arrington, *J. Chem. Phys.*, 1989, **91**, 3368–3377.
47 H. Tanaka, M. Ichinohe and A. Sekiguchi, *J. Am. Chem. Soc.*, 2012, **134**, 5540–5543.
48 (*a*) E. Niecke, A. Fuchs, F. Baumeister, M. Nieger and W. W. Schoeller, *Angew. Chem., Int. Ed.*, 1995, **34**, 555–557; (*b*) N. Roques, P. Gerbier, U. Schatzschneider, J.-P. Sutter, P. Guionneau, J. Vidal-Gancedo, J. Veciana, E. Rentschler and C. Guérin, *Chem. – Eur. J.*, 2006, **12**, 5547–5562; (*c*) W. G. Bentrude, S.-G. Lee, K. Akutagawa, W.-Z. Ye and Y. Charbonnel, *J. Am. Chem. Soc.*, 1987, **109**, 1577–1579.
49 H. Cox, P. B. Hitchcock, M. F. Lappert and L. J.-M. Pierssens, *Angew. Chem., Int. Ed.*, 2004, **43**, 4500–4504 (*Angew. Chem.*, 2004, **116**, 4600–4604).
50 C. Cui, M. Brynda, M. M. Olmstead and P. P. Power, *J. Am. Chem. Soc.*, 2004, **126**, 6510–6511.
51 K. Takeuchi, M. Ichinohe and A. Sekiguchi, *J. Am. Chem. Soc.*, 2011, **133**, 12478–12481.
52 S.-H. Zhang, H.-W. Xi, K.-H. Lim, Q. Meng, M.-B. Huang and C.-W. So, *Chem. – Eur. J.*, 2012, **18**, 4258–4263.
53 V. Lavallo, Y. Canac, C. Präsang, B. Donnadieu and G. Bertrand, *Angew. Chem., Int. Ed.*, 2005, **44**, 5705–5709 (*Angew. Chem.*, 2005, **117**, 5851–5855).
54 (*a*) D. Martin, M. Melaimi, M. Soleilhavoup and G. Bertrand, *Organometallics*, 2011, **30**, 5304–5313; (*b*) D. Martin, Y. Canac, V. Lavallo and G. Bertrand, *J. Am. Chem. Soc.*, 2014, **136**, 5023–5030.
55 O. Back, M. Henry-Ellinger, C. D. Martin, D. Martin and G. Bertrand, *Angew. Chem., Int. Ed.*, 2013, **52**, 2939–2943 (*Angew. Chem.*, 2013, **125**, 3011–3015).
56 D. Martin, M. Soleilhavoup and G. Bertrand, *Chem. Sci.*, 2011, **2**, 389–399.
57 K. C. Mondal, H. W. Roesky, M. C. Schwarzer, G. Frenking, I. Tkach, H. Wolf, D. Kratzert, R. Herbst-Irmer, B. Niepötter and D. Stalke, *Angew. Chem., Int. Ed.*, 2013, **52**, 1801–1805 (*Angew. Chem.*, 2013, **125**, 1845–1850).
58 K. C. Mondal, P. P. Samuel, M. Tretiakov, A. P. Singh, H. W. Roesky, A. C. Stückl, B. Niepötter, E. Carl, H. Wolf, R. Herbst-Irmer and D. Stalke, *Inorg. Chem.*, 2013, **52**, 4736–4743.
59 K. C. Mondal, H. W. Roesky, M. C. Schwarzer, G. Frenking, B. Niepötter, H. Wolf, R. Herbst-Irmer and D. Stalke, *Angew. Chem., Int. Ed.*, 2013, **52**, 2963–2967 (*Angew. Chem.*, 2013, **125**, 3036–3040).
60 S. Roy, K. C. Mondal, L. Krause, P. Stollberg, R. Herbst-Irmer, D. Stalke, J. Meyer, A. C. Stückl, B. Maity, D. Koley, S. K. Vasa, S. Q. Xiang, R. Linser and H. W. Roesky, *J. Am. Chem. Soc.*, 2014, **136**, 16776–16779.
61 K. C. Mondal, H. W. Roesky, A. C. Stückl, F. Ihret, W. Kaim, B. Dittrich, B. Maity and D. Koley, *Angew. Chem., Int. Ed.*, 2013, **52**, 11804–11807 (*Angew. Chem.*, 2013, **125**, 12020–12023).
62 K. C. Mondal, P. P. Samuel, H. W. Roesky, B. Niepötter, R. Herbst-Irmer, D. Stalke, F. Ehret, W. Kaim, B. Maity and D. Koley, *Chem. – Eur. J.*, 2014, **20**, 9240–9245.
63 (*a*) A. V. Lalov, S. E. Boganov, V. I. Faustov, M. P. Egorov and O. M. Nefedov, *Russ. Chem. Bull.*, 2003, **52**, 526–538; (*b*) M. T. Swihart and R. W. Carr, *J. Phys. Chem. A*, 1998, **102**, 785–792.
64 K. C. Mondal, B. Dittrich, B. Maity, D. Koley and H. W. Roesky, *J. Am. Chem. Soc.*, 2014, **136**, 9568–9571.
65 J. R. Koe, D. R. Powell, J. J. Buffy, S. Hayase and R. West, *Angew. Chem., Int. Ed.*, 1998, **37**, 1441–1442.
66 K. C. Mondal, H. W. Roesky, B. Dittrich, N. Holzmann, M. Hermann, G. Frenking and A. Meents, *J. Am. Chem. Soc.*, 2013, **135**, 15990–15993.
67 K. C. Mondal, P. P. Samuel, H. W. Roesky, R. R. Aysin, L. A. Leites, S. Neudeck, J. Lübben, B. Dittrich, M. Hermann and G. Frenking, *J. Am. Chem. Soc.*, 2014, **136**, 8919–8922.
68 Y. Wang, Y. Xie, P. Wie, R. B. King, H. F. Schaefer III, P. V. R. Schleyer and G. H. Robinson, *J. Am. Chem. Soc.*, 2008, **130**, 14970–14971.
69 (*a*) R. Martens and W.-W. duMont, *Chem. Ber.*, 1992, **125**, 657–658; (*b*) R. Martens and W.-W. duMont, *Chem. Ber.*, 1993, **126**, 1115–1117.
70 S. Roy, A. C. Stückl, S. Demeshko, B. Dittrich, J. Meyer, B. Maity, D. Koley, B. Schwederski, W. Kaim and H. W. Roesky, *J. Am. Chem. Soc.*, 2015, **137**, 4670–4673.
71 S. Roy, P. Stollberg, R. Herbst-Irmer, D. Stalke, D. M. Andrada, G. Frenking and H. W. Roesky, *J. Am. Chem. Soc.*, 2015, **137**, 150–153.
72 S. Roy, B. Dittrich, T. Mondal, D. Koley, A. Claudia Stückl, B. Schwederski, W. Kaim, M. John, S. K. Vasa, R. Linser and H. W. Roesky, *J. Am. Chem. Soc.*, 2015, **137**, 6180–6183.
73 D. Geiß, M. I. Arz, M. Straßmann, G. Schnakenburg and A. C. Filippou, *Angew. Chem., Int. Ed.*, 2015, **54**, 2739–2744 (*Angew. Chem.*, 2015, **127**, 2777–2782).
74 V. Lavallo, Y. Canac, B. Donnadieu, W. W. Schoeller and G. Bertrand, *Angew. Chem., Int. Ed.*, 2006, **45**, 3488–3491.
75 D. Martin, C. E. Moore, A. L. Rheingold and G. Bertrand, *Angew. Chem., Int. Ed.*, 2013, **52**, 7014–7017 (*Angew. Chem.*, 2013, **125**, 7152–7155).
76 (*a*) J. K. Mahoney, D. Martin, C. E. Moore, A. L. Rheingold and G. Bertrand, *J. Am. Chem. Soc.*, 2013, **135**, 18766–18769; (*b*) J. K. Mahoney, D. Martin, F. Thomas, C. E. Moore, A. L. Rheingold and G. Bertrand, *J. Am. Chem. Soc.*, 2015, **137**, 7519–7525.
77 (*a*) J. Stubbe and W. A. vander Donk, *Chem. Rev.*, 1998, **98**, 705–762; (*b*) W. Buckel and B. T. Golding, *Annu. Rev. Microbiol.*, 2006, **60**, 27–49.
78 S. Styra, M. Melaimi, C. E. Moore, A. L. Rheingold, T. Augenstein, F. Breher and G. Bertrand, *Chem. – Eur. J.*, 2015, **21**, 8441–8446.
79 R. Kinjo, B. Donnadieu, M. A. Celik, G. Frenking and G. Bertrand, *Science*, 2011, **333**, 610–613.
80 P. Bissinger, H. Braunschweig, A. Damme, I. Krummenacher, A. K. Phukan, K. Radacki and S. Sugawara, *Angew. Chem., Int. Ed.*, 2014, **53**, 7360–7363 (*Angew. Chem.*, 2014, **126**, 7488–7491).
81 O. Back, M. A. Celik, G. Frenking, M. Melaimi, B. Donnadieu and G. Bertrand, *J. Am. Chem. Soc.*, 2010, **132**, 10262–10263.
82 (*a*) W. W. Dulley and D. A. A. Williams, *Interstellar Chemistry*, Academic Press, New York, 1984; (*b*) Y. L. Yung and

W. B. DeMore, *Photochemistry of Planetary Atmospheres*, Oxford University Press, Oxford, 1998.

83 R. Kinjo, B. Donnadieu and G. Bertrand, *Angew. Chem., Int. Ed.*, 2010, **49**, 5930–5933 (*Angew. Chem.*, 2010, **122**, 6066–6069).

84 O. Back, B. Donnadieu, M. V. Hopffgarten, S. Klein, R. Tonner, G. Frenking and G. Bertrand, *Chem. Sci.*, 2011, **2**, 858–861.

85 P. Agarwal, N. A. Piro, K. Meyer, P. Muller and C. C. Cummins, *Angew. Chem., Int. Ed.*, 2007, **46**, 3111–3114 (*Angew. Chem.*, 2007, **119**, 3171–3174).

86 O. Back, B. Donnadieu, P. Parameswaran, G. Frenking and G. Bertrand, *Nat. Chem.*, 2010, **2**, 369–373.

87 M. Y. Abraham, Y. Wang, Y. Xie, R. J. Gilliard Jr., P. Wei, B. J. Vaccaro, M. K. Johnson, H. F. Schaefer III, P. V. R. Schleyer and G. H. Robinson, *J. Am. Chem. Soc.*, 2013, **135**, 2486–2488.

88 (*a*) Y. Li, K. C. Mondal, P. P. Samuel, H. Zhu, C. M. Orben, S. Panneerselvam, B. Dittrich, B. Schwederski, W. Kaim, T. Mondal, D. Koley and H. W. Roesky, *Angew. Chem., Int. Ed.*, 2014, **53**, 4168–4172 (*Angew. Chem.*, 2014, **126**, 4252–4256); (*b*) L. Jin, M. Melaimi, L. Liu and G. Bertrand, *Org. Chem. Front.*, 2014, **1**, 351–354.

89 J. Park, H. Song, Y. Kim, B. Eun, Y. Kim, D. Y. Bae, S. Park, Y. M. Rhee, W. J. Kim, K. Kim and E. Lee, *J. Am. Chem. Soc.*, 2015, **137**, 4642–4645.

90 D. Weinberger, M. Melaimi, C. E. Moore, A. L. Rheingold, G. Frenking, P. Jerabek and G. Bertrand, *Angew. Chem.*, 2013, **125**, 9134–9137 (*Angew. Chem., Int. Ed.*, 2013, **52**, 8964–8967).

91 D. S. Weinberger, N. A. SK, K. C. Mondal, M. Melaimi, G. Bertrand, A. C. Stückl, H. W. Roesky, B. Dittrich, S. Demeshko, B. Schwederski, W. Kaim, P. Jerabek and G. Frenking, *J. Am. Chem. Soc.*, 2014, **136**, 6235–6238.

92 P. P. Samuel, K. C. Mondal, H. W. Roesky, M. Hermann, G. Frenking, S. Demeshko, F. Meyer, A. C. Stückl, J. H. Christian, N. S. Dalal, L. Ungur, L. F. Chibotaru, K. Pröpper, A. Meents and B. Dittrich, *Angew. Chem., Int. Ed.*, 2013, **52**, 11817–11821 (*Angew. Chem.*, 2013, **125**, 12033–12037).

93 A. P. Singh, P. P. Samuel, H. W. Roesky, M. C. Schwarzer, G. Frenking, N. S. Sidhu and B. Dittrich, *J. Am. Chem. Soc.*, 2013, **135**, 7324–7329.

